Gezamenlijke opleiding Universiteit Hasselt en KU Leuven

2016•2017
FACULTEIT INDUSTRIËLE INGENIEURSWETENSCHAPPEN
master in de industriële wetenschappen: bouwkunde

Masterproef

Experimental and numerical analysis on a reinforced concrete structure using structural similitude laws

Promotor :
Prof. dr. ir. Herve DEGEE

Copromotor :
De heer Dan DRAGAN

Maikel Renette
Scriptie ingediend tot het behalen van de graad van master in de industriële wetenschappen: bouwkunde

2016•2017
Faculteit Industriële ingenieurswetenschappen
master in de industriële wetenschappen: bouwkunde

Masterproef
Experimental and numerical analysis on a reinforced concrete structure using structural similitude laws

Promotor :
Prof. dr. ir. Herve DEGEE

Copromotor :
De heer Dan DRAGAN

Maikel Renette

Scriptie ingediend tot het behalen van de graad van master in de industriële wetenschappen: bouwkunde

ACKNOWLEDGEMENTS

The experimental analysis of this master's thesis was a very challenging and intensive parkour. Also, the building of the portal frame and the reinforcement cages had to be done very precisely. The completion of this master's thesis could not be successful without the advice and help of several people out of the Structural Department and beyond.

I would like to express my sincere acknowledgement to my promotor Professor Hervé Degée and my copromotor PhD. engineer Dan Dragan. Also, I would like to thank the other Professors and teachers in the Structural Department and specially Professor Bram Vandoren. This experience was much more interesting due to their teaching and knowledge. Renaat van Heinsbergen from the company Jans Creacar is recognized for his assistance in ordering and manipulating of the steel for the reinforcement cages. Life is much more interesting when the experience can be shared with others. I would like to thank the numerous students who took part in this project, gave me advice, and made this experience satisfying.

Finally, I would like to thank my family and friends. Thank you for the support and perseverance you gave me. Also, thank you for the interest and enthusiasm that you showed as well as for the reading of this master's thesis. I would like to express explicitly my gratitude to Glynis Bogaard for the reading and improving of this master's thesis.

ABSTRACT

Buildings from around 1960 that were built out of reinforced concrete portals were often constructed without proper knowledge of the influence from lateral loads. The lack of this knowledge caused several buildings to fail in a disastrous brittle shear manner. Nonetheless, reinforced concrete structures and their sensitivity to moments and shear forces have not been studied well. Moreover, reliable numerical software's to study shear-critical structures are rare. Therefore, the purpose of this master's thesis is to predict the behaviour of a real life reinforced concrete structure using a scaled model and to calibrate a finite element model to obtain this prediction.

The starting point for this master's thesis was a thesis which was carried out at the University of Toronto, in which they tested a full size reinforced concrete frame under seismic loading. The same single-span, two-storey, reinforced concrete frame was constructed on scale one to three. An experimental and numerical analysis was carried out when the reinforced concrete frame was subjected to lateral loading, to investigate the critical shear behaviour of the portal frame. This numerical analysis was done with the software TNO DIANA.

The experimental- and numerical analyses showed that a difference in behaviour and failure mode arose between the prototype and the scaled model when a scale factor of three was applied. This change in behaviour between the prototype and the scaled model is removed by a modified model. The finite element model proved that this modification is accurate and that the behaviour of the prototype can be predicted by a scaled model and by the calibrated finite element model.

ABSTRACT - NEDERLANDS

Gebouwen van rond de jaren 1960 die opgebouwd zijn aan de hand van gewapende betonnen draagstructuren, zijn vaak geconstrueerd zonder de juiste kennis te hebben over de invloed van laterale belastingen. Hierdoor kunnen gebouwen door brosse afschuifkrachten op catastrofale wijze bezwijken. De oorzaak hiervan is dat er in het verleden weinig onderzoek is gevoerd naar deze moment- en afschuifkracht gevoelige gebouwen. Ook betrouwbare numerieke software om dit te onderzoeken was zeldzaam. Het doel van deze master thesis is daarom om het gedrag van een gewapende beton structuur te voorspellen aan de hand van een schaalmodel. Om dit gedrag te voorspellen wordt er binnen deze master thesis ook een eindige elementen model ontwikkelt.

In dit thesisonderzoek is een betonnen portaal uit een referentie artikel geschaald met factor drie. Op dit betonnen portaal is vervolgens een laterale belasting aangebracht waarna op experimentele- en numerieke wijze het kritisch afschuifgedrag van het portaal onderzocht is. De numerieke analyse is bekomen aan de hand van de software TNO DIANA.

De experimentele- en numerieke resultaten tonen aan dat er een verschil in gedrag en bezwijkmechanisme ontstaat tussen het prototype en het schaalmodel wanneer een schaalfactor van drie wordt toegepast. Dit verschil is weggewerkt aan de hand van een aangepast model. Het eindige elementen model bewijst dat deze aanpassing accuraat is. Het gedrag van het prototype kan dus voorspelt worden aan de hand van een schaalmodel en een gekalibreerd eindige elementen model.

TABLE OF CONTENTS

LIST OF TABLES

LIST OF FIGURES

Chapter 1

Chapter 2

Chapter 3

Chapter 4

Chapter 5

Chapter 7

LIST OF GRAPHS

Chapter 2

Chapter 3

Chapter 4

Chapter 5

Chapter 7

0. INTRODUCTION

This master's thesis describes a study on predicting the behaviour of a real life reinforced concrete frame (prototype) using a scaled structure (model). The scaled model has a scale of 1:3 related to the prototype. The scaling of the dimensions, the materials characteristics, the boundary conditions, and the loadings of the prototype are based on the similitude theory.

The main advantages of scaled experiments are the simple manner of manipulation of the structure, the low fabrication costs and the small size of the equipment. The main disadvantages of this method are the time for fabrication of the models and the challenges in simulating the entire behaviour of the prototype. To make the testing on scaled models possible, some carefully chosen adjustments are necessary. These adjustments will lead to small differences between the expected and the obtained results. The current study uses an experimental quantitative design.

Two aspects are inextricably linked with this research topic: reinforced concrete frames and the similitude theory. Before an experimental – and numerical investigation can be carried out, it is necessary to give a precise definition of these subjects. To this end, five cases are studied, which demonstrate the behaviour of a separated reinforced concrete element. Next, the behaviour of the connection between several elements is discussed. This investigation is carried out in chapter one *Literature review*.

The second chapter of this master's thesis elaborates on the experimental design. This is done by a representation of the dimensions of the test specimens. In the next section, the properties of the used materials are explained, followed by an overview of the construction of the mould and the reinforcement cages supplemented with a description of the casting process. Lastly, the used test setup is discussed together with the used measure instrumentation.

Chapter three focusses on the processing of the results, gathered from the experimental program that is mentioned in the previous chapter. These results are transformed into graphs per specimen and clarified by pictures that were taken during the experimental tests.

The fourth chapter discusses the finite element modelling by a description of the support conditions, the material model that is used for the mathematical FE modelling of the concrete – and reinforcement elements and the loading conditions. Next, the incremental-iterative solution procedure is explained in the section *Analysis procedure*. The model is built using the finite element software TNO DIANA. Following, the results of this numerical research are discussed in chapter five. Here, the focus is on the crack-widths in the z-direction, the displacement of the frame and its elements in the x-direction, the total compression stresses in the concrete, and the total stresses in the reinforcement in the x- and z-direction.

Chapter six makes a comparison between the experimental program and the numerical program and chapter seven makes a comparison between the results of the reference article and the results obtained from the current study.

The conclusions out of these two previous comparison chapters are formulated in chapter eight. Also, a general conclusion related to the research topic is mentioned in this chapter. Moreover, these conclusions were used for the formulation of research topics that could be investigated in future work, which are discussed in chapter nine. Finally, the derived sources are formulated in the last chapter of this master's thesis.

1. LITERATURE REVIEW

1.1 Reinforced concrete frames

1.1.1 Background

A reinforced concrete frame is a constructive combination of elements (columns and beams) which is frequently used in building constructions. Reinforced concrete is an artificial, stone like material that contains steel bars and is used for various structural purposes. It is made by mixing cement and various aggregates with water, for example, sand, pebbles, gravel, or shale.

Concrete and its usage became more popular after inauguration of Portland cement in the 19th century. Because unreinforced concrete only governs a good behaviour in compression, steel bars were introduced in the tensile zone of the concrete, which led to the development of a composite material named *reinforced concrete*. This material has excellent characteristics in compression and tension by the cooperation between the concrete and the steel bars. Therefore, the material is used in several types of civil engineering constructions such as high-rise buildings, dams, bridges, etc.

Reinforced concrete is widely used because to the broad availability of the cement ingredients and the steel bars. Also, the production of concrete is much cheaper than that of steel. A reinforced concrete frame consists out of vertical elements which are called columns, and horizontal elements, are called beams. These elements are connected to each other by fixed joints. To increase the frame strength, the elements are usually cast together during the construction work. Two types of frames can be distinguished, the braced- and the unbraced frames. Braced frames can resist higher lateral loads than unbraced frames. This because the bracing system prevents that the structure sways away due to a horizontal load.

Reinforced concrete frames are frequently used in high-rise buildings because it has more safety advantages than other materials. More precisely, reinforced concrete has more resistance against high temperature depending on the thickness of the concrete cover, with more thickness meaning longer heat resistance. Also, concrete has a good explosion resistance, and it can resist a wind force up to 300 kilometres per hour, given that the structure is designed properly of course [1].

1.1.2 Frame analysis

Frame analyses are carried out to study the behaviour of these frames when they are subjected with vertical –and horizontal forces. In practice, reinforced concrete constructions are designed on linear elastic assumptions. Analyses that use these assumptions are commonly plausible if the building is designed according the Eurocode. This means that serviceability conditions and strength are met, joints are detailed in the correct way, the length of the rebar's are developed efficiently and the failure modes are ductile. Designs according to Eurocode are commonly conservative.

The proper knowledge of the structural performance is not necessary, as these buildings are designed to withstand the external and internal loads in a safe way. However, when inspected structures are considered to be inadequate according to general standards, a more adequate analysis is demanded to revalue the capacity of these structures for safety. In this case, second-order effects such as geometric nonlinearities and material properties become more directive. These effects can affect the ultimate capacity and the failure modes. For this reason, a detailed structural calculation is necessary to account for these second-order effects. This analysis has two advantages; first, the rehabilitation strategy can be evaluated and secondly the crack pattern can be predicted. This can warn engineers for potential failure.

The last 25 years, a lot of effort is done to improve and implement nonlinear numerical analysis procedures for reinforced concrete frames. Transparent and realistic models out of tests are implemented in design formulations and analysis procedures. These formulations and procedures are in a next stage applied to the design and evaluation of real life structures. TNO DIANA (Displacement Analyser) is a comprehensive multi-purpose Finite Elements software, focused on calculations of a wide spectrum of civil engineering and geotechnical applications and is used in this thesis. The rational of TNO DIANA is based on the Modified Compression Field Theory (MCFT) [2].

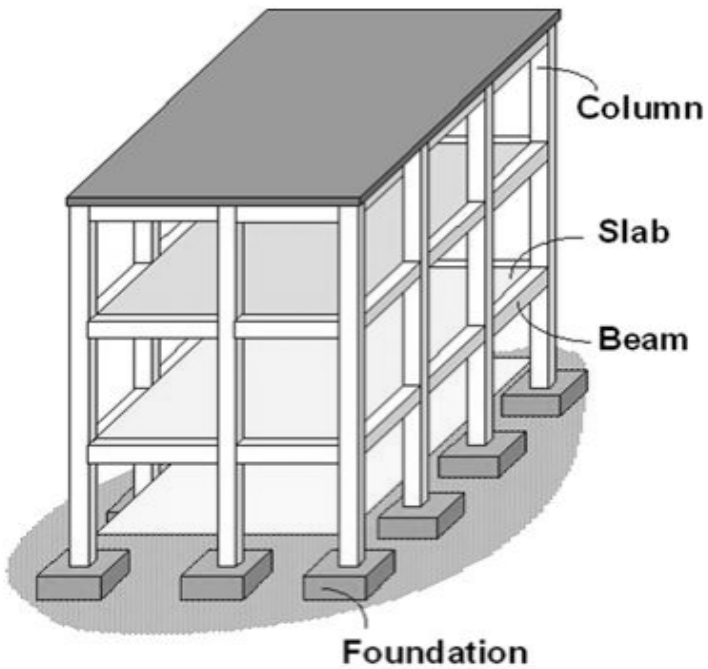

Fig. 1.1: Reinforced concrete frame building [3]

1.1.3 Modified Compression Field Theory (MCFT)

The Modified Compression Field Theory was originally proposed by Vecchio & Collins in 1986. The essential relations behind the MCFT were obtained out of experimental tests of thirty reinforced concrete panels which were subjected to a combination of axial loads and shear or pure shear. Out of these test results, compatibility, stress and strain-strain and equilibrium relationships were defined in average stresses and strains. The equilibrium conditions secure balance of the external applied forces to the internal forces in the elements; compatibility imposes agreement between deformation experienced by the concrete to an identical deformation of the reinforcement; and fundamental relationships relate average stresses to average strains for the cracked concrete but also for the cracked reinforcement.

The Modified Compression Field Theory treats the cracked reinforced concrete elements as an orthotropic material wherein the cracks can rotate and re-orient. This MCFT also accounts on softening compression behaviour. This refers to the reduced concrete compressive strength in the presence of large transversal tensile strains. Also, tension stiffening is included and this counts for the tensile stresses in the concrete which occurs between the cracks. The local failure mechanisms are considered with yielding or fracture from the reinforcement at the position of the cracks. Also, sliding shear failure along the crack openings is considered [4].

1.1.4 Case studies

To increase the research in this academic writing, this part will focus on previous experimental work of cyclic –or monotone loaded reinforced concrete frames. The testing of reinforced concrete frames has already been studied for years at several universities around the world.

In this section, the shear-critical beam column connection is examined. Finally, the study of reinforced concrete frames at the University of Toronto will be investigated in more depth because one of the pioneers in this topic, namely Frank J. Vecchio was a professor at this University. Also, the reinforced concrete frame on which the experiment in this thesis is based on, was part of a thesis written at the University in Toronto [2].

A Shear-critical beam column connection

In the past, many beam column connections had been examined and tested to understand the behaviour of reinforced concrete portals. To understand this behaviour, it suffices to build and to examine only the joint between these two elements. Thus, it is not necessary to build a whole frame. The disadvantage of this method is that only results of the local behaviour of the joint can be used, and not the global frame behaviour. With this in mind, two studies will be discussed in detail below. The first study is executed by Celebi and Penzien (1973), who investigated the behaviour of reinforced components by building a connection that existed out of a part of an interior beam and a column. In the second study, Ghobarah, Aziz and Biddah (1996) built a connection between a weak beam and a strong column, to examine the flexural shear in the connection. This connection was subjected to a cyclic loading.

A.1 A connection by Celebi and Penzien (1973)

Celebi and Penzien tested twelve connections subjected to a cyclic loading. The variable parameters they used for the beam were width to depth ratio, the spacing between the stirrups, the dimensions of the cross-section, the longitudinal reinforcement ratio, and the dynamic versus static loading percentage. To understand the shear degradation due to a static load, they focused on just one specimen. Below are the properties, the way of testing the specimen and the results for beam twelve mentioned.

Beam twelve has a length of 183 millimetres and a cross-section of 230 millimetres on 380 millimetres (width x depth). A column is located in the middle of the beam, causing the ratio between shear span and width to have a value of 2,30. The beam is equipped with longitudinal reinforcement (1%) but also with reinforcement against shear (0,75%). The yield strength of the steel has a value of 345 MPa and the compressive strength of the concrete was almost 32 MPa. The configuration of the specimen is given in *Figure 1.3*.

For measuring the loads and displacements they used actuator load cells, LVDTs and DCDTs which where mounted on an external frame. With the LVDTs the diagonal displacement is measured and with the DCDTs (direct current displacement transducers) the strains in the rebar's are measured. The column stud is subjected with a vertical reverse cyclic load in a quasi-static way. The loading cycles are illustrated in *Figure 1.4*. Because of the cyclic load, the connection degraded in resistance which is shown in load deflection curve in *Figure 1.4*. The squeeze in the graph occurs because of the low ratio between the shear span and width and also due to the high value of the shear stresses. The deformations due to shear have an effect on the global total deformation of the joint and the structure [5].

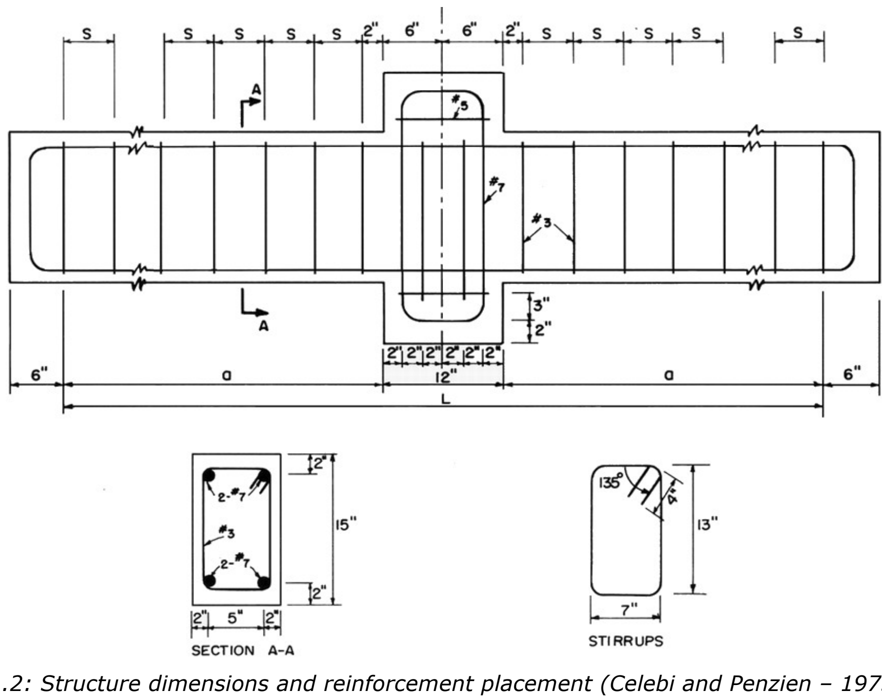

Fig. 1.2: Structure dimensions and reinforcement placement (Celebi and Penzien – 1973) [5]

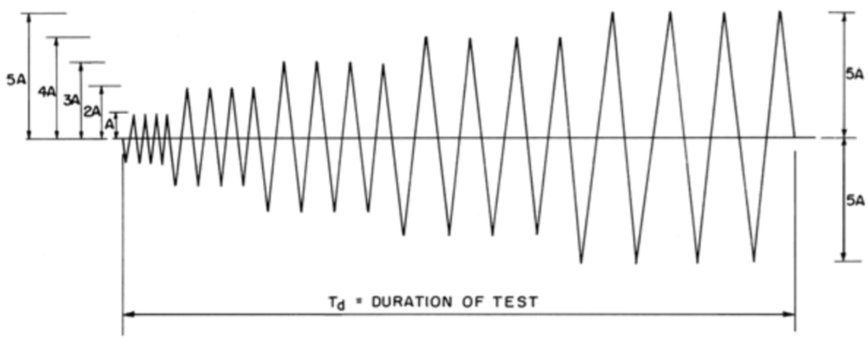

Fig. 1.3: Loading Sequence of beam twelve (Celebi and Penzien – 1973) [5]

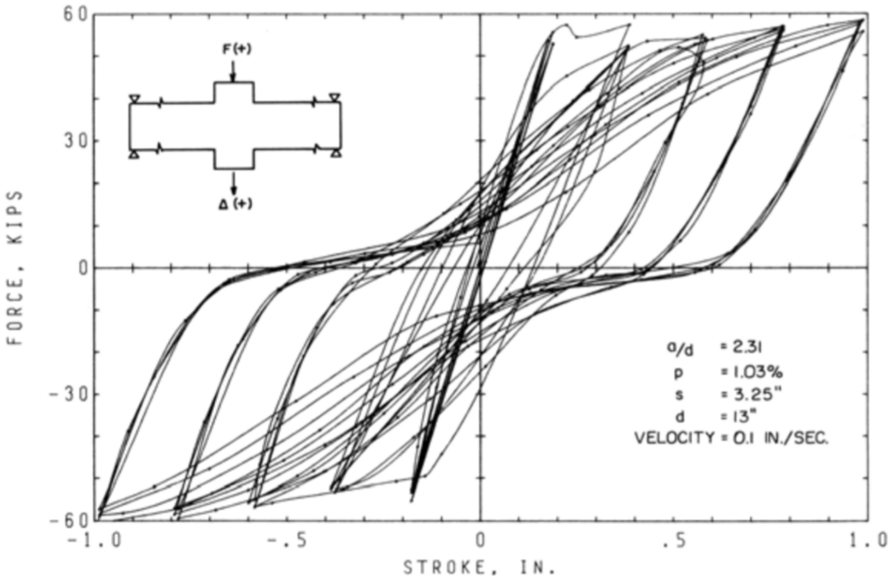

Fig. 1.4: Cyclic Response of beam twelve (Celebi and Penzien – 1973) [5]

A.2 A connection by Ghobarah, Aziz and Biddah (1996)

Ghobarah, Aziz and Biddah investigated a beam column connection for seismic design, which was based on a technique where curved steel jacks are used. Those curved steel jacks were applied in the zones were the failure in the connections occur. After placing the jacks in those weak zones the openings between the reinforcement and the concrete are filled with a shrink resistant grout. In this case, four specimens were tested. Below are the properties, the way of testing the specimen and the results for joint four mentioned.

The joint between the constructive elements is built on a scale of one to three. The yield strength of the transversal rebar's has a value of 448 MPa and the 2,8 millimetres thick curved steel jacket has a strength of 363 MPa. The compressive strength of the concrete was 23 MPa. The configuration of the specimen is given in *Figure 1.5*. *Figure 1.6* shows the layout of the reinforcement.

The first load cycle was a compression load which was applied on the top of the column with a value of 505 kN. This force was kept constant during the entire test. At the end of the beam they applied a vertical reverse cycle with a size of 15% of the strength of the specimen (60 kN), followed by two load cycles until failure of the concrete occurs (120 kN), and two cycles until failure of the reinforcement (340 kN). In the next stage, the displacement increases to two times the yield displacement. This continued until the total strength capacity of the specimen was lower than 25% of the eventual strength. The strains at the surface and the displacement of the structure were measured by strain meters and displacement converters. In *Figure 1.7* is the load displacement curve given. The first crack occurs at the joint between the beam and the column. This is followed by yielding of the reinforcement in the length direction of the beam (320 kN). During this phenomenon, the first cracks in the beam appears. The highest resistance what was reached was 430 kN when the displacement was equal to four times the displacement at yielding of the rebar's. The failure was analysed as a failure due to shear at the plastic hinge region in the beam [6].

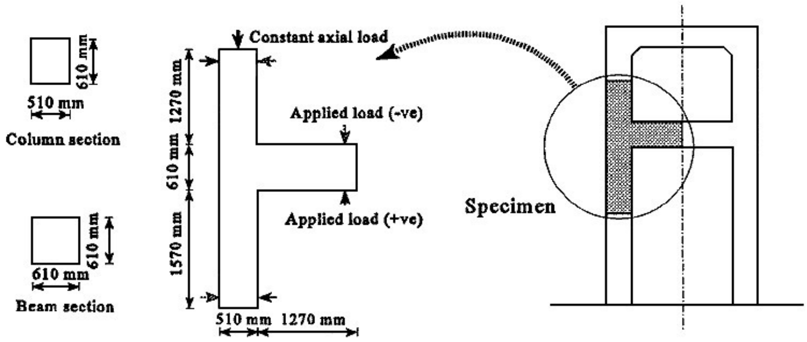

Fig. 1.5: Dimensions and loading locations of beam column joint (Ghobarah, Aziz and Biddah) [6]

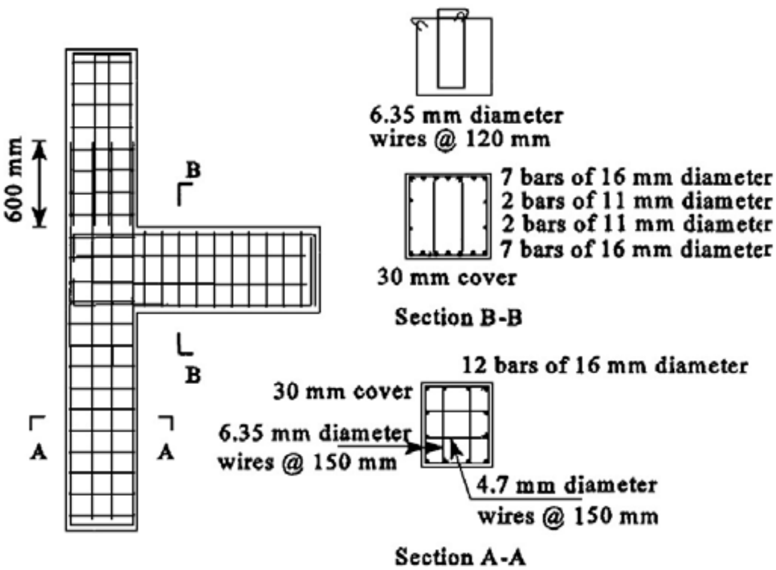

Fig. 1.6: Reinforcement placement (Ghobarah, Aziz and Biddah) [6]

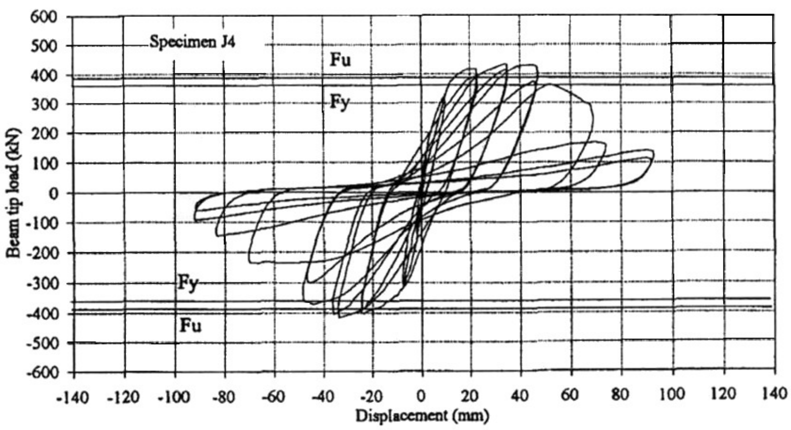

Fig. 1.7: Reverse cyclic load vs. displacement (Ghobarah, Aziz and Biddah) [6]

B Reinforced concrete frames at the University of Toronto

B.1 The Vecchio and Balopoulou frame (1990)

The study on the behaviour of reinforced concrete frames at the University of Toronto has been conducted in the last twenty years. The two most famous frames in this work field are the ones tested by Vecchio and Balopoulou in 1990 and by Vecchio and Emara in 1992. Based on these projects, Kien Vinh Duong wrote his thesis at the University of Toronto in 2006. His frame, the Duong frame established the base for the experiment in this thesis [2].

Vecchio and Balopoulou (1990) tested the parameters that cooperate to the nonlinear behaviour of RC frames. In this case, the frames where subjected to short-term loadings. These tests have been executed on a real life scaled reinforced concrete frame. Also, a research on the current formulations which predict analytically the reinforced concrete response was carried out.

The frame tested by Vecchio and Balopoulou (1990) was scaled one to one and constructed out of two columns and two horizontal beams to simulate a two-storey high reinforced concrete building. The test specimen had a width of 3500 millimetres between the axes of the two columns, and the height of one storey was captured at 2000 millimetres. The total height of the specimen including de height of the foundation and the height of the beams, was 4600 millimetres. The dimensions of the frame and the placement of the reinforcement is depicted in *Figure 1.8*. The connections between columns and beams are fixed joints and the columns are clamped on the foundation. The reinforcement anchorage of the whole structure was accomplished by welding the ends of each rebar on a steel plate. This steel plate serves as a bearing for all the rebar's, to keep the whole reinforcement of the structure in place. The concrete they used to build the frame was a concrete with a compressive strength of 29 MPa. The specimen was lab cured for three weeks and the tests on the frame were executed after a period of almost six months.

When running the tests, the experimenters applied a vertical stabilizing point load of 350 kN at the centre of the upper beam. The whole structure was monitored to understand the behaviour of the frame and the behaviour of the reinforcement. To measure the total displacement of the frame, they applied twelve linear variable displacement transducers (LVDTs). Vecchio and Balopoulou also added a speckled pattern on the frame to measure the deformations of the surfaces with a camera. In total, they executed thirty-six load stages.

When studying the test results, they mentioned that the second-order effects have a big influence on the general behaviour of the frame. The effects that were responsible for this influence were nonlinearities in the geometry, nonlinearities in the material, stiffening effects in tension, deformations due to shear, membrane action and shrinkage of the concrete. Finally, the structure failed due to a combination of crushing of the concrete at the middle of the bottom beam and yielding of the steel in the tensile zone. Another phenomenon that was observed was that hinges arose at the joints between column and beam at this bottom beam. These hinges developed just before the critical load of failing was reached. At the point of failing, the frame was subjected with a force of 517 kN. *Figure 1.9* shows the load-displacement curve of this test.

This test was executed in the year 1990, in which the testing of fully scaled reinforced concrete models was rare. Back then, they only could apply vertical forces on the structure. Therefore, this project is considered a pilot project in its field of work. Thus, to completely understand the behaviour of a reinforced concrete structure, more complex load combinations were necessary [7].

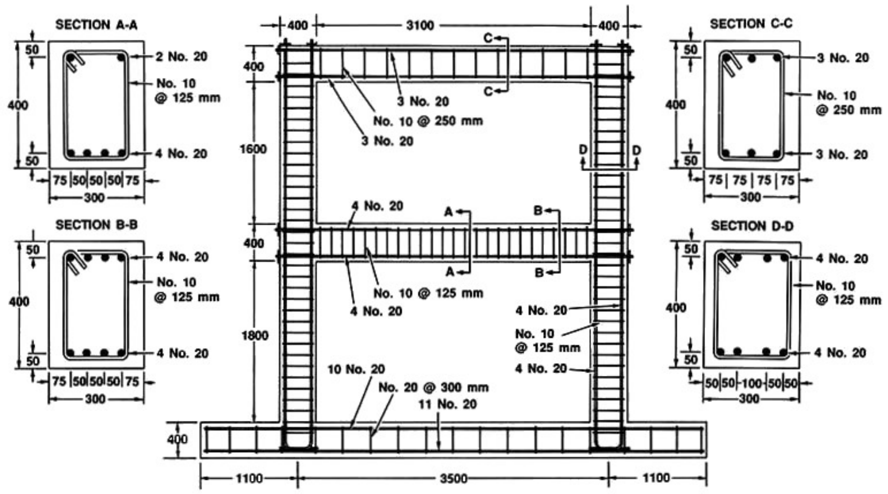

Fig. 1.8: Frame dimensions and reinforcement placement (Vecchio and Balopoulou - 1990) [7]

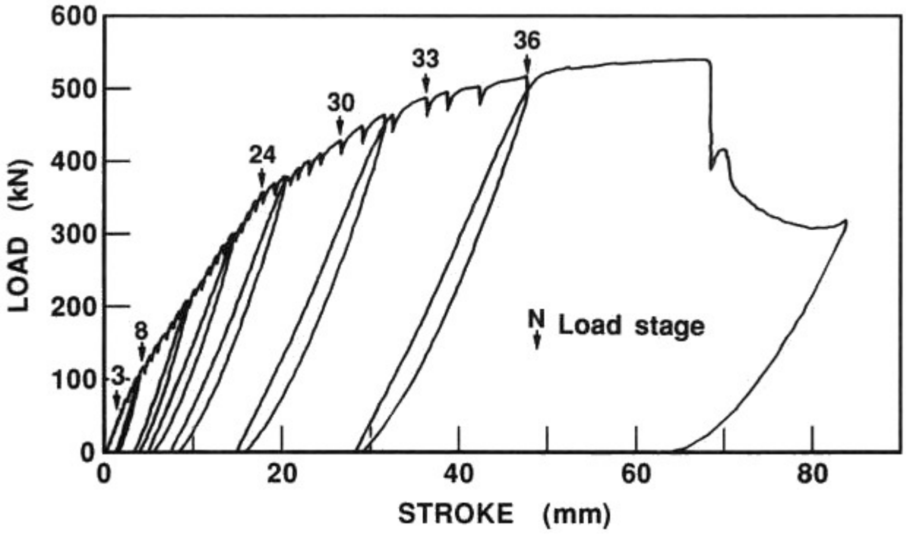

Fig. 1.9: Vertical Load vs. Vertical Displacement at the Midspan of the First Storey Beam (Vecchio and Balopoulou - 1990) [7]

B.2 The Vecchio and Emara frame (1992)

A second important study that has been carried out at the University of Toronto is the frame tested by Vecchio and Emara (1992). This test is a follow-up of the test proceeded by Vechhio and Balopoulou (1990). Vechhio and Emara aimed to investigate the influence of shear on the behaviour of a concrete structure. *Figure 1.10* shows the details of the test setup. The difference between the frame from Vecchio and Emara (1992) and the frame from Vechhio and Balopoulou (1990) is that they made another layout for the reinforcement, see *Figure 1.11*. All the other parameters, like the material properties and measurement tools, were identical between the studies.

In this test setup, the experimenters used two vertical stabilizing forces instead of one. These forces were applied on the top of each column. The value of these forces was 700 kN. These vertical forces were combined with a horizontal increasing load which was placed at the left corner of the second-storey beam. This lateral load was applied by a 1000 kN displacement-controlled actuator.

At the point of failing the frame was subjected to a lateral force of 329 kN. The frame failed at this point because there was a transition from a clamp to a hinge. These hinges arose at the left –and right side of each beam and at the base of each column. In *Figure 1.12* the lateral load-displacement of this test setup is shown. Due to this force, some shear cracks arose in the constructive elements. These shear cracks amounted 20% of the total deflection in the lateral way. The size of this influence depends on several parameters, such as the size of the loads and the geometry of the frame. The shear strains that arises due to the deflection decreases the lateral stiffness and the rigidity of the columns and beams. Besides this, the axial and rotational strains increase. When the displacement of a frame is affected by the previously mentioned second-order effects, the failure mechanism can be influenced by deflection increase.

Between 1990 and 1992 a lot of progress was made in testing and examining reinforced concrete frames. This resulted in more insight into the response of reinforced concrete frames and about the shear deflection in those frames. The frame tested by Vecchio and Emara failed due to flexure. To understand completely the effect due to shear and flexural behaviour of reinforced concrete frames, specific shear tests need to be carried out on this type of frames [8].

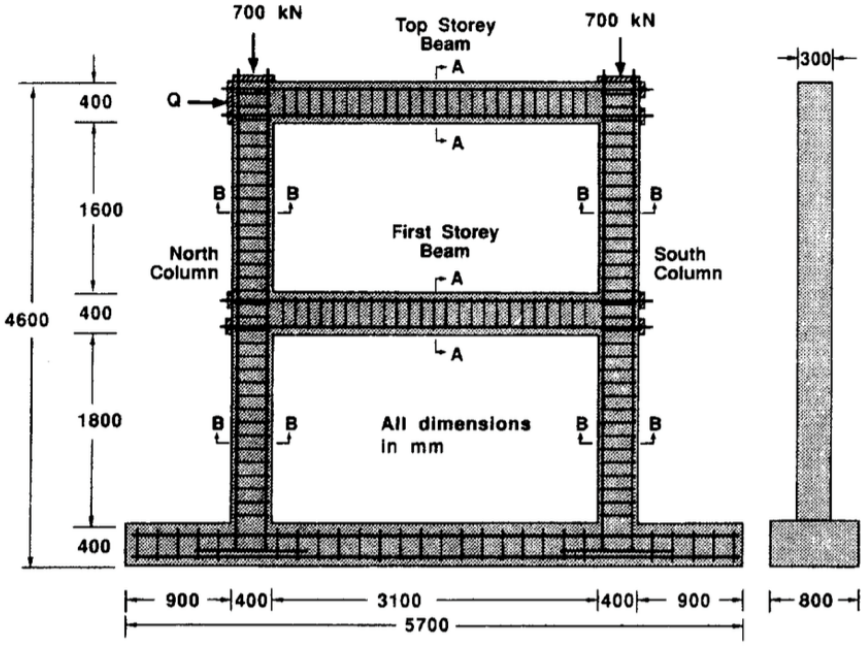

Fig. 1.10: Detail of the test setup
(Vecchio and Emara - 1992) [8]

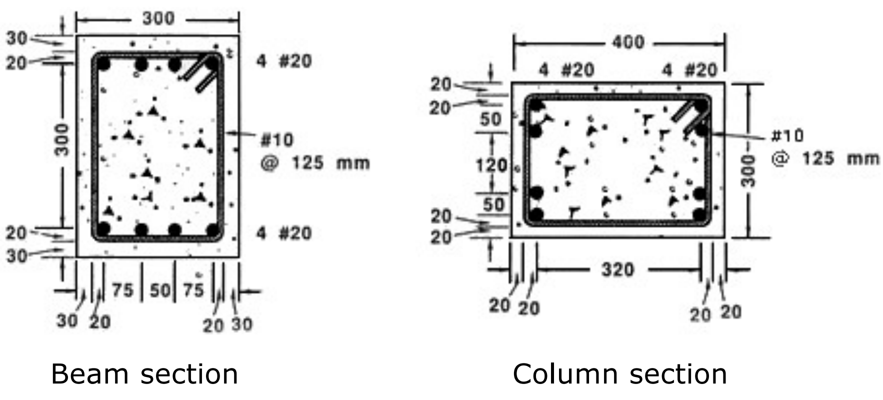

Fig. 1.11: Cross-sections of the constructive elements
(Vecchio and Emara - 1992) [8]

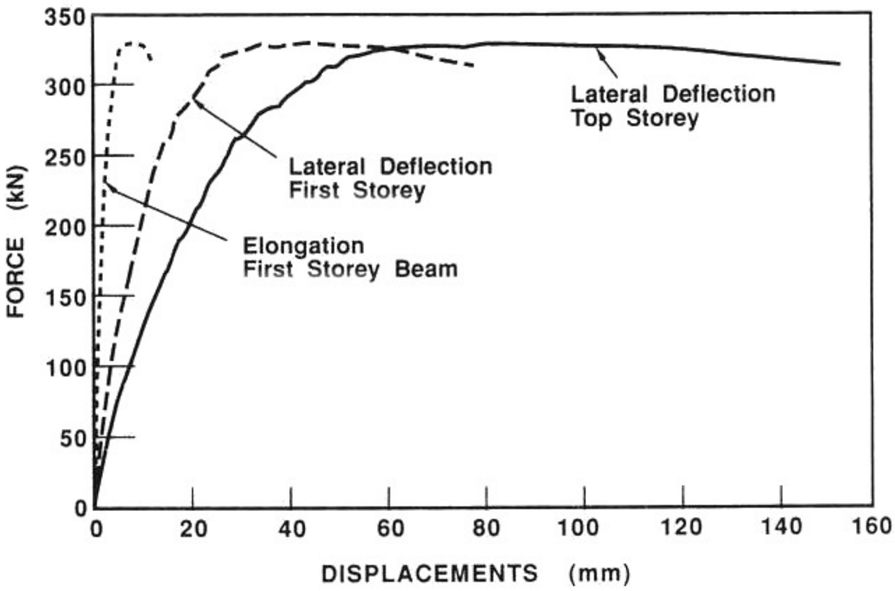

Fig. 1.12: Second-Storey Lateral Force vs. Lateral Storey Deflection (Vecchio and Emara - 1992) [8]

B.3 The Duong frame (2006)

The Duong frame forms the base for the experiment in this thesis. The Duong frame is developed by Kien Vinh Duong at the University of Toronto as part of a thesis to obtain the degree of Masters of Applied Science. The specimen is formed by a single-span, two-storey, shear-critical reinforced concrete frame with a clamped foundation. The specimen is developed and tested in the laboratories of the University of Toronto. Below the properties, the way of testing the specimen and the results are explained.

The frame which was used was also the scaled version of a real-life building frame. The scale factor in this project was two to three. The frame has a height of 4,6 meters and a width of 2,3 meters. The beams have a cross-section of 300 millimetres by 400 millimetres just like the columns. This to ensure that the columns can be fixed properly to the foundation. The base of the specimen is 4,1 meters in length, 800 millimetres wide and 400 millimetres thick. In the next stage, this foundation is fixed by a post-tensioning to the floor. The beams span a length of 1,5 meters and the height of a storey is captured at 1,7 metres. Due to these measurements, a span to depth ratio of 3,8 is obtained. This high value for the ratio caused shear failure in the beams. The concrete cover for the beams and columns is defined on 30 millimetres and 20 millimetres. The concrete cover for the foundation is 40 millimetres.

In this test setup, they used two vertical stabilizing forces. These forces were applied on the top of each column. These vertical forces were combined with a horizontal increasing load which was placed at the left corner of the second-storey beam. Due to this lateral force, there arise high bending stresses at the bottom of the columns. To prevent those stresses in those zones, an extra reinforcement layer is added. The table below gives an overview of the used parameters in the frame. *Figures 1.13, 1.14* and *1.15* show the dimensions of the structure and the dimensions and placement of the reinforcement for each cross-section of each member [2].

Table 1.1: Cross-section details of constructive frame elements [2]

Member	b (mm)	h (mm)	Bottom steel	Top steel	Stirrup	ρx (%)	ρy (%)
Beam	300	400	4Ø20	4Ø20	Ø9,5 at 300	1,143	0,158
Column	300	400	4Ø20	4Ø20	Ø10 at 130	1,111	1,018
Column top	300	400	8Ø20	4Ø20	Ø10 at 130	1,111 or 2,39	1,018
Column base	300	400	8Ø20	8Ø20	Ø10 at 130	2,39	1,018
Foundation	800	400	8Ø20	8Ø20	Ø10 at 175	0,857	0,429

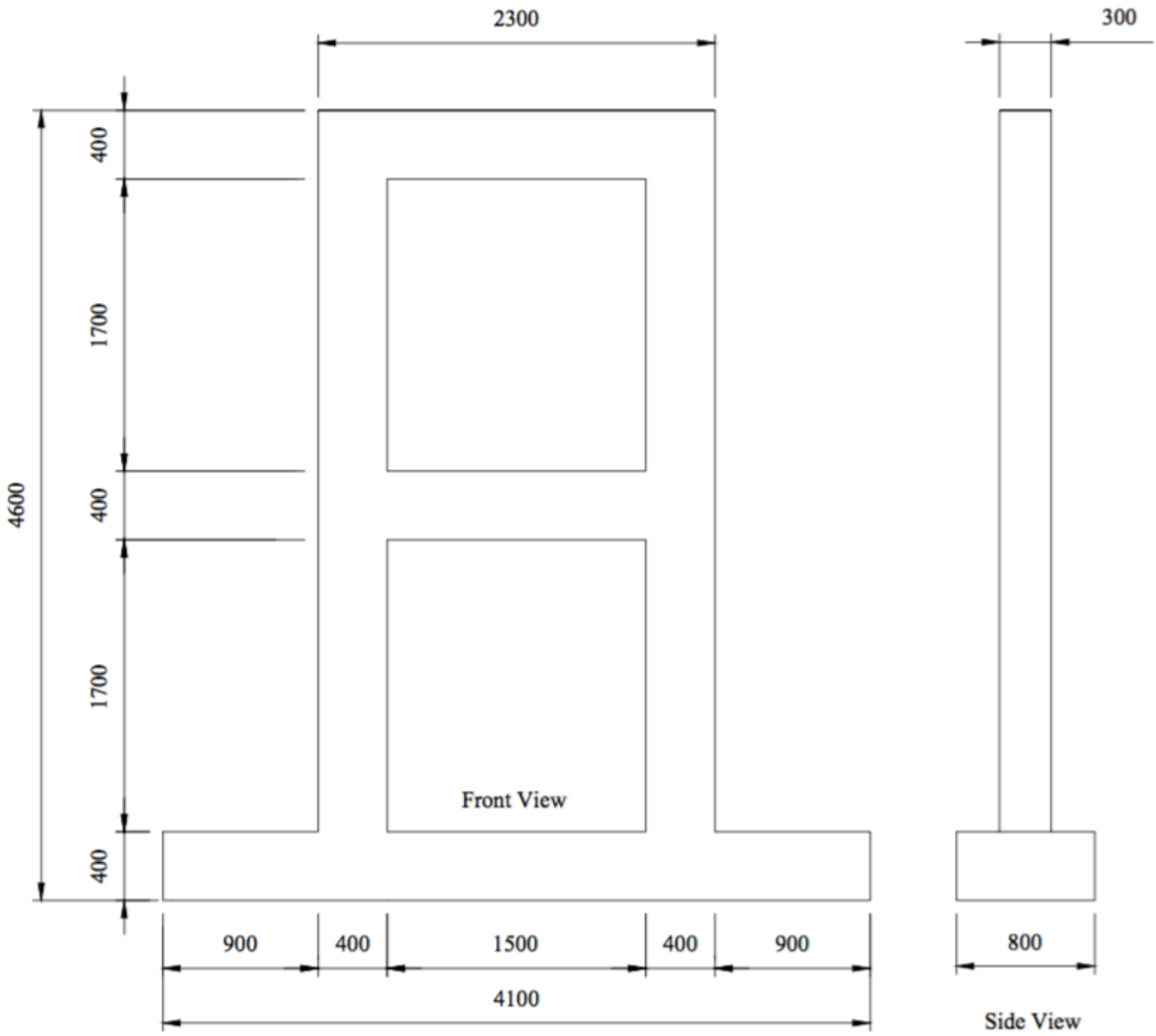

Fig. 1.13: Frame dimensions in millimetres (Duong - 2006) [2]

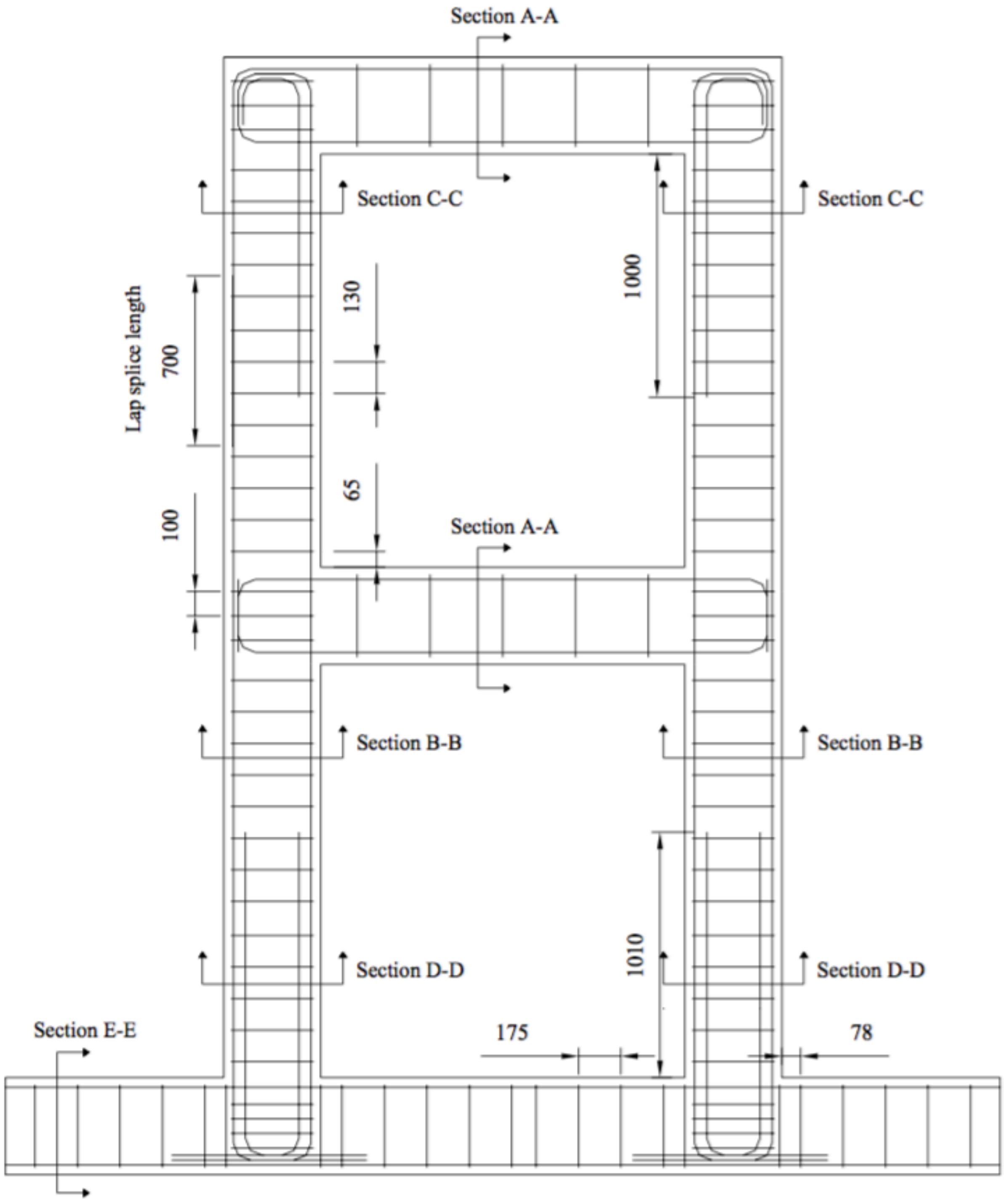

Fig. 1.14: Frame reinforcement placement (Duong - 2006) [2]

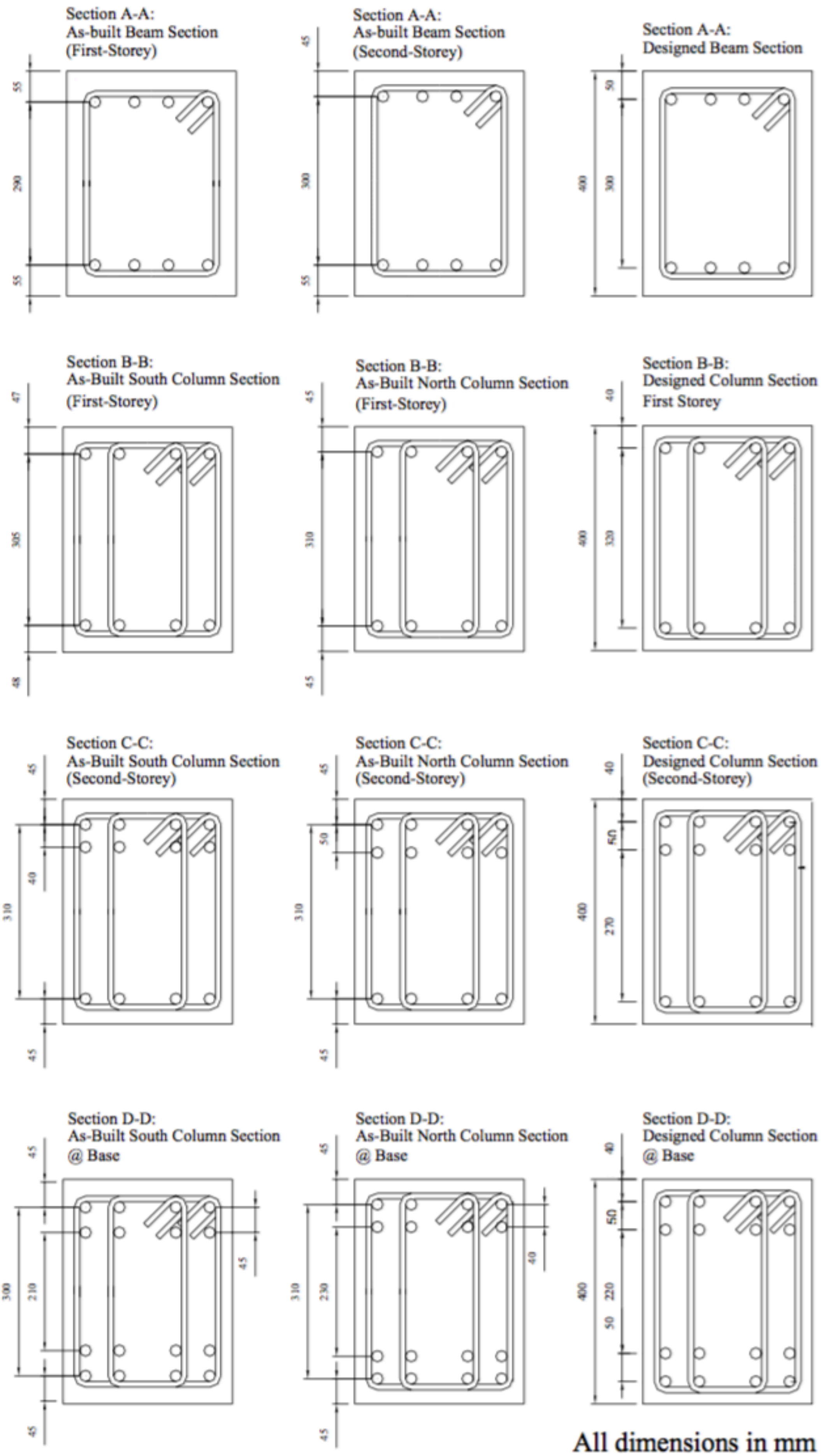

Fig. 1.15: Cross-section constructive members (Duong - 2006) [2]

The concrete strength, which was specified to build the specimen, should have had a compressive strength of 20 MPa after 28 days. In reality, this concrete had a compressive strength of 30 MPa after 28 days. This extra strength of 10 MPa is a safety margin prescribed by the cement manufacturers. The slump of the concrete was 75 millimetres and the largest dimensions of the granulates were 10 millimetres. The compressive strength on the test cylinders are shown in *Table 1.2*. The cylinders were subjected to lab cured conditions, or moist cured conditions, and the moist cured cylinders were only tested at 28 days [2].

Table 1.2: Compressive strength tests [2]

Casting days	**f'c (MPa) lab cured**	**f'c (MPa) moist cured**	**f'r (MPa) lab cured**	**f'r (MPa) moist cured**
8	21,3			
28	34,4	35,1	3,33	5,69
9 months (test)	42,9			

The properties of the different sizes of reinforcing bars are listed in *Table 1.3*. The results for the tensile strength of the used reinforcement diameters 9,5; 10 and 20 are listed in *Table 1.4*. All these values mentioned above and below are used to build the numerical model. This numerical method is further illustrated in the following chapters [2].

Table 1.3: Reinforcement details [2]

Bar size	**Nominal diameter (mm)**	**Area cross-section (mm^2)**	**Location in specimen**
$\emptyset 9,5$	9,5	71	Transversal (Column + base)
$\emptyset 10$	10	100	Longitudinal
$\emptyset 20$	20	300	Transversal (beam)

Table 1.4: Reinforcement properties [2]

Bar size	**Sample**	$\varepsilon y\ (x10^{-3})$	$\varepsilon sh\ (x10^{-3})$	**fy (MPa)**	**fu (MPa)**	**E (MPa)**	**Esh (MPa)**
$\emptyset 9,5$	Mean	2,41	28,3	506	615	210000	1025
$\emptyset 10$	Mean	2,38	22,8	455	583	192400	1195
$\emptyset 20$	Mean	2,25	17,1	447	603	198400	1372

To obtain data from these tests, Duong used three types of measurement tools. The first type is the strain gauges. Those gauges are monitoring the steel deformation during tests. The deformation of the whole portal is measured by a total of thirty-six strain gauges. This way of testing is mentioned in *Figure 1.16*.

The second type is the Zurich gauge. These gauges are small metal studs that were attached to the concrete surface of the portal to measure the strains in this concrete surface. Surface strains were registered after each load step by measuring the relative movement between the points. As well in the horizontal and vertical way as well diagonal. This test setup is given by *Figure 1.17*.

The last type is the LVDTs (Linear variable differential transducers). These were placed on several places on the frame to measure lateral and vertical deflections, as well as any possible base slip and out-of-plane movement. Those deflections and movements were measured by a total of seventeen LVDTs. This test setup is given by *Figure 1.18* [2].

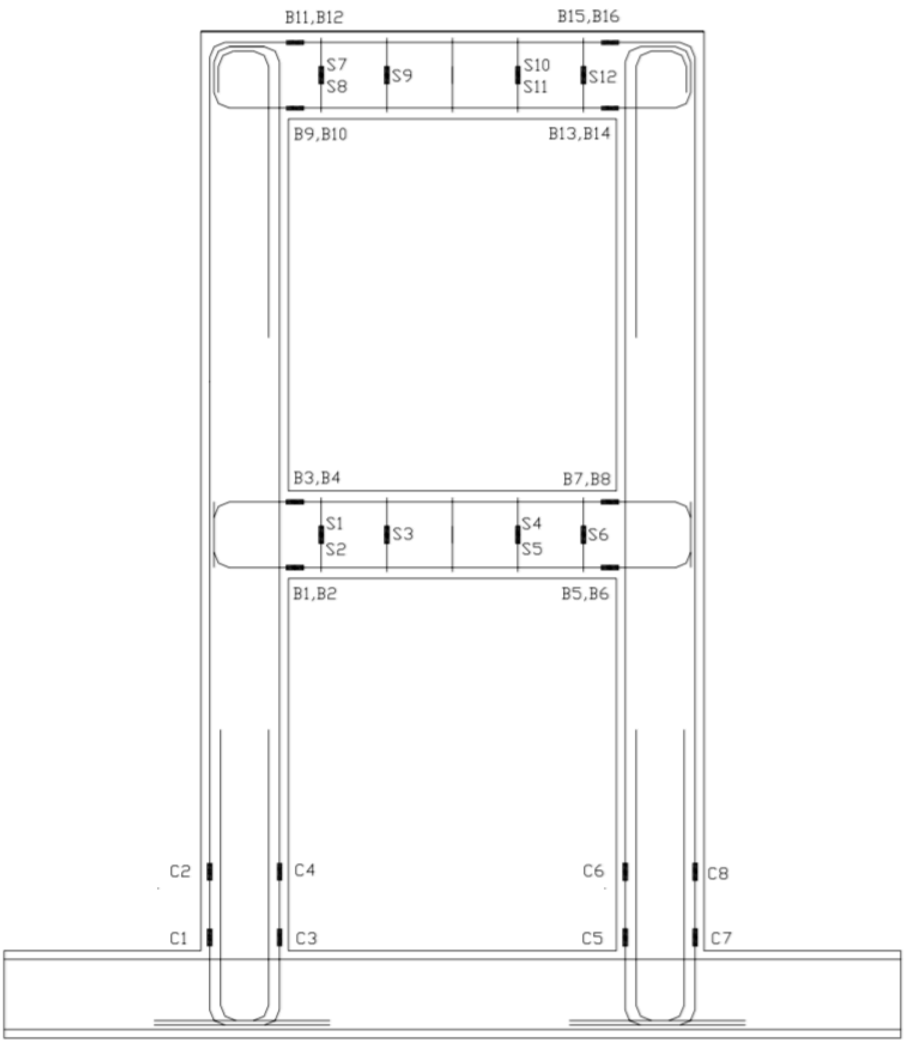

Fig. 1.16: Layout of the steel strain gauges (Duong - 2006) [2]

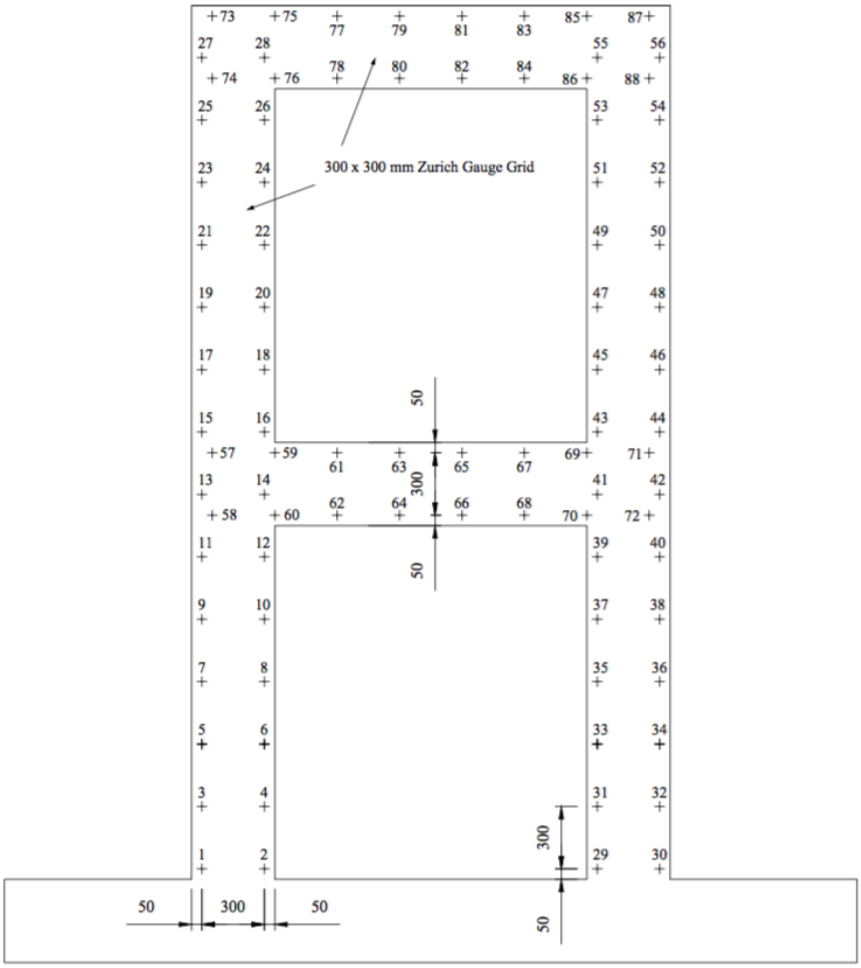

Fig. 1.17: Layout of Zurich gauges (Duong - 2006) [2]

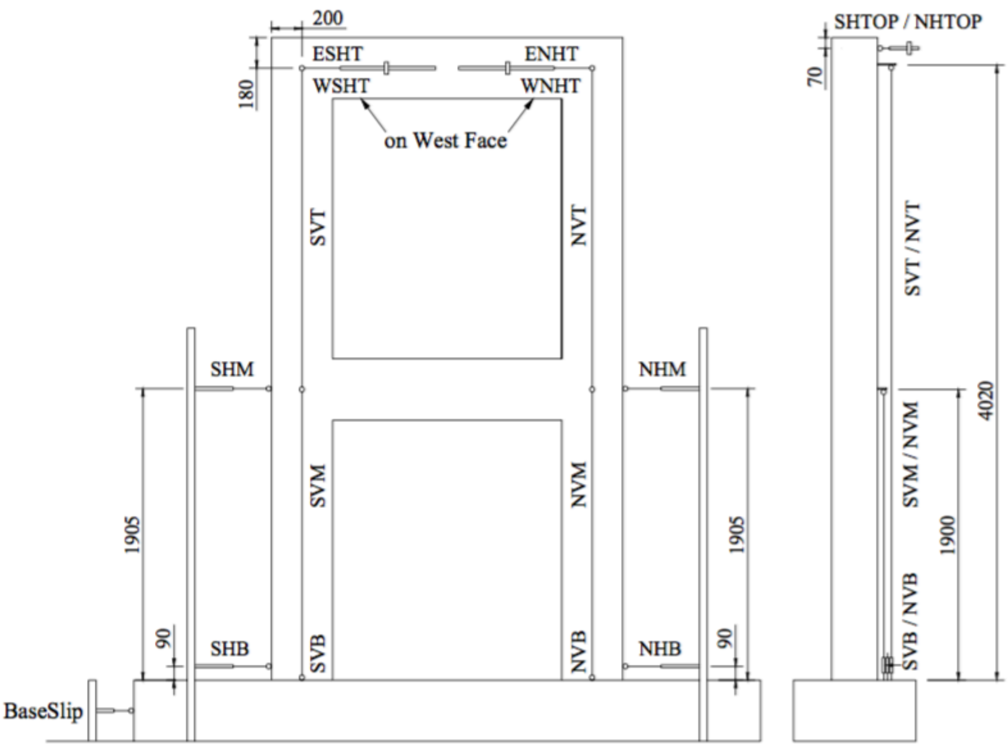

Fig. 1.18: Layout of the LVDTs (Duong - 2006) [2]

As mentioned before, two vertical stabilizing forces were used. These forces were applied on the top of each column. The value of these forces was 420 kN and were sustained during the entire test. Those vertical forces were combined with a horizontal increasing load, which was placed at the left corner of the second-storey beam. This force was implement in displacement-controlled situation. At the load steps in the beginning, the horizontal force was a constant force, however, at the loads steps later in the procedure, these were decreased to 80% as a safety margin. The load steps for the forward half-cycle are summarized in the table below. *Figure 1.19* shows the load displacement curve for the second storey beam [2].

Table 1.5: Load steps [2]

Load step	Load (kN)	Lateral displacement (mm)
	FORWARD HALF-CYCLE	
0	0	0
1	25	1,13
2	50	2,23
3	75	2,65
4	99	4,13
5	125	5,46
6	150	8,56
7	175	10,07
8	197	11,70
9	221	13,80
10	250	19,98
11	275	23,78
12	295	25,50
13	320	30,00
14	325	32,30
15	327	44,70

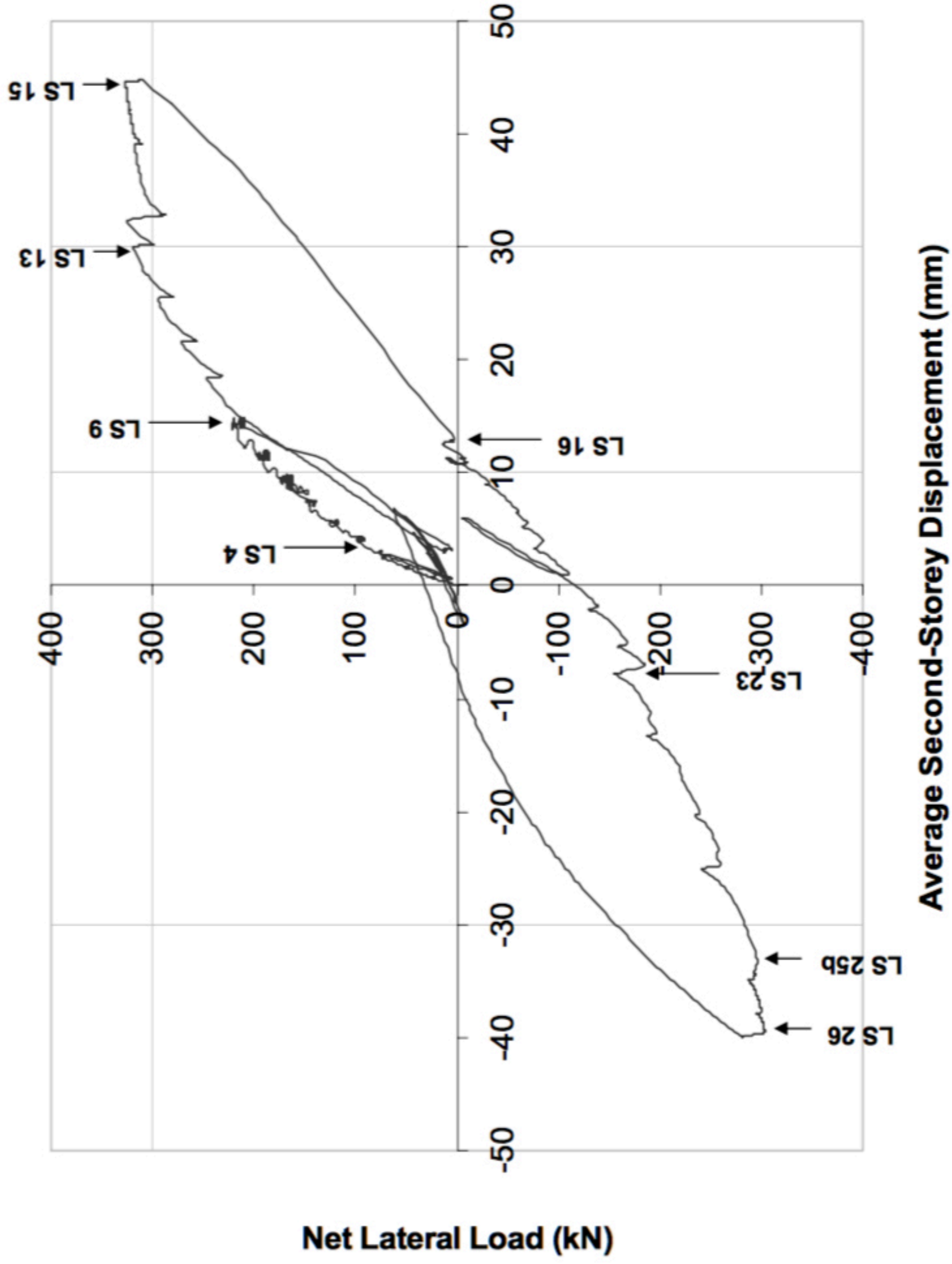

Fig. 1.19: Load displacement second storey beam (Duong - 2006) [2]

1.2 The similitude theory (scaling laws)

1.2.1 Background

Every new design is subjected to several investigations like theoretical analyses and experimental investigations before it is produced. For complicated systems, mathematical models are usually formulated to understand the model properly. This is necessary to evaluate the models' reliability and – performance. Most of these physical experiments are associated with destruction of the test specimens, whereby a lot of specimens are needed.

For civil constructions like bridges, dams and tall buildings, but also for large systems, like airplanes and space crafts, testing of the prototype (scale 1:1) is impossible. Even when it is possible to test a prototype it will not be executed due to the high costs, the long testing time and the difficult manageable conditions. For this reason, it is valuable to executed the tests on a similar scaled model. This is much more workable. The only possible way to gather experimental data of the performance of the system and the interaction between the internal elements is to design a similar scaled model with the same behaviour as the prototype. The reliability of the prototype's behaviour is dependent on the relationship between the interrelated parameters and variables of the scaled model and the prototype.

In similar systems, it is necessary that the proper system parameters are identical and these systems are directed by a set of characteristic equations. So, an equitation or variable is valid for all the systems with the same similarity conditions. Each model variable is related to the corresponding prototype variable. This ratio is called scale-factor and has a crucial role in predicting the link between the model and the prototype.

Models have already been used for years as a tool. Rayleigh was the first to discuss the specific use of models in a scientific way, based on geometrical analysis. The usability of the similitude theory was first discussed by Goodier and Thompson in 1944. They searched for a systematic method for establishing similarity based on geometric analysis.

Establishing this similarity can divided into two procedures. In the first procedure, the similarity conditions can be established out of the field equations or out the dimensional analysis. In the second procedure, all the parameters and variables that influence the behaviour of the system should be known. So, similarity is a link between a prototype and a model and can be used to extrapolate the gathered data of a much cheaper scaled model to predict the behaviour of the prototype [9].

As mentioned before, Rayleigh was in 1915 the first researcher in history that discussed the dimensional analysis or similitude from small scaled models. Based on Fourier's work he found the main principals of the dimensional analysis. In a later period, this theory of Rayleigh is several times studied and completed by other researchers like Bickhoff, Bridgman, Buckingham, Langhaar and Riabouchinsky. [9]

The usability of the similitude theory was first discussed by Goodier and Thompson in 1944 and in 1955 by Goodier. In this period of history (1950 – 1970) a lot of interesting literature is written about this subject by researchers as Murphy (1950), Langhaar (1951), Sedov (1959), Kline (1965) and Skoglund (1967). Most of those authors described the concept of similarity as a geometrical analysis. Only Kline (1965) involved the characteristic equations into geometrical analysis [10].

Many studies on static –and dynamic behaviour of structural systems like reinforced concrete structures have been executed. For instance, Krawinkler (1978) described for instance the dynamic earthquake resistance of reinforced concrete models. The growth of testing on scaled models is arose since reinforced composite components need to elaborate experimental interpretations.

In contemporary times, due to large dimensions and difficult structural design solutions, testing on small scaled models in association with the similitude theory has become a rare solution to gather experimental data. The studies which were mentioned above used the complete similarity between the prototype and the model in their theories. The objectives in their investigations were:

- to search two methods of similarity;
- to obtain similar conditions to create and build an accurate distorted model;
- to evaluate analytically the obtained similar conditions and to adapt the experimental data of the prototype to the predictions of the scaled model [11].

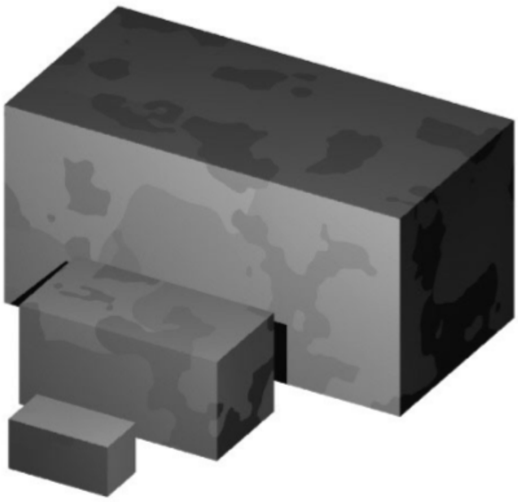

Fig. 1.20: Similar shapes due to geometrical similitude [12]

1.2.2 Theory of similitude

This chapter describes the concepts and foundations of the similitude theory. The concept will be explained and two important methods to use this similarity conditions are described.

The similitude theory develops important and necessary conditions between two phenomena's in the field of similarity. This similarity between systems provides researchers with the ability to predict the behaviour of one system by the results of an already investigated second system. Similitude between those systems means a similarity in behaviour in some particular forms. In other words, if one knows how a system reacts to an input, it is possible to predict the response of a similar system.

The essential similitude theory for obtaining dimensional similarity for plane geometrical figures is developed by Euclid. This means that when the dimensions of a figure are contracted or enlarged with a ratio (=scale –or similarity factor), a new figure is developed and this one is similar to the original one.

The behaviour of a system is determined by several parameters, for instance dynamic –and energy characteristics, geometry and material behaviour. Each system can be designed in a mathematical way by parameters and variables. In this case, it should be noted that the prototype and the model are two different systems, whereby the parameters and variables are also different. The set-up of the similitude theory is to transform the mathematical model of the scaled model into the mathematical model of the prototype. This is done through bi-unique mapping or vice versa. This means that if the vector X_m the unique vector is of the model and X_p the unique vector is of the prototype the next transformation matrix Δ can be find between the two systems so that:

$$Xm = \Delta^{-1} Xp \quad \text{or} \quad Xp = \Delta\, Xm \tag{1.1}$$

Vector X contains all the parameters and variables of the system. Transforming the matrix Δ in the diagonal way is the simplest way of transformation. The diagonal of the matrix Δ represents the scale factors of the vector X.

$$\Delta = \begin{matrix} \lambda_{x1} & 0 & 0 \\ 0 & \lambda_{x2} & 0 \\ 0 & 0 & \lambda_{xn} \end{matrix} \tag{1.2}$$

In this matrix is the scale factor X_i given by $\lambda_{xi} = \frac{X_{ip}}{X_{im}}$. The similitude theory can be used in a lot of different ways to investigate a particular system. Most of the times the geometrical similarity is combined with the characteristic equations to obtain the similarity between two systems [13].

A Dimensional analysis

The main objective of dimensional analysis is to lower the number of parameters and variables by developing groups of parameters and variables ($\pi - \text{terms}$). As a result, all those terms become self-reliant and dimensionless.

Rayleigh developed the main principles of this dimensional analysis, derived from the work from Fourier, where after those principles were proved by Riabouchinsky. Out of those theorems, Buckingham did a reformulation of them. After that there followed a discussion of the theorems by Brand, Brickhoff, Bridgman, Langhaar and Van Driest and they were called the Buckingham's $\pi - \text{Theorems}$.

Those $\pi - \text{Theorems}$ allowing a reduction of *n* variables into a set of *n* - *r* dimensionless $\pi - \text{terms}$. The parameter *r* represents the grade of the matrix.

$$\phi(x_1, x_2, x_3, \dots, x_n) = 0 \quad \text{or} \quad \phi(\pi_1, \pi_2, \pi_3, \dots, \pi_{n-r}) = 0 \tag{1.3}$$

In this equation is Φ the functional relation but it is not necessary that this function is a known function for the system. It only gives the downsized form of the related variables. Each system can be described by several combinations of amounts like for instance time (t), force (F), length (L), mass (M) but also second-rated amounts like area (A), stress (σ) and velocity (v).

First, the characteristic quantities need to be selected. After that the system variables can be described. It should be mentioned that it is very important that all the obvious parameters, like for example gravity (g), etcetera, are included in the equations, because otherwise the analysis gives an unrealistic and wrong output.

Through time several dimensional analysis methods have been developed, such as the Rayleigh method, the Buckingham method, the Basic Stepwise method, the Echlon Matrix method, and the Proportionalities method.

To illustrate, consider an easy supported beam with a spring support in the middle whose buckling load need to be find. The configuration is given in *Figure 1.21*. The main variables are given in *Table 1.6* [14].

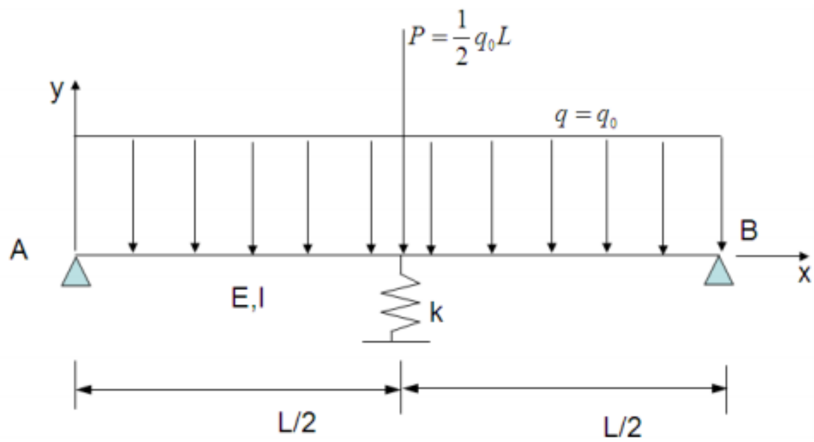

Fig. 1.21: Easy supported beam [14]

Table 1.6: Main variables for the configuration out Figure 21

Variable	Dimension
Deflection (w)	L
Span (L)	L
Modulus of elasticity (E)	$F\,L^{-2}$
Moment of inertia (I)	L^4
Spring stiffness (k)	$F\,L^{-1}$
Axial load (P)	F

$$\phi(w, L, E, I, k, P) = 0 \tag{1.4}$$

The dimensional matrix and related $\pi - \mathrm{terms}$ are given by:

$$\begin{array}{c|cccccc} & L & E & w & I & k & P \\ \hline L & 1 & -2 & 1 & 4 & -1 & 0 \\ F & 0 & 1 & 0 & 0 & 1 & 1 \end{array} \Rightarrow \begin{array}{c|cccccc} & L & E & w & I & k & P \\ \hline L & 1 & 0 & 1 & 4 & 1 & 2 \\ E & 0 & 1 & 0 & 0 & 1 & 1 \end{array} \tag{1.5}$$

$$\pi_1 = \frac{w}{L}, \quad \pi_2 = \frac{I}{L^4}, \quad \pi_3 = \frac{k}{LE}, \quad \pi_4 = \frac{P}{EL^2}$$

A not specific set of π – terms is calculated by applying a dimensional analysis method. This is not a specific set because other combinations of the variables are also possible. Some variables are much easier to control then other variables whereby it is designated to use the easiest variables in the analysis. π – Terms to the power or a product of two π – terms is also possible and the results of these are also non-dimensional. The final result of the π – terms is equal to

$$\phi(\pi_1, \pi_2, \pi_3, \pi_4) = 0 \tag{1.6}$$

It is also possible to write an independent variable in function of the other variables:

$$\pi_1 = \phi(\pi_2, \pi_3, \pi_4) \tag{1.7}$$

The purpose of π – terms is that because of the similarity between two systems, the equations of those systems are also similar or the same. This means that $\phi_1 = \phi_2$ even when the specific equations of the systems are not known exactly. This equality between the two π – terms of the two systems are called the similarity conditions or scaling laws between them and also for other specific phenomenon's.

$$\pi_{1p} = \phi_p(\pi_{2p}, \pi_{3p}, \pi_{4p}) \quad , \quad \pi_{1m} = \phi_m(\pi_{2m}, \pi_{3m}, \pi_{4m}) \tag{1.8}$$

$$\text{If} \quad \pi_{im} = \pi_{ip} \quad \text{for} \quad i = 2, 3, 4 \quad \text{then}$$

$$\phi_p(\pi_{2p}, \pi_{3p}, \pi_{4p}) = \phi_m(\pi_{2m}, \pi_{3m}, \pi_{4m})$$

$$\pi_{1m} = \pi_{1p}$$

The above described π – terms define relationships between dynamic -, geometric -, kinematic – and material variables of the two systems [15].

B Direct use of the applicable equations

A system with convenient boundary conditions determines the systems behaviour by its variables and parameters. The defining variables are in this case a function of the undefined variables. If under transformation Δ and Δ^{-1}, the convenient equations from the prototype and the scaled version of it are similar, there is a similarity between the two systems. This is also demonstrated by *equation (1.1)*. This conversion gives us the scaling laws between all the variables but also between the input and the output of the two systems.

Consider again the easy supported beam with a spring support in the middle *(Figure 1.21)*. The reaction of this spring support is equal to $k\delta$, where δ is the deflection at the centre of the beam. Because of the symmetrical system, the reaction force at $0 \leq x \leq L/2$ is equal to $k\delta/2$. The corresponding equation becomes:

$$EI_{w,xx} + P\omega = \frac{k\delta\omega}{2} \tag{1.9}$$

$$\omega(0) = 0$$
$$\omega_x(L/2) = 0$$
$$\omega(L/2) = \delta$$

For the prototype and the scaled models this becomes:

$$E_p I_P \frac{d^2\omega_p}{dx_p^2} + P_p\omega_p = \frac{k_p\delta_p\omega_p}{2} \tag{1.10}$$
$$E_m I_m \frac{d^2\omega_m}{dx_m^2} + P_m\omega_m = \frac{k_m\delta_m\omega_m}{2}$$

The scale factor between the prototype and the model can be defined by λ_i. Because of this, the variables of the systems become $x_{ip} = \lambda_{xi} \,.\, x_{im}$. The similarity between the prototype and the model are defined by replacement of $\lambda_{xi} \,.\, x_{im}$ into the differential equation of the prototype. This differential equation equals the differential equation of the model *(equation 1.10)*.

$$\left(\frac{\lambda_E\lambda_I\lambda_\omega}{\lambda_x^2}\right) E_m I_m \frac{d^2\omega_m}{dx_m^2} + (\lambda_P\lambda_\omega)\, P_m\omega_m = (\lambda_k\lambda_\delta\lambda_\omega)\, \frac{k_m\delta_m\omega_m}{2} \tag{1.11}$$

Equation (1.10) is equal to *equation (1.11)* if:

$$\left(\frac{\lambda_E\lambda_I\lambda_\omega}{\lambda_x^2}\right) = (\lambda_P\lambda_\omega) = (\lambda_k\lambda_\delta\lambda_\omega) \tag{1.12}$$

Using one of these terms to divide *equation (1.12)* gives (first term):

$$1 = \frac{\lambda_P\lambda_x^2}{\lambda_E\lambda_I} = \frac{\lambda_k\lambda_\delta\lambda_x^{\,2}}{\lambda_E\lambda_I} \tag{1.13}$$

or:

$$1 = \frac{\lambda_P\lambda_x^2}{\lambda_E\lambda_I} \qquad or \qquad \lambda_p = \lambda_x^{-2}\lambda_E\lambda_I \tag{1.14}$$

and:

$$1 = \frac{\lambda_k\lambda_\delta\lambda_x^{\,2}}{\lambda_E\lambda_I} \qquad or \qquad \lambda_k\lambda_\delta\lambda_x^{\,2} = \lambda_E\lambda_I \tag{1.15}$$

and for the boundary conditions:

$$\frac{\lambda_w}{\lambda_\delta} = 1 \qquad or \qquad \lambda_w = \lambda_\delta \tag{1.16}$$

The *equations 1.14, 1.15* and 1*.16* are showing the conditions between the prototype and the model for complete similarity. There are seven unknown λ's related to three relationships. This means that four λ's can be chosen, and the other three unknown variables can be determined with the *equations* 1*.14, 1.15* and 1*.16* [15].

1.2.3 Partial similarity and deformed model

Two systems are similar when the similarity conditions between them are fulfilled or when the before mentioned $\pi - \text{terms}$ from the prototype and the model are the same. Complete similarity, however, is often not achieved. When a model has some small differences, it is called a distorted or deformed model.

In the case of complete similarity, the $\pi - \text{terms}$ are $\pi_{im} = \pi_{ip}$ with $\text{i} = 1, \dots, \text{N}$ and for not complete fulfilled similarity the $\pi - \text{terms}$ are $\pi_{im} = \pi_{ip}$ with $\text{i} = 1, \dots, \text{k}$ with $\text{k} < \text{N}$. These small similarity differences cause a difference in model behaviour between the prototype and the model. It is necessary to understand these small differences to modify the output data of the tests from the model and to be more precise in predicting the behaviour of the prototype.

A Dimensional analysis

Dimensional analysis means that the similarity between $\pi - \text{terms}$ of the prototype and $\pi - \text{terms}$ of the model are related to the variables' scale factor. For instance, when there are m-r $\pi - \text{terms}$, there will be m-r functions, with the result that there will be m scale factors. When two systems are completely similar, the dimensional matrix r determines the number of scale factors which can be chosen. *Table 1.7* gives an overview of the interpretation between complete –and not complete similarity.

Table 1.7: Complete similarity versus not complete similarity

Complete Similarity	Not complete similarity
$\pi_{1m} = \pi_{1p}$	$\pi_{1m} = \pi_{1p}$
$\pi_{2m} = \pi_{2p}$	$\pi_{2m} = \pi_{2p}$
…	…
$\pi_{km} = \pi_{1p}$	$\pi_{km} = \pi_{kp}$
$\pi_{k+1m} = \pi_{k+1p}$	$\pi_{k+1m} \neq \pi_{k+1p}$
…	…
$\pi_{nm} = \pi_{np}$	$\pi_{nm} \neq \pi_{np}$

In case of a deformed model, the scale factors related to their $\pi - \text{terms}$ can change due to a difference in equality. Consequently, a difference in $\pi - \text{terms}$ can occur, resulting in more unknown scale factors then that there are similarity equations. Thus, extra variables are necessary. These should be searched by the general equations of a systems like there are equations related to the boundary conditions, the behaviour of the material, the compatibility, etcetera. To obtain those extra variables by extra equations, additional tests should be carried out to gather more data to solve the systems [16].

B Direct use of the applicable equations

When general equations of the system are used to obtain conditions of similarity, the relationship between those variables are constrained by these general equations. For instance, a system has *m* variables and due to the similarity conditions of the general equations there are defined *n* relationships according to m unknown scale factors related to those variables.

When the two systems share a complete similarity, m – n scale factors can be chosen. The remaining scale factors can be found by n conditions of similarity. When, for example, one condition cannot be fulfilled, 'not complete similarity' is achieved. Each variable has his own influence on the systems' behaviour, whereby also the final result of the similarity conditions gives a different result or influence. When the influence of each variable is known, it is allowed and possible to neglect the variables with the lowest influence, without a failing of the system [17].

To give an example, suppose a large rectangular plate that is easy supported at the edges and subjected with a uniform load q. The cross-section of the configuration consists out of an isotropic material and the general differential equation is given by *equation (1.17)*. The configuration is given in *Figure 1.22* [18].

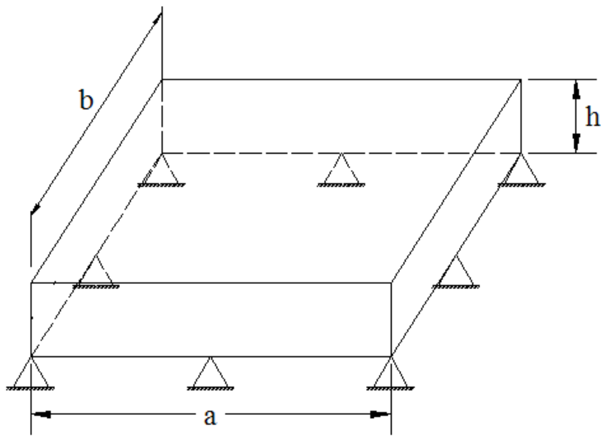

Fig. 1.22: Easy supported rectangular plate

$$\frac{d^4\omega}{dx^4} + 2\,\frac{d^4\omega}{dx^2dy^2} + \frac{d^4\omega}{dy^4} = \frac{q}{D} \tag{1.17}$$

and B.C at $x = 0,\ a$:

$$\omega = 0 \tag{1.18}$$

$$M_x = -D\,\frac{d^2\omega}{dx^2} = 0 \tag{1.19}$$

and at $y = 0,\ b$:

$$\omega = 0 \tag{1.20}$$

$$M_y = -D\,\frac{d^2\omega}{dy^2} = 0 \tag{1.21}$$

and similitude gives:

$$\frac{\lambda_\omega}{\lambda_x^4} = \frac{\lambda_\omega}{\lambda_x^2\,\lambda_y^2} = \frac{\lambda_\omega}{\lambda_y^4} = \frac{\lambda_q}{\lambda_D} \tag{1.22}$$

To find the scaling laws out of *equation (1.22)* there are three possibilities. Firstly, it is possible to divide *equation (1.22)* by the yield of the first term:

$$\lambda_x = \lambda_y \quad , \quad \lambda_\omega = \frac{\lambda_q\,\lambda_x^4}{\lambda_D} \tag{1.23}$$

Or to divide *equation (1.22)* by the yield of the second term:

$$\lambda_x = \lambda_y \quad , \quad \lambda_\omega = \frac{\lambda_q\,\lambda_x^2\,\lambda_y^2}{\lambda_D} \tag{1.24}$$

And finally, by dividing *equation (1.22)* by the yield of the third term:

$$\lambda_x = \lambda_y \quad , \quad \lambda_\omega = \frac{\lambda_q\,\lambda_y^4}{\lambda_D} \tag{1.25}$$

From these three equations (*(1.23), (1.24), (1.25)*) the most sufficient equation needs to be chosen. This is the equation that predicts the behaviour of the prototype the most precise by comparing the theoretical deflection of the model with the theoretical deflection of the prototype. The three equations give the same results in case of a complete similarity between the two systems. To avoid an unrealistic size for the cross-section of the configuration, different scale factors for each direction (x, y, z) need to be chosen [18].

If $\lambda_y = C.\lambda_x$ and $C > 0$, the *equations (1.23), (1.24)* and *(1.25)* become:

$$\lambda_\omega = \frac{\lambda_q\,\lambda_x^4}{\lambda_D} = \bar{C}\,\frac{\lambda_q\,\lambda_x^4}{\lambda_D} \quad , \quad \bar{C} = 1 \tag{1.26}$$

$$\lambda_\omega = \frac{\lambda_q\,\lambda_x^2\,\lambda_y^2}{\lambda_D} = \bar{C}\,\frac{\lambda_q\,\lambda_x^4}{\lambda_D} \quad , \quad \bar{C} = C^2 \tag{1.27}$$

$$\lambda_\omega = \frac{\lambda_q\,\lambda_y^4}{\lambda_D} = \bar{C}\,\frac{\lambda_q\,\lambda_x^4}{\lambda_D} \quad , \quad \bar{C} = C^4 \tag{1.28}$$

Out of these three equations (*(1.26), (1.27), (1.28)*) the most sufficient equation needs to be chosen. This is the equation who predicts the behaviour of the prototype the most proper by comparing the theoretical deflection of the model with the theoretical deflection of the prototype. Thus, for the prototype there are three possibilities:

- Inverse rectangular $\frac{a}{b} < 1$
- Square $\frac{a}{b} = 1$
- Rectangular $\frac{a}{b} > 1$

Based on the scale factors were the characteristics of the model calculated. The theoretical deflection of the prototype and the model are also determined with the scale factors and is given by Timoshenko:

$$\omega = \frac{16\, q_0}{\pi^6\, D} \sum_{m=1}^{\infty} \sum_{n=1}^{\infty} \frac{\sin \frac{m\pi x}{a} \,.\, \sin \frac{n\pi y}{b}}{mn \left[\left(\frac{m}{a}\right)^2 + \left(\frac{n}{b}\right)^2 \right]^2} \tag{1.29}$$

By using *equations (1.26), (1.27), (1.28)* the model data is transformed to predict the prototype behaviour. Next, a comparison between the predicted deflection and the theoretical deflection of the prototype is made. Out of this comparison follows a discrepancy result follows, which gives the ratio between predicted –and theoretical deflection of the prototype.

$$\%Discr. = \frac{\left|\omega_{th.} - \omega_{pr.}\right|}{\omega_{th.}} \,.\, 100 \tag{1.30}$$

These discrepancy results are calculated for different C-values because thereby also belong different model ratio's. Each distortion of the y-direction is investigated for each corresponding model ratio. The experimental output of the model is obtained from a theoretical deflection of the model by introducing 10% discrepancy. Besides, for each configuration it is assumed that $\lambda_E = \lambda_\upsilon = \lambda_p = 1$ [18].

Case 1: the prototype is an inverse rectangular plate with a model ratio of $\left(\frac{a}{b}\right)_m < 1$. *Equation (1.26)* gives a good prediction of the behaviour when C goes to 0,01 *(Figure 1.23)*. On the other hand, *Equations (1.27)* and *(1.28)* are not giving a good prediction of the behaviour because the discrepancy increase very fast *(Figure 24)*.

Case 2: the prototype is a square plate. *Equation (1.26)* and *(1.27)* are giving a good prediction of the behaviour when the value of C is near one *(Figure 1.25)*. When the value of C goes to ten the prediction is very inaccurate and none of the equations is usable *(Figure 1.26)*.

Case 3: the prototype is a rectangular plate with a model ratio of $\left(\frac{a}{b}\right)_p > 1$. *Equation (1.28)* gives an excellent prediction when the value of C goes to ten *(Figure 1.27)*. This means that each rectangular plate can be changed by another plate with other dimensions if the model ratio is equal to $\left(\frac{a}{b}\right)_p \geq 1$. *Equation (1.26)* and *(1.27)* are giving inferior results in this situation and are not usable *(Figure 1.28)* [18].

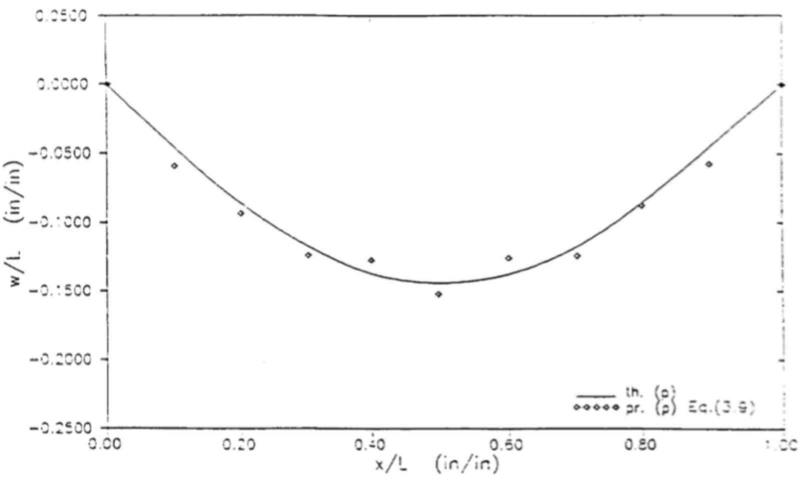

Fig. 1.23: Inverse rectangular plate: good prediction by equation (1.26) *C → 0,01 [17]*

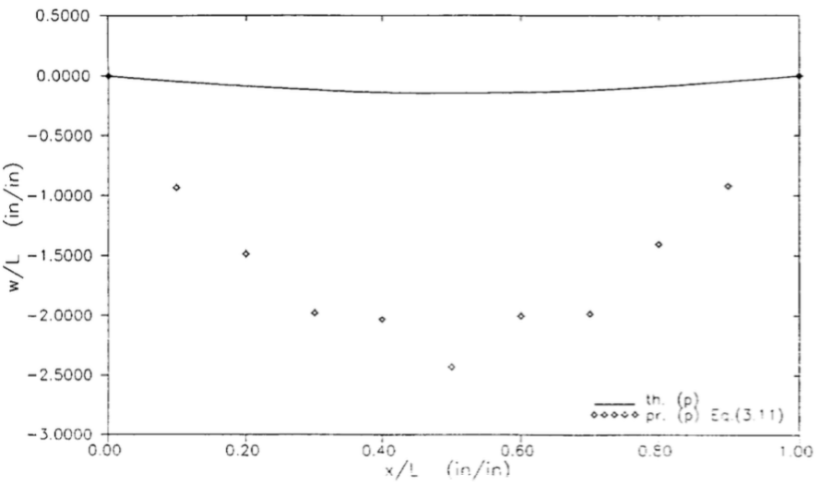

Fig. 1.24: Inverse rectangular plate: bad prediction by equation (1.27) *and* (1.28) *[18]*

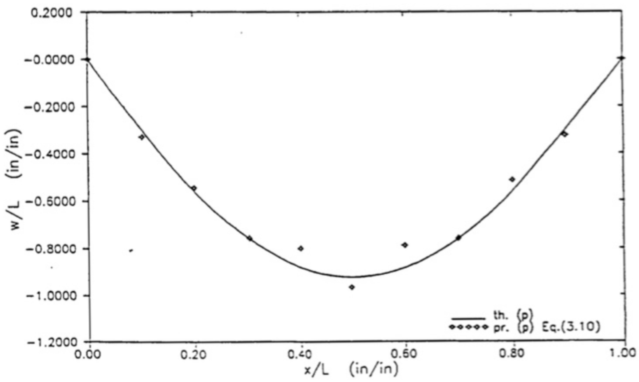

Fig. 1.25: Square plate: good prediction by equation (1.26) *and* (1.27) *C → 1 [18]*

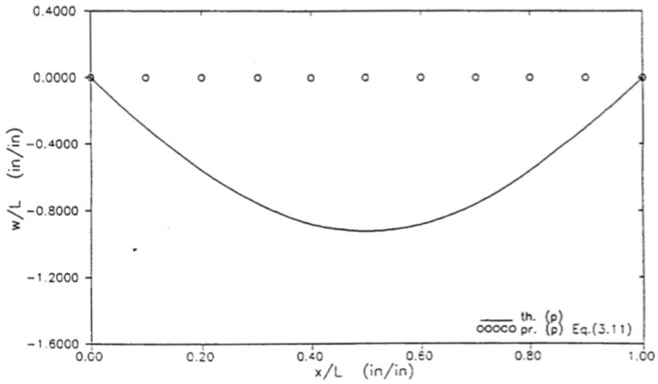

Fig. 1.26: Square plate: bad prediction by equation (1.28) *C → 0,01 [18]*

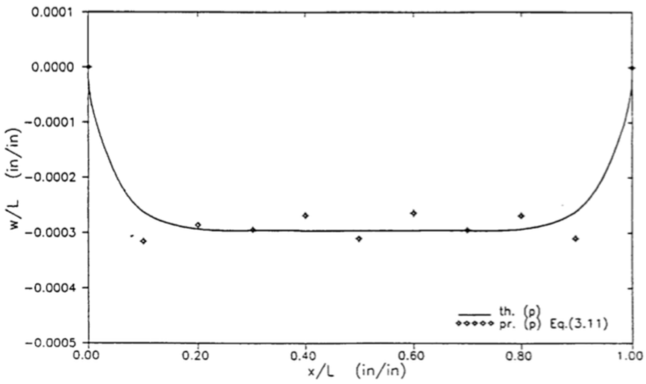

Fig. 1.27: Rectangular plate: good prediction by equation (1.28) *C → 10 [18]*

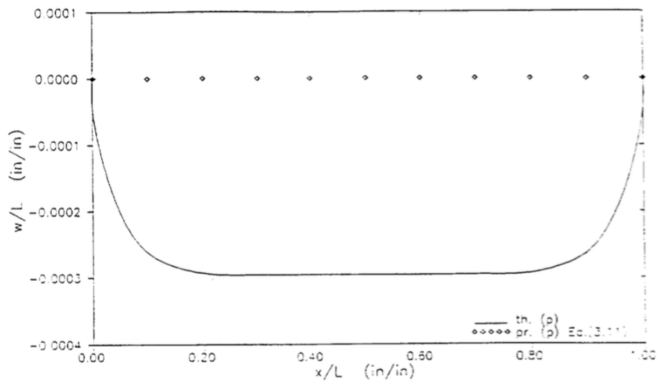

Fig. 1.28: Rectangular plate: bad prediction by equation (1.26) *and* (1.27) *C → 0,01 [18]*

2. EXPERIMENTAL PROGRAM

2.1 Introduction

This chapter is a detailed summarization of the experiment combined with the information about the characteristics of the frame, the material properties and the way of construction of the model. Also, the way of testing the model and the used measurement instrumentation are described.

2.2 Test Specimens

The Duong frame *(described in part B.3)* forms the base for the experiment in this thesis. This frame was also a scaled version of a real-life building frame. The scale factor was two to three. The frame has a height of 4,6 meters and a width of 2,3 meters. The beams have a cross-section of 300 millimetres by 400 millimetres just like the columns. The base of the specimen is 4,1 meters in length, 800 millimetres wide and 400 millimetres thick. The beams span a length of 1,5 meters and the height of a storey is captured at 1,7 metres. The concrete cover for the beams and columns is defined on thirty millimetres and twenty millimetres. The concrete cover for the foundation is 40 millimetres. The main reinforcement bars have a diameter of twenty millimetres. For the stirrups of the beams is a diameter 9,5 millimetres used and for the columns and foundation a diameter of ten millimetres.

The scale factor which is applied in this research thesis is a factor three. This means that all the dimensions of the Duong frame are divided by three. So, the height of the frame has become 1,53 metres and the width 0,77 metres. The cross-section of the beams has become 100 millimetres by 133 millimetres just like the columns. The base of the specimen is 1,37 meters in length, 267 millimetres wide and 133 millimetres thick. The beams span a length of 0,5 meters and the height of a storey is captured at 0,57 metres. The concrete cover for the beams and columns is defined on ten millimetres and seven millimetres. The concrete cover for the foundation is thirteen millimetres. The main reinforcement bars have a diameter of six millimetres. For the stirrups of the beams, the columns and the foundation, a uniform diameter of three millimetres is used.

At the upper right corner of the frame a lateral increasing load will be applied. Because of this load high bending stresses near the bottom of the columns will arise, but also at the inner side of the top of the columns. For this reason, an extra layer of reinforcement bars is applied, with a diameter of ten millimetres at these points to avoid instant failure of the frame when the lateral force increases. These extra bars increase the flexural capacity of the whole frame. The reinforcement bars diameter ten millimetres are also equipped with hooks and extra lengths to provide an anchorage.

The table below gives an overview of the used parameters in the developed frame. *Figures 2.1, 2.2, 2.3, 2.4 and 2.5* show the dimensions of the structure and the dimensions and placement of the reinforcement for each cross-section of each member. To obtain well-grounded and realistic values for the several parameters, two of these specimens are built to conduct the tests.

Table 2.1: Cross-section details of constructive frame elements

Member	b (mm)	h (mm)	Bottom steel	Top steel	Stirrup
Beam	100	133	4Ø6	4Ø6	Ø3 at 100
Column	100	133	4Ø6	4Ø6	Ø3 at 45
Column top	100	133	8Ø6	4Ø6	Ø3 at 45
Column base	100	133	8Ø6	8Ø6	Ø3 at 45
Foundation	267	133	8Ø6	8Ø6	Ø3 at 60

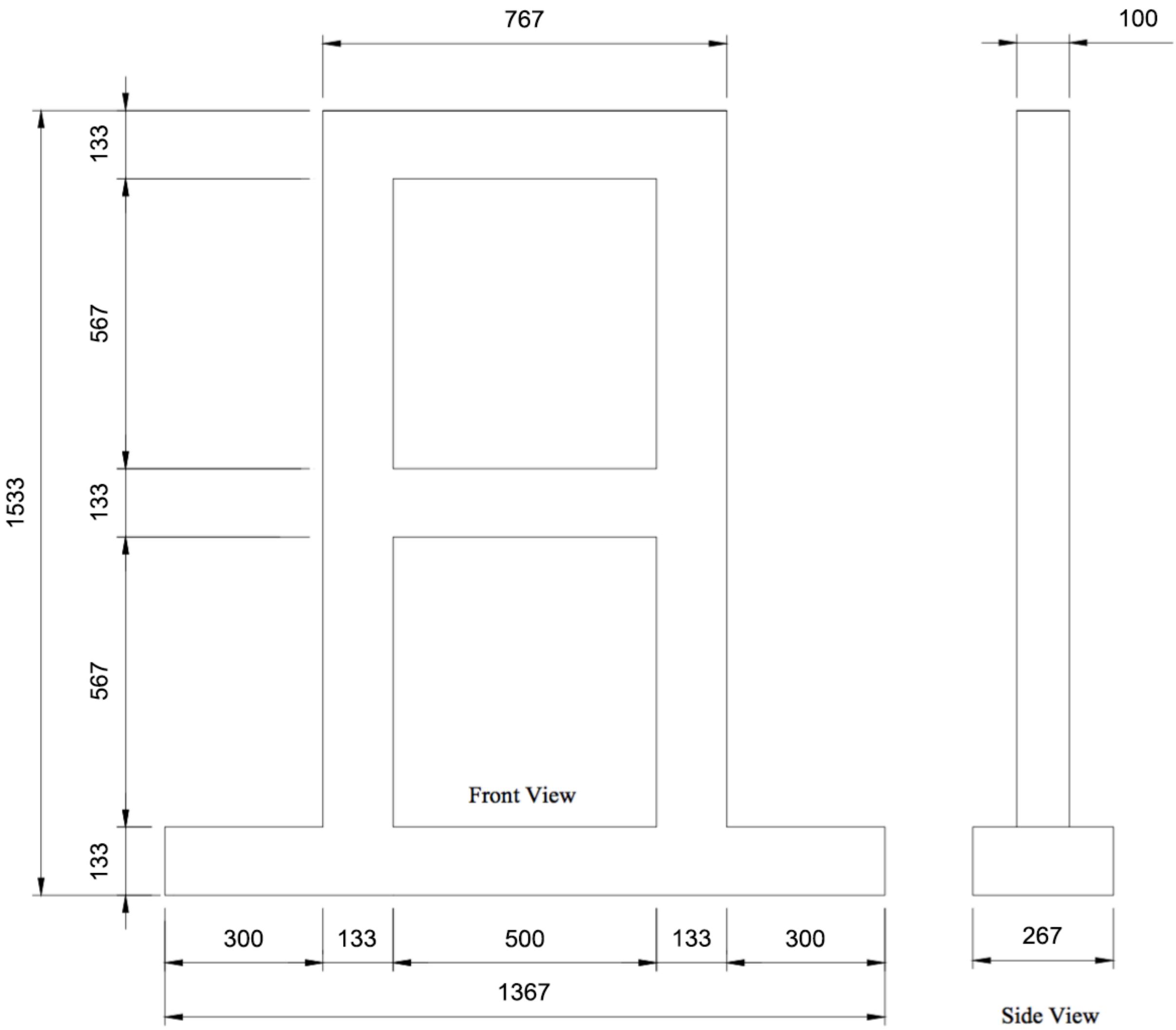

Fig. 2.1: Frame dimensions in millimetres

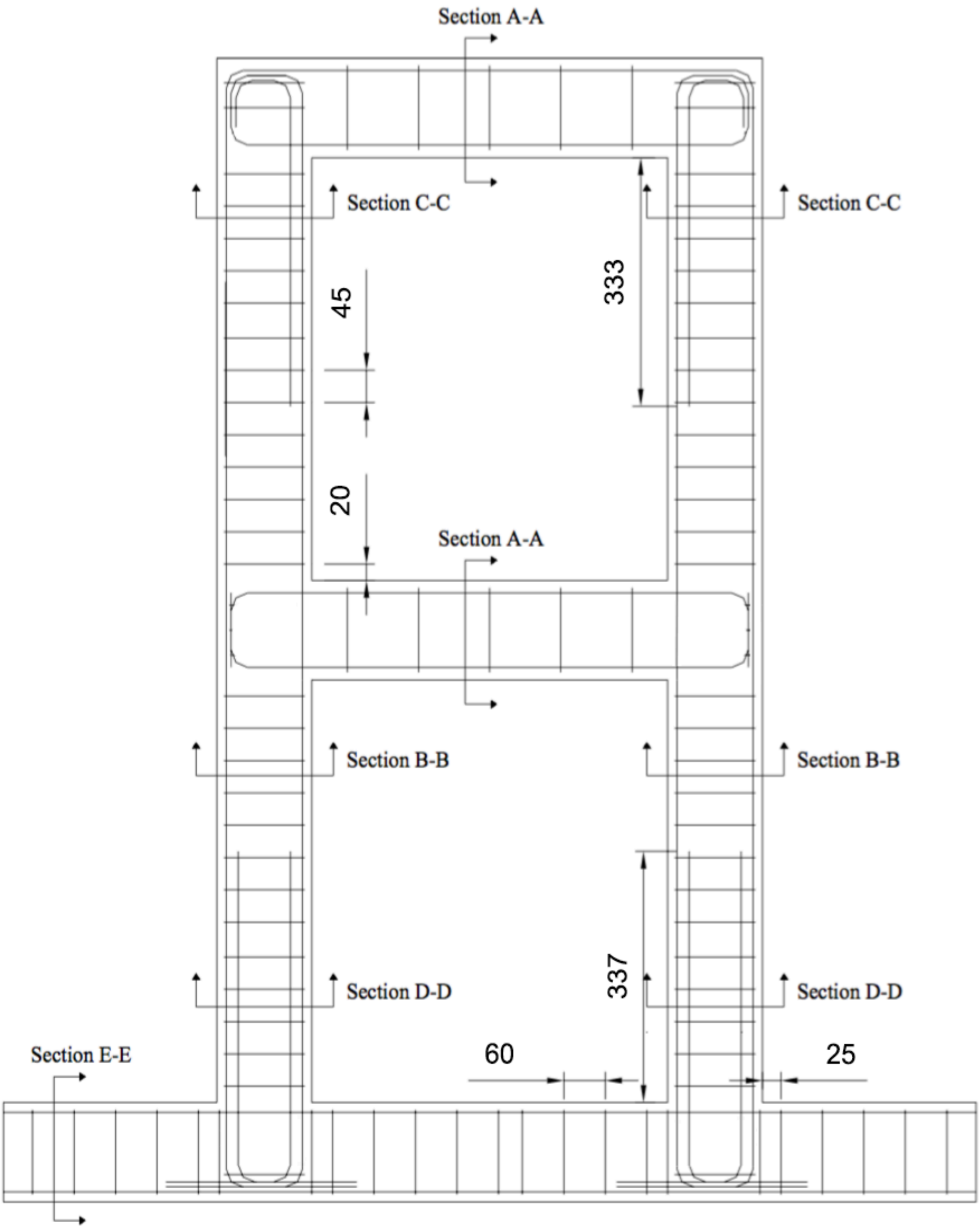

Fig. 2.2: Frame reinforcement placement

Section A-A:
As-built Beam section

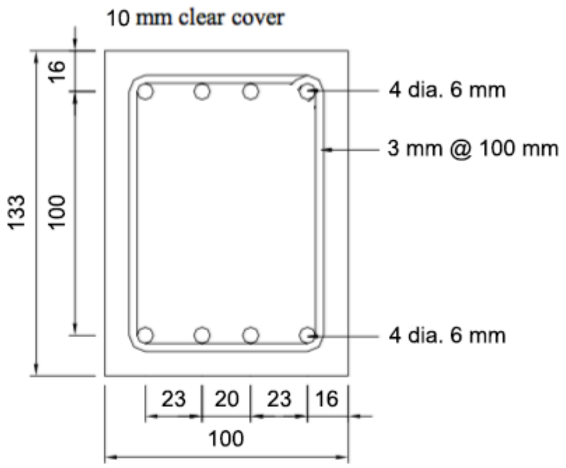

Section B-B:
As-built Column section

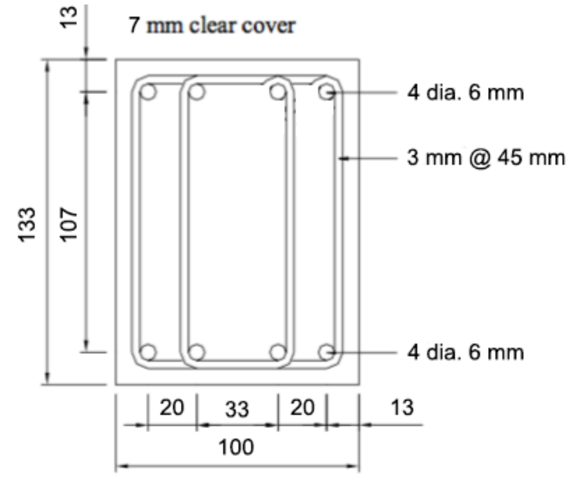

Fig. 2.3: As-built Beam and Column cross-section

Section C-C:
As-built Column section (top)

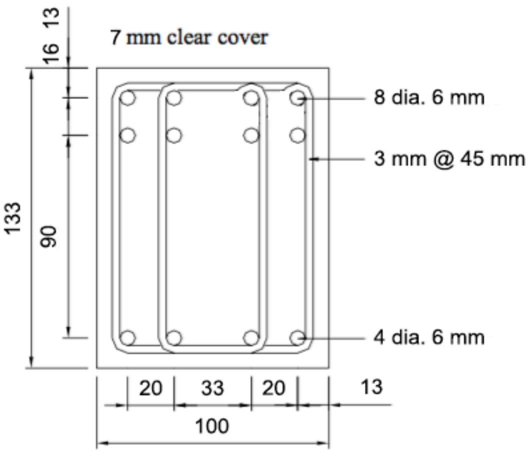

Section D-D:
As-built Column section (base)

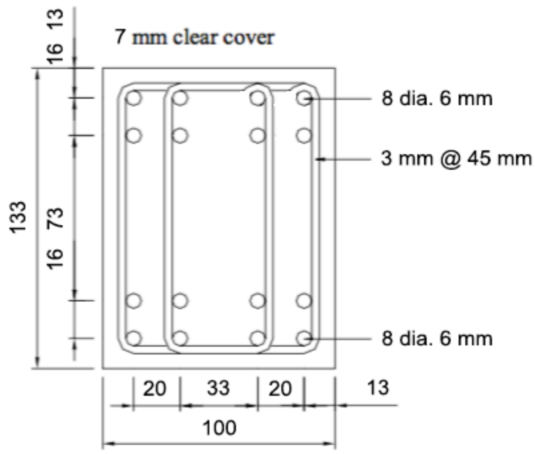

Fig. 2.4: As-built Column cross-section

Section E-E:
As-built Foundation section

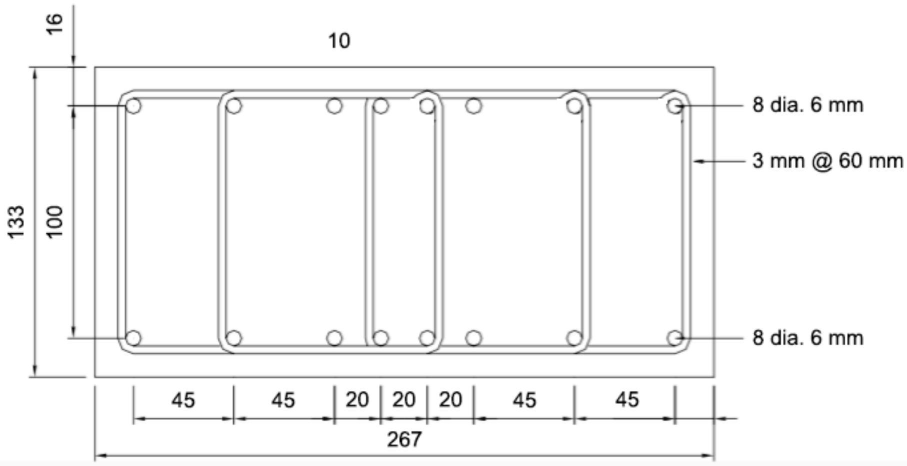

Fig. 2.5: As-built foundation cross-section

2.3 Material properties

2.3.1 Concrete

A Testing

To obtain the correct concrete behaviour, several different concrete mixtures are made. From each recipe were made nine cubes from 150 millimetres on 150 millimetres. Three of them are lab cured and six of them are moist cured. This is done to see the difference in compressive strength between the two specimen types with different boundary conditions. The recipes that are tested on compressive strength are C8/10 CEM II 32,5 (*Graph 2.1*), C12/15 CEM II 32,5 (*Graph 2.2*), C28/35 CEM II 32,5 (*Graph 2.3*) and a C35/45 CEM III 42,5 (*Graph 2.4*). The different recipes were all tested after eight days (8) and after 28 days (28). The horizontal red line in each graph represents the compression force that was applied on the concrete in the test on the Duong Frame. The value for the compression force is given by *Equation 2.1*. The compressive strength of the concrete on the date of testing is given in *Table 1.2 (part B.3)*.

$$\sigma = \frac{F}{A} \tag{2.1}$$

$$F = \sigma \,.\, A$$

$$F = 0{,}0429 \; \frac{kN}{mm^2} \,.\, (150\; mm \,.\, 150\; mm)$$

$$F = 0{,}0429 \; \frac{kN}{mm^2} \,.\, (22500\; mm^2)$$

$$F = 965{,}25\; kN$$

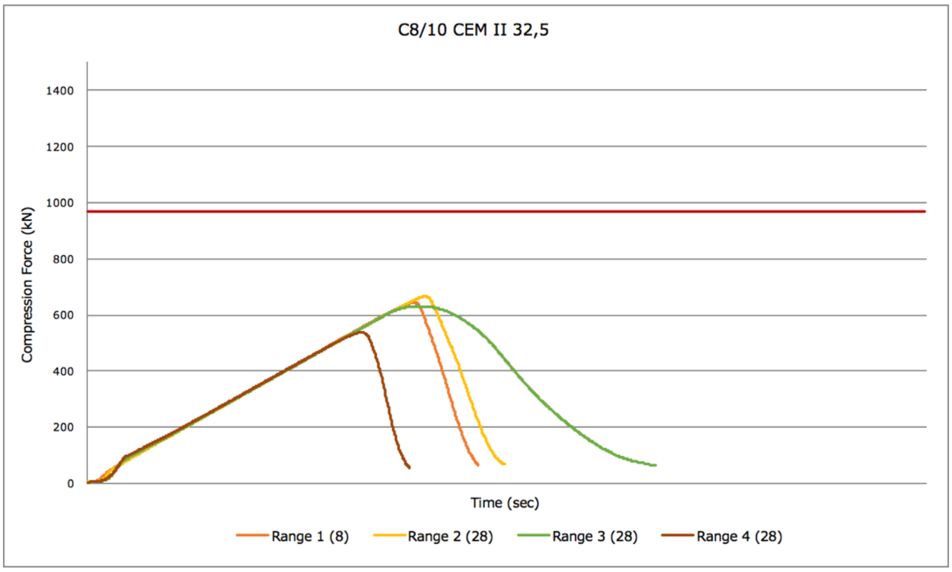

Graph 2.1: Compressive strength C8/10 CEM II 32,5

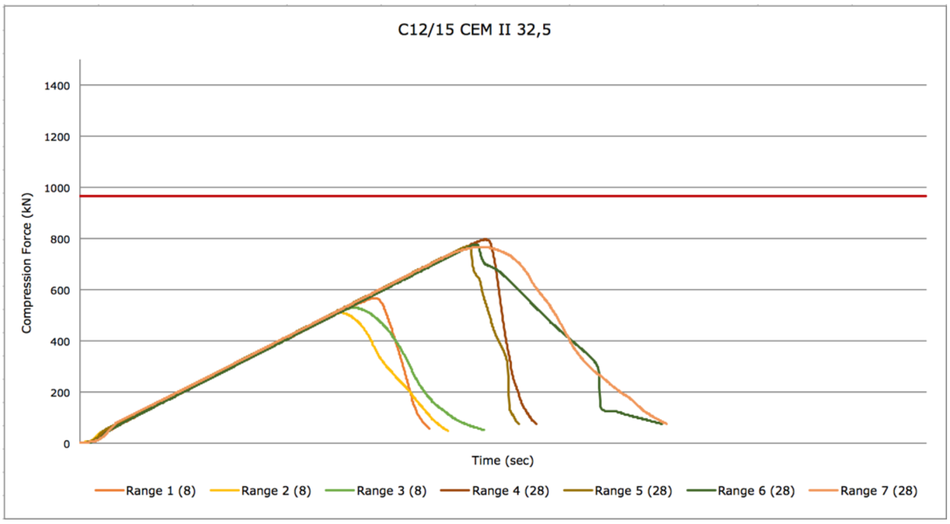

Graph 2.2: Compressive strength C12/15 CEM II 32,5

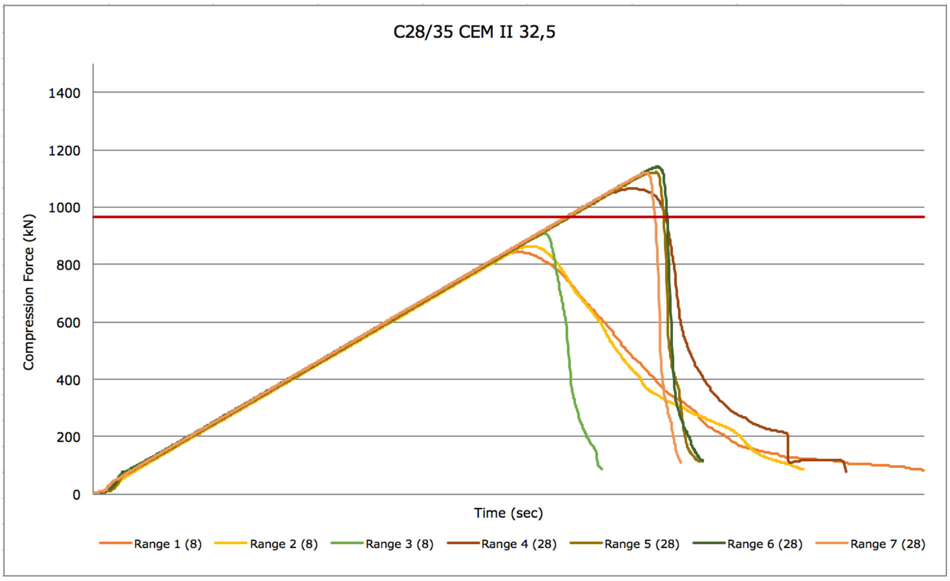

Graph 2.3: Compressive strength C28/35 CEM II 32,5

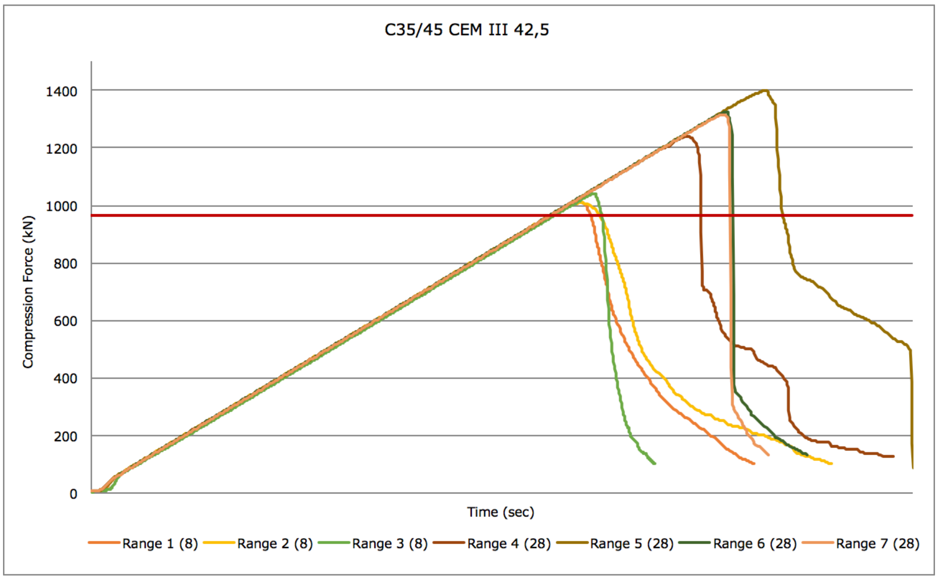

Graph 2.4: Compressive strength C35/45 CEM III 42,5

B Used concrete

Due to a delay in delivery of the steel for the reinforcement, there is chosen to use a stronger cement class so that the desired strength of the concrete is achieved much faster. Otherwise there would arise a time problem to perform the tests on the frames. The finally applied recipe is a C25/30 CEM I 52,5 because this concrete class lies between C12/15 and C28/35, and will approach the value of 965,25 kN the best *(Graph 2.5)*. The characteristics and calculations of this concrete are given in *Table 2.2.* The delivered granulates had a humidity of 2%. The specific amount of raw materials for one frame are given in *Table 2.3*. One specimen has a volume of 0,1 m^3.

Table 2.2: Characteristics concrete C25/30 CEM I 52,5

C25/30 CEM I 52,5 (1m^3)	
W/C Factor	$W/C = 0{,}60 + 20\% = 0{,}72$
	$W/C = 0{,}55$
Slump S2 (75mm)	$W = 185L + 20\%$
	$W = 240L$
(Humidity of 2%)	$W = 240\ L - (1605\ KG \,.\, 2\%)$
	$W = 210\ L$
Cement dosage	$C = \frac{W}{W/C}$
	$C = \frac{240\text{ L}}{0{,}55}$
	$C = 437\text{ KG}$
Aggregates (0-8mm)	$Ag = \rho\,.(1000 - \frac{C}{3} - \frac{W}{1} - 20)$
	$Ag = 2{,}7\,.(1000 - \frac{437}{3} - \frac{240}{1} - 20)$
	$Ag = 1605\ KG$
(Humidity of 2%)	$Ag = 1605\ KG\,.\,1{,}02\%$
	$Ag = 1635\ KG$
Summary (1m^3)	$\boldsymbol{W = 210\ L}$
	$\boldsymbol{C = 437\text{ KG}}$
	$\boldsymbol{Ag = 1635\ KG}$

Table 2.3: The specific amount of raw materials for one specimen

C25/30 CEM I 52,5 (1m^3)	**C25/30 CEM I 52,5 (0,1m^3)**
$\boldsymbol{W = 210\ L}$	$\boldsymbol{W = 21\ L}$
$\boldsymbol{C = 437\ \mathrm{KG}}$	$\boldsymbol{C = 43,7\ \mathrm{KG}}$
$\boldsymbol{Ag = 1635\ KG}$	$\boldsymbol{Ag = 163,5\ KG}$

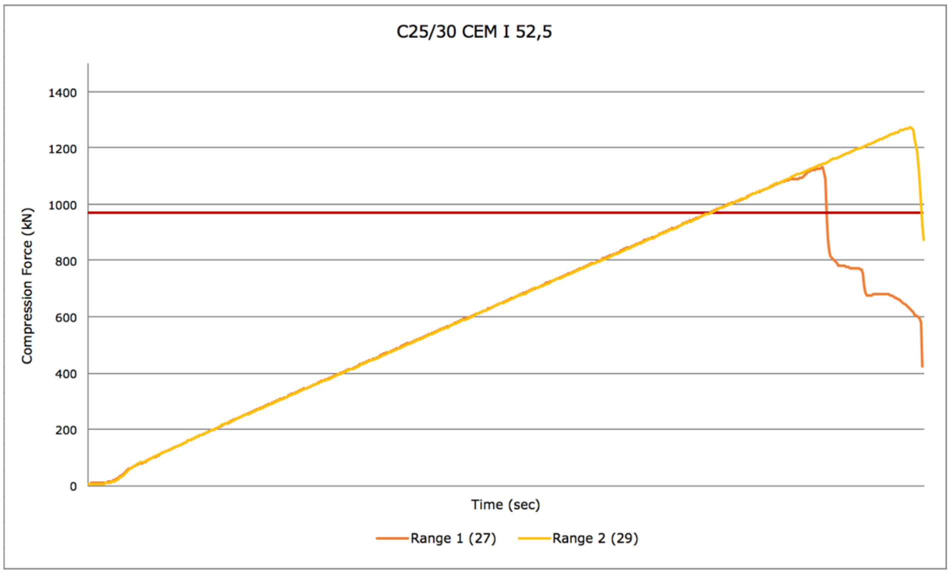

Graph 2.5: Compressive strength C25/30 CEM I 52,5

$$\sigma = \frac{F_{MAX}}{A} \tag{2.2}$$

$$\sigma_{27} = \frac{1129{,}225\,.\,10^3\ N}{150\ mm\,.\,150\ mm} \qquad \sigma_{29} = \frac{1270{,}638\,.\,10^3\ N}{150\ mm\,.\,150\ mm}$$

$$\sigma_{27} = 50{,}19\ MPa \qquad \sigma_{29} = 56{,}47\ MPa$$

$$\sigma_{average} = 53{,}33\ MPa$$

This value of the compressive strength is a little bit higher than the compressive strength out of the reference article (42,9 MPa). This difference in compressive strength of the concrete will be modified in the numerical analysis, to enable the comparison between experimental- and numerical analysis.

2.3.2 Steel reinforcement

In this scaled down model are use two different diameters instead of three that are used in the reference model. This is due to the scale process. The properties of the different sizes of reinforcing bars are listed in *Table 2.4*. The results for the tensile strength of the used reinforcement diameters three millimetres (400 MPa) and six millimetres (500 MPa) are mentioned in *Graph 2.6* and *Graph 2.7.* These tensile tests were conducted in the Laboratory of the University of Hasselt with a testing machine of 125 kN.

Table 2.4: Reinforcement details

Bar size	Nominal diameter (mm)	Area cross-section (mm^2)	Location in specimen
∅3	3	7	Transversal
∅6	6	28	Longitudinal

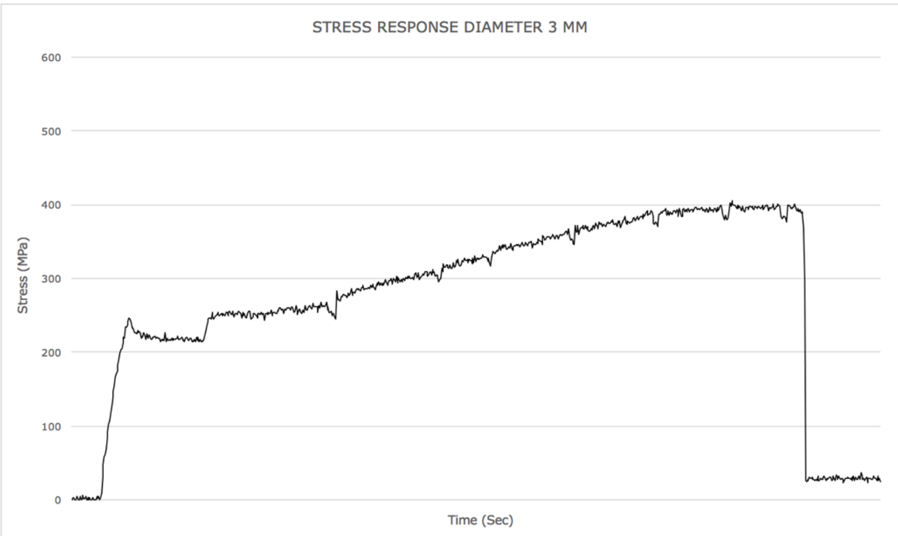

Graph 2.6: Stress response transversal reinforcement diameter three millimetres

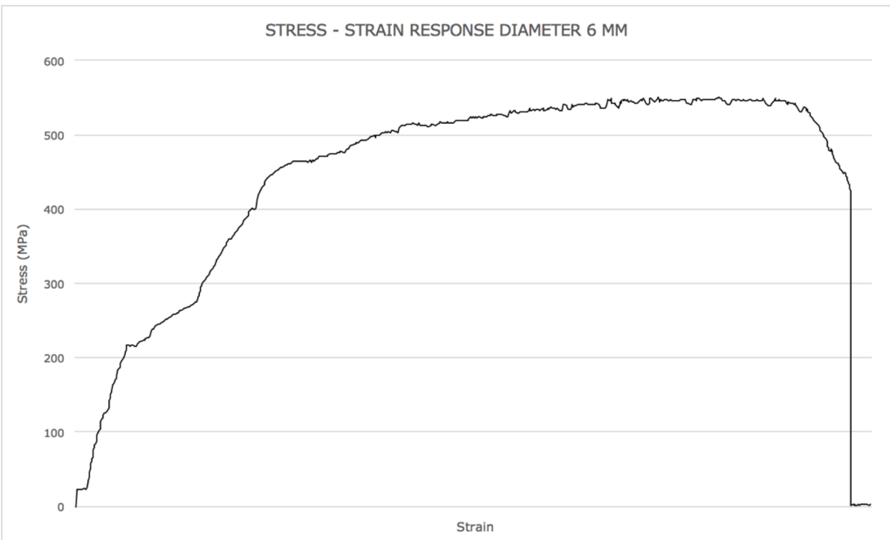

Graph 2.7: Stress – Strain response longitudinal reinforcement diameter six millimetres

2.4 Construction

The complete construction of the specimens can be divided into four parts; the construction of the mould, the construction of the reinforcement, the placement of the reinforcement in the mould and the concrete casting. In a traditional construction of a portal frame on site, the frame is built in an upstanding position. In this case, there is chosen to build the frame in a horizontal position so that the casting of the specimens becomes much easier. This is depicted in *Figure 2.6*.

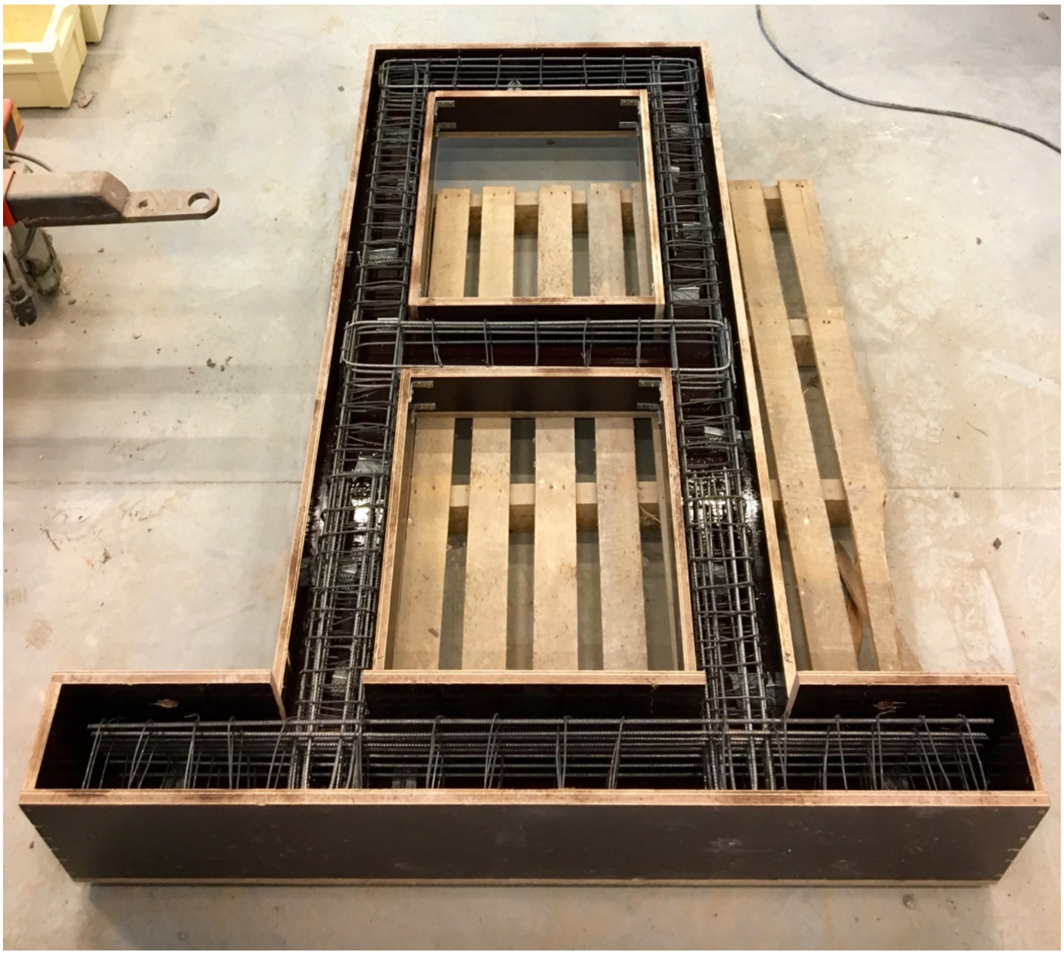

Fig. 2.6: Casting position of assembled frame [19]

2.4.1 Construction of the mould

The mould is constructed out of concrete plywood panels with a thickness of eighteen millimetres which have been cut by a specialized company. De panels per element (foundation, beam or column) are assembled with screws with a spacing of 50 millimetres, to give the mould enough strength against the pressure of the concrete. The elements are attached to each other by steel hooks and screws. In the upper panel of the foundation have been drilled four holes (two on each side) with a diameter of twenty millimetres, in order to insert aluminium tubes that will be cast in place. Through these tubes can enter threaded bars (anchorages) with a diameter of sixteen millimetres so that the frame can be connected to the test setup. Because of this, sliding of the specimen will be prevented when the forces are applied.

2.4.2 Construction of the reinforcement

The construction of the reinforcement cages started with the cutting and bending of the six millimetres' bars at the specific distances. The bars were cut at the company Jans Creacar in Hoeselt *(Figure 2.7)* and were bended by a self-made setup *(Figure 2.8)*. The three millimetres' bars were manual cut with a grinding wheel and bended in the same manner then the six millimetres' bars. After that, the bended bars *(Figure 2.9)* were assembled in the following way. First, the foundation cage was assembled wherein the longitudinal bars of the columns were connected *(Figure 2.10)*. Secondly, the first beam was put together and moved into place *(Figure 2.11)*, where after the stirrups around the upper parts of the columns were placed. Last, the upper beam was assembled and moved into place. Each connection between the stirrups and the longitudinal bars are tied with a 1,2 millimetres' steel wire. Finally, the extended bars from the entire reinforcement cage *(Figure 2.12)* were cut with the grinding wheel.

Fig. 2 7: Cutting machine [19]

Fig. 2.8: Bending setup [19]

Fig. 2.9: Bended reinforcement [19]

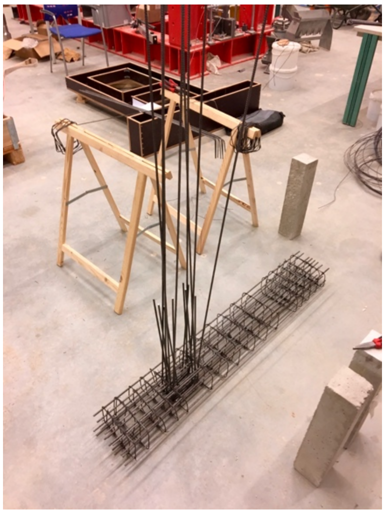

Fig. 2.10: Foundation cage [19]

Fig. 2.11: Placement 1^{st} beam [19]

Fig. 2.12: Complete cage [19]

2.4.3 Placement of the reinforcement

Once the moulds and the reinforcement cages were assembled, the cages could be placed inside the moulds. First, the moulds were cleaned properly and after that they were oiled with formwork releasing oil. Secondly, spacers of ten millimetres were placed at the bottom off the moulds to obtain a sufficient concrete cover on the reinforcement. Thirdly, the cages were put into the moulds and bent into position with a hammer. Last, the aluminium tubes for the anchorages were tied into the cages of the foundations *(Figure 2.13)*.

Fig. 2.13: Full mould and full reinforcement assembly [19]

2.4.4 Concrete casting

The fourth and final phase of the construction consisted of casting the specimens. First, the foundation is being poured and after that the columns and the beams. The concrete is consolidated with a vibrating needle to compact the concrete and to release air bubbles out of the mixture. The top surfaces of the specimens are levelled with trowels and the surfaces that are exposed to the environment were kept wet for two days. Also, seven cubes of 150 millimetres on 150 millimetres are made, to measure when the concrete has the same compressive strength as the concrete out of the reference article, so that the specimens can be tested at the same compressive strength.

Fig. 2.14: Casted specimen [19]

2.5 Test setup

To perform the test, the frame had to be demoulded, placed into the test position (into the test bench) and, the test instrumentation had to be assembled and placed on the specimen's surface. Ten days after the specimen was casted, it was lifted by an overhead crane to demould it and, to put it into the test position afterwards. Once the specimen was placed into the test bench, the specimen was connected to the bench by threaded bars diameter sixteen millimetres and bearing nuts. The test setup is depicted in *Figure 2.15* and *Figure 2.16*. The test bench consists of two beams and to columns, which are HEA 300 profiles. These serve as stability for the test equipment as well as for stability of the specimen. The columns also provided a support point to mount the LPT's. The test setup also contained a horizontal and vertical loading system. A hydraulic cylinder with a range of 200/400 kN was placed between the upper steel plate and the test bench on top of the columns. A load cell was placed between the steel plates to measure the applied force of the cylinder. A load of 45 kN was applied by the cylinder and was kept constant during the entire test by tightening the nuts after the pre-tensioning of the threaded bars. The lateral loading was applied by a 400 kN hydraulic cylinder in the centre of the second storey beam. This cylinder was connected to the right HEA 300 column of the test bench.

Table 2.5: Specifications and members of test setup

1	Steel plate (50 millimetres)
2	Vertical hydraulic cylinder – 200/400 kN
3	Steel plate (fifteen millimetres)
4	Vertical load cell – 360 kN (2x)
5	Horizontal hydraulic cylinder – 100 kN
6	Horizontal load cell – 125 kN
7	Steel distribution plate (ten millimetres)
8	Test specimen mounted in the test bench
9	Tensioning bars (dia. sixteen millimetres + nuts - 8x)
10	Test bench (HEA 300)
11	Steel distribution plate (30 millimetres)
12	Anchorage of specimen (threaded bars dia. sixteen millimetres + nuts)
13	Wooden leveling/spacing plate (eighteen millimetres)
14	Linear Potentiometer one – Linear Position Transducer (LPT)
15	Linear Potentiometer two – Linear Position Transducer (LPT)
16	Test specimen – portal frame
17	Inclinometer one – top beam
18	Linear Potentiometer three – Linear Position Transducer (LPT)
19	Inclinometer two – bottom beam

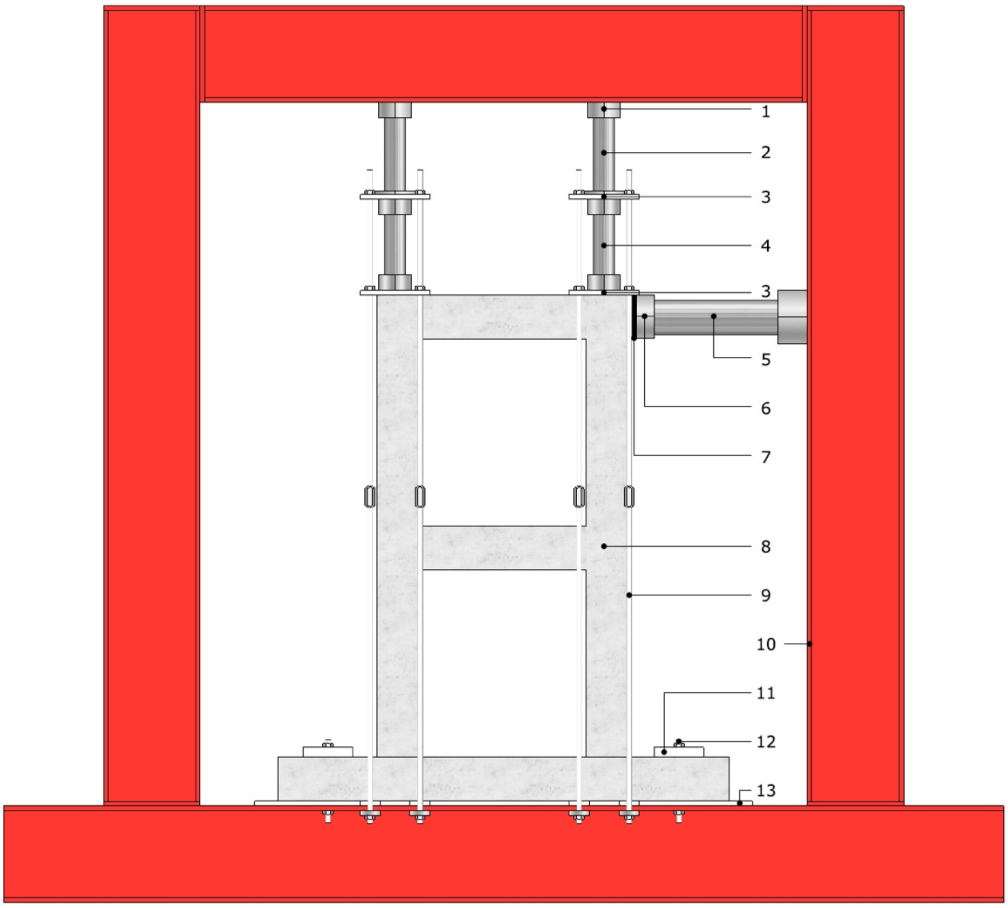

Fig. 2.15: Scheme - front view of test bench with mounted test specimen - members' description

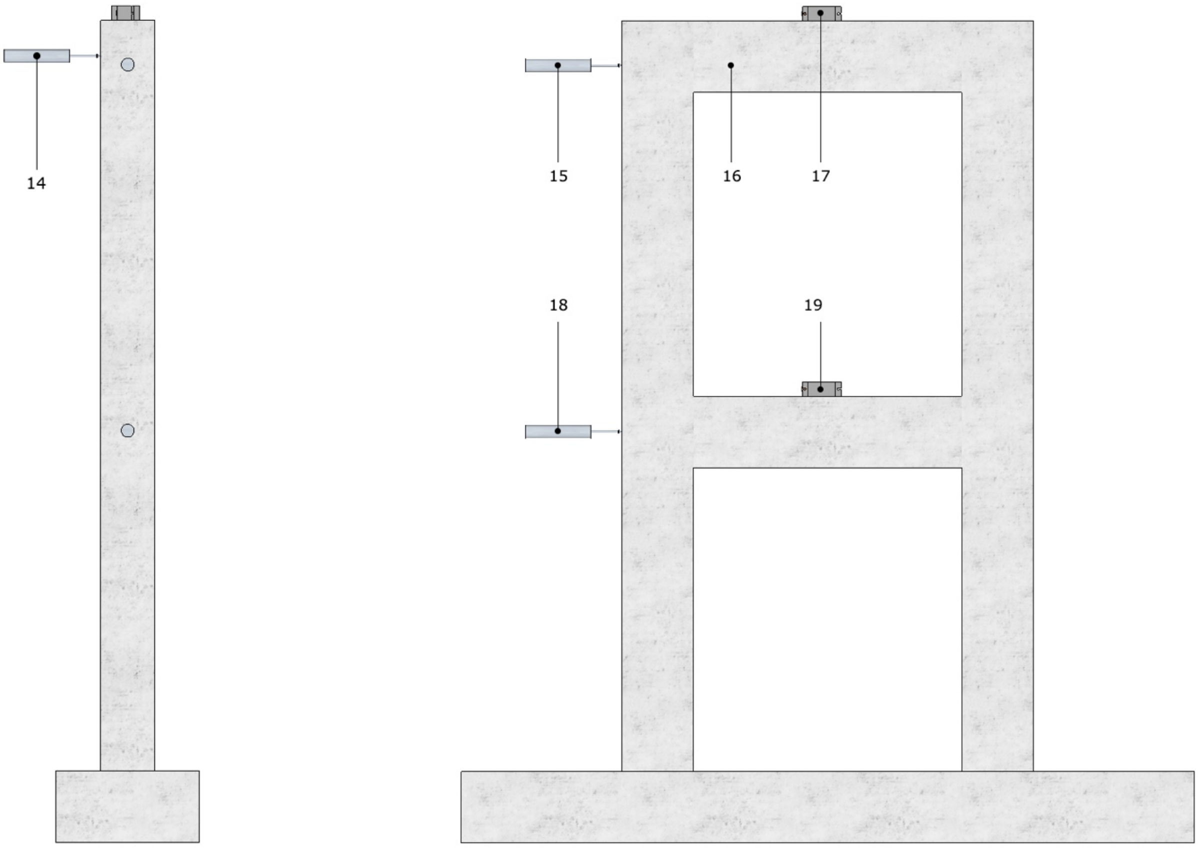

Fig. 2.16: Scheme - left view + front view of test specimen with measurement equipment

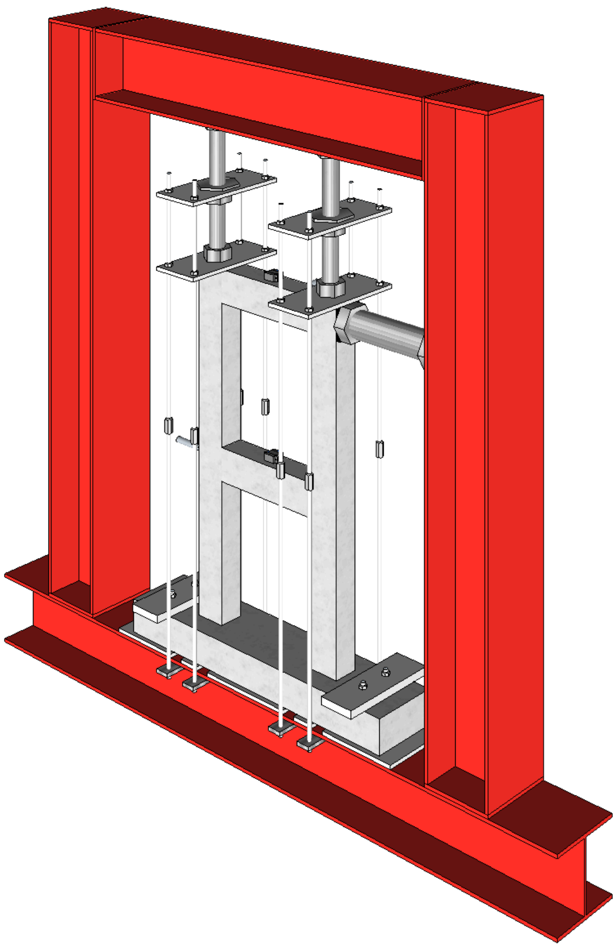
Fig. 2.17: 3D scheme of test bench with mounted test specimen and measurement equipment

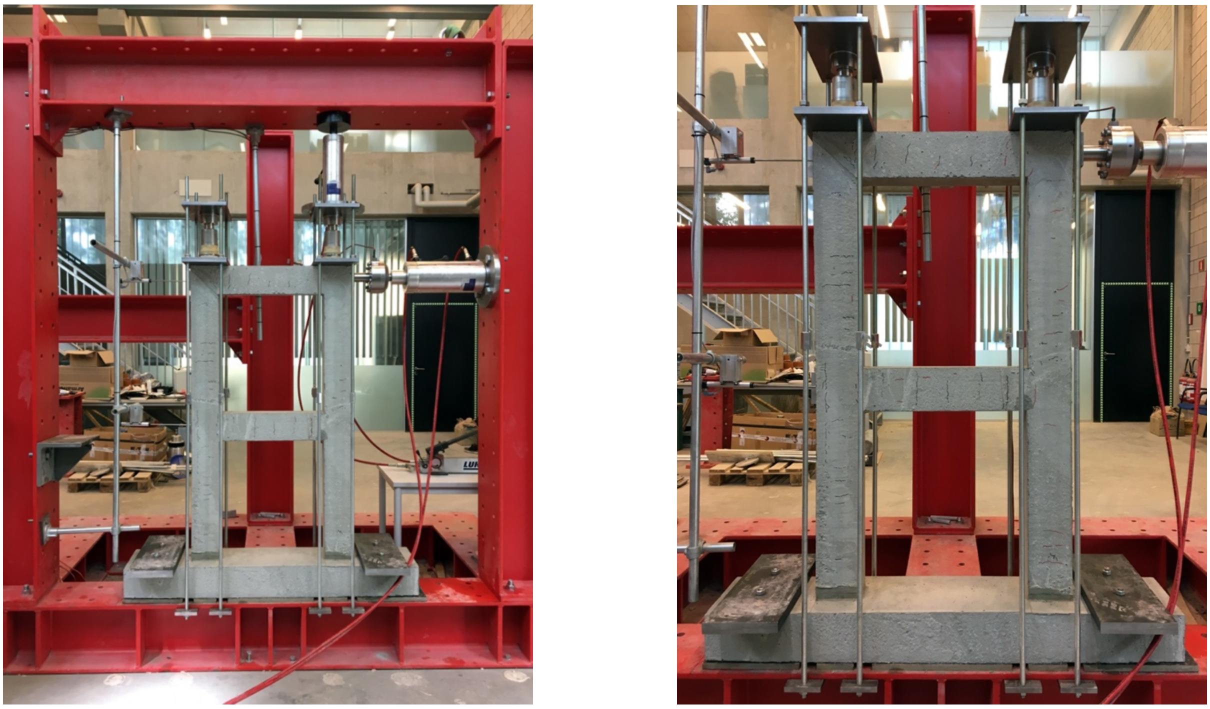

Front elevation during pre-tensioning　　　　Front elevation after pre-tensioning

Fig. 2.18: Overall view of test setup [19]

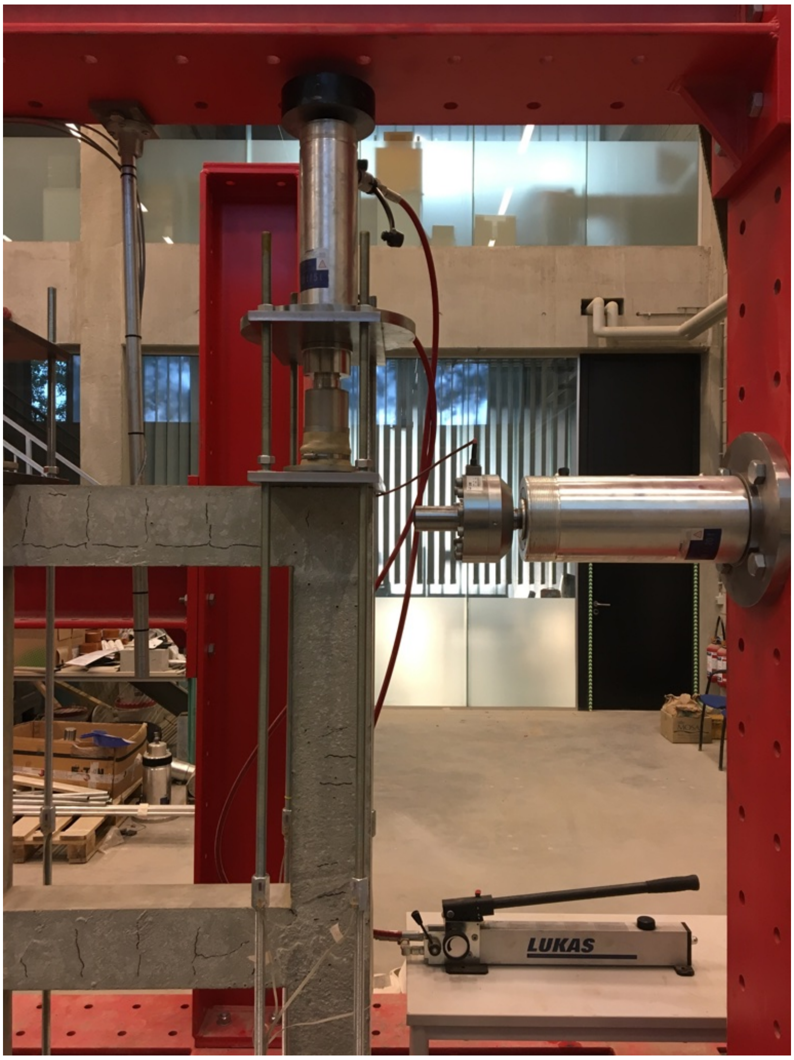

Fig. 2.19: Vertical – and lateral loading system [19]

2.6 Instrumentation

The data acquirement system is a computer controlled system that gathers electronic test data out of the following measurement devices: inclinometers and LPT's. The various gauges are described below.

2.6.1 Inclinometer

An inclinometer or clinometer *(Figure 2.20)* is an instrument that measures angles, elevations or depressions of objects that are respecting the gravity. Inclinometers measure inclines and declines by two different measure units: degrees and percentages. These gauges are recording the angular displacement of the beams due to the lateral increasing load. Before the loads were applied, two of these targets were attached on the specimen. One is attached at the lower beam and the other one is attached at the upper beam using a thin layer of glue. The gauges were placed in the centre of these beams because the rotation will be the largest in those points. However, the calibration of these measuring devices did not succeed. Because of this, no results have been acquired about the distortion of the beams.

Fig. 2.20: Used inclinometer [19]

2.6.2 Linear Position Transducer (LPT)

A Linear Position Transducer (LPT) *(Figure 2.21)* is a type of electrical transformer used for measuring linear displacement. They were placed at three locations on the specimen which is depicted in *Figure 2.16* and *Figure 2.17*. These gauges measure the lateral deflections of the specimen due to the lateral increasing load. They were placed at the level of the first storey beam and, the second storey beam and perpendicular on the second storey beam. The LPT's were placed at the centreline of these parts on the left side of the specimen and, attached to the left HEA 300 column of the test bench. There were no LPT's placed at the right side of the specimen because there will only be applied a forward static load (pushing) and no reversed static load (pulling).

Fig. 2.21: Used Linear Position Transducer [19]

2.7 Loading

In these experiments only a forward static load (push-over) is applied because a reversed cyclic load is only necessary in a seismic experiment. The specimens were loaded forward until damage due to shear arose. These testing phases had a duration of circa one hour per specimen to reach the point of failure.

The testing of the specimens started with applying the constant vertical load of 45 kN on the top of each column. The calculation of this load is derived out of the reference article and recalculated for the scaled model. This calculation is mentioned by *Formula 2.3*. This load was applied in force-controlled modus and was preserved during the entire test period. The lateral load was also applied in force-controlled modus. This lateral load was applied at the centre of the second storey beam by a hydraulic cylinder that creates a force on a steel distribution plate as described in part *2.5 Test setup*.

The load increased constant during the forward static loading, with a reading precision of the load cell of 50 Newton. At 10, 20, 25 and 30 kN the lateral force was kept constant for a few minutes so that there was the possibility to mark the occurring cracks.

The data out of these tests is collected accurate because the results were used in the results- and discussion chapters of this master's thesis.

$$f_{cd}(scaled) = \alpha_{cc} \, . \frac{f_{ck}(scaled)}{\gamma_m} \qquad (2.3)$$

$$f_{cd}(scaled) = 0{,}85 \, . \frac{53{,}33 \, MPa}{1{,}0} = 42{,}66 \, MPa$$

$$N_d(scaled) = N_{s1} + N_{s2} + N_c = \left((A_{s1} + A_{s2}) \, . \sigma_{sd}\right) + \left(A_c \, . f_{cd}(scaled)\right)$$

$$N_d(scaled) = \left(\left(\left(8 \, . \frac{\pi \, . 6^2}{4}\right) + \left(8 \, . \frac{\pi \, . 6^2}{4}\right)\right) . 500 \, MPa\right) + \left(\left((133{,}33 \, . 100) - \left(2 \, . \left(8 \, . \frac{\pi \, . 6^2}{4}\right)\right)\right) . 42{,}66 \, MPa\right)$$

$$N_d(scaled) = 775{,}746 \, kN$$

$$N_d(prototype) = N_{s1} + N_{s2} + N_c = \left((A_{s1} + A_{s2}) \, . \sigma_{sd}\right) + \left(A_c \, . f_{cd}(prototype)\right)$$

$$N_d(protoype) = \left(\left(\left(8 \, . \frac{\pi \, . 20^2}{4}\right) + \left(8 \, . \frac{\pi \, . 20^2}{4}\right)\right) . 447 \, MPa\right) + \left(\left((400 \, . 300) - \left(2 \, . \left(8 \, . \frac{\pi \, . 20^2}{4}\right)\right)\right) . 42{,}9 \, MPa\right)$$

$$N_d(prototype) = 7179{,}205 \, kN$$

$$\frac{N_d applied \ (prototype)}{N_d(prototype)} = \frac{420 \, kN}{7179{,}205 \, kN} = 0{,}0585 = 5{,}85\%$$

$$\frac{N_d applied \ (scaled)}{N_d(scaled)} = \frac{N_d applied \ (scaled)}{775{,}746 \, kN} = 5{,}85\%$$

$$N_d \ applied \ (scaled) = N_d(scaled) \, . \% = 775{,}746 \, kN \, . 5{,}85\% = 45{,}38 \, kN$$

$$N_d \ applied \ (scaled) \approx 45 \, kN$$

3. EXPERIMENTAL RESULTS

3.1 Introduction

This chapter is a detailed summary of the experimental results and test considerations. First, there is given a global explanation about the test conventions, followed by an overview of the loading stages and the gathered test results. Information has been processed about the crack pattern, crack widths in the z-direction, the shear failing locations and the displacement in the x-direction. Out of these results a force-displacement curve is plotted. The most important phenomena at the end of each load step are given by a representative photo. Graphs that are related to the specific results are shown at the end of the chapter. The discussion of these results is given in part *3.4 Discussion of results*.

3.2 Test conventions

A description of the complete test setup is given by *Figure 3.1*. Note that some elements that are used during these tests are not mentioned in the figure for clarity. The specimen is connected to the ground beam of the test bench. The three hydraulic cylinders are connected to the right column and between the upper steel plates and the test bench on the top of each column. These cylinders were used to apply the forces on the frame as described in part *2.5 Test setup*.

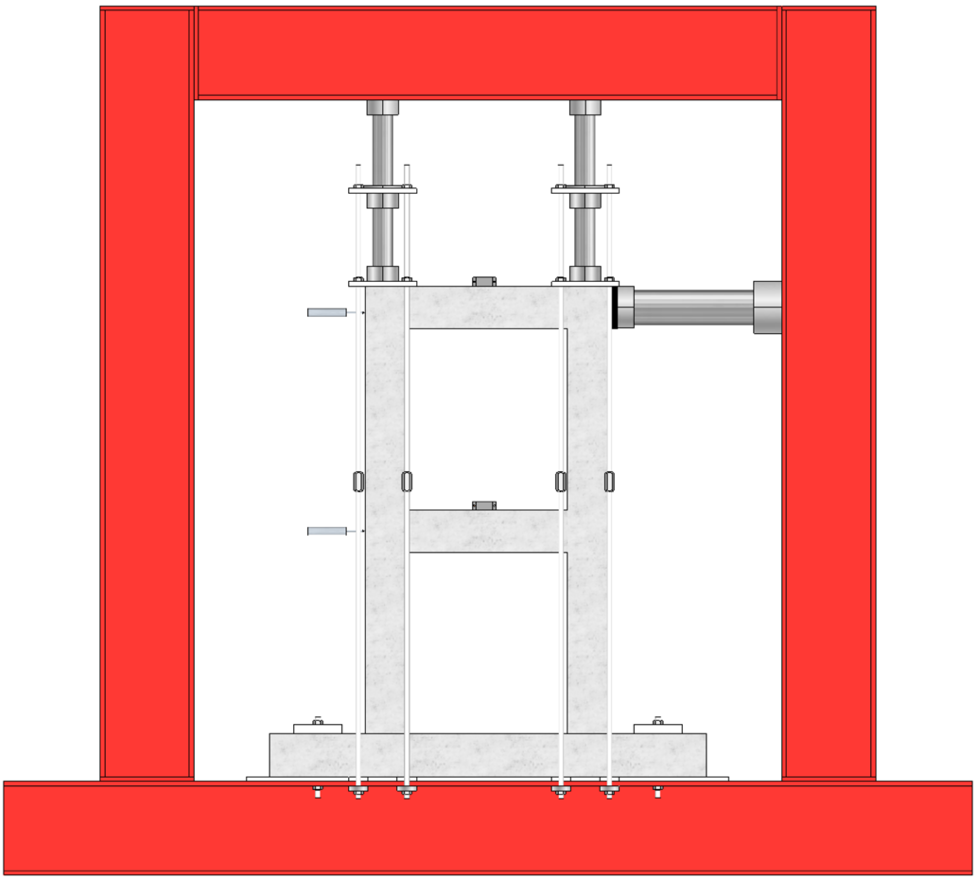

Fig. 3.1: Front view of test bench with mounted test specimen

In this part, there is talked about the net horizontal force. This is the total horizontal force minus the horizontal part of the force that is developed by the vertical cylinder. This is necessary because when the frame starts to deform, the forces applied in the columns do not remain vertical. At this point of the test there is developed a horizontal- and vertical part in the compression force. For this reason, the horizontal part of the vertical force had to be subtracted from the total horizontal load to know the exact applied horizontal load. These additional horizontal forces derived from the compression force were calculated at each load step using trigonometry between the height of the column and the lateral displacement of the second storey beam. Although these additional forces were very small they were considered in the calculations.

To make an observation of the cracks and to make a difference between the cracks, five colours are used to indicate the different types. Cracks can arise due to the testing of the specimen and due to the shrinkage of the concrete. A black coloured marker was used for cracks that are caused from the shrinkage of the concrete. An orange coloured marker was used to indicate the cracks derived after a lateral loading of 10 kN, a green coloured marker after 20 kN, a blue coloured marker by opening of the first significant cracks and a red coloured marker to mention the failing cracks.

3.3 Results

3.3.1 Initial condition

Before the loads were applied on the frame, the portal was completely checked for cracks caused from the shrinkage of the concrete or by the tensioning of the frame to the test bench by the threaded bars and bearing nuts. The portal contained a very small amount of shrinkage cracks and no tensioning cracks. The shrinkage cracks were less than 0,1 millimetres wide and were therefore not a problem. The foundation had a small curvature caused the mould opened a little bit by the pressure of the concrete during the casting. These gaps were filled by wood panels before the portal frame was tensioned on the test bench. In the final stage of the tests, the foundation suffered because of a bending moment in the foundation due to the lateral loading.

Fig. 3.2: Initial condition of the test specimen with the marked shrinkage cracks [19]

3.3.2 Detailed test results

One loading phase is applied on the test specimens in the forward direction until the specimens failed due to shear. The load stages of the forward static loading are summarized in *Table 3.1* for the first specimen and in *Table 3.3* for the second specimen. *Table 3.2* summarizes the applied load corresponding to the lateral drift mentioned in percentages for specimen one. The same summarization for specimen two is mentioned in *Table 3.4*. The lateral drift is calculated as:

$$Lateral\ Drift\ \% = \frac{\Delta\ LPT_2}{H}\ .100 \tag{3.1}$$

$\Delta\ LPT_2 = Lateral\ displacement\ at\ the\ centre\ of\ second\ storey\ beam\ (mm)$

$H = Column\ height\ from\ top\ foundation\ to\ centre\ of\ second\ storey\ beam\ (1320mm)$

Table 3.1: Load stages of forward static load - specimen one

Load interval	Load (kN)	Comment
0	0	-
1	10	Continuation shrinkage cracks
2	20	Corner cracks
3	25	Crack opening bottom beam
4	30	Fail of bottom beam + Crack opening top beam
5	31,35	Fail of specimen Crack 14,80 mm (top beam) $\Delta\ LPT_2$ 29,02 mm

Table 3.2: Lateral load + lateral drift - specimen one

Load interval	Load (kN)	$\Delta\ LPT_2\ (mm)$	Lateral Drift (%)
0	0	0,05	0,0037
1	10	4,23	0,32
2	20	9,10	0,69
3	25	12,49	0,95
4	30	19,85	1,50
5	31,35	29,02	2,20

Table 3.3: Load stages of forward static load - specimen two

Load interval	Load (kN)	Comment
0	0	-
1	10	Continuation shrinkage cracks
2	20	Corner cracks
3	24	Crack opening bottom beam
4	25	Fail of bottom beam + Crack opening top beam
5	27,55	Fail of specimen Crack 14,67 mm (top beam) $\Delta\, LPT_2$ 26,70 mm

Table 3.4: Lateral load + lateral drift - specimen two

Load interval	Load (kN)	$\Delta\, LPT_2\ (mm)$	Lateral Drift (%)
0	0	0,23	0,017
1	10	4,25	0,32
2	20	9,34	0,71
3	24	12,94	0,98
4	25	16,44	1,25
5	27,55	26,70	2,02

Table 3.5 (specimen one) and *Table 3.6* (specimen two) gives a detailed summary of the observations at each load interval out of *Table 3.1* to *Table 3.4*. Reference is made to *Figure 3.3* to *Figure 3.7* (specimen one) and to *Figure 3.10* to *Figure 3.13* (specimen two). All the LPT's were calibrated and set to zero before the compression loads on the columns were applied. Also, all the shrinkage cracks were marked in black before the lateral load was applied.

The maximum forward static load during de first test was 31,35 kN with a related lateral displacement of the second storey beam of 29,02 millimetres. After failing of the specimen, the lateral force increased again until a maximum displacement of 69,17 millimetres was reached. The specimen failed due to shear. Cracks in the lower beam were first observed around 25 kN and failing of the lower beam occurred around 30 kN. Immediately hereafter shear cracks developed in the second storey beam and the whole specimen collapsed at 31,35 kN. The shear crack in the first storey beam was 7,68 millimetres wide and in the second storey beam 14,80 millimetres.

Table 3.5: Summary of observations during push-over of test specimen one

Specimen One		**Comment**
Load interval	**Load (kN)**	
0	0	Application of the compression loads on the columns.
1	10	Existing shrinkage cracks were continued about twenty millimetres in length and new cracks were observed at the height of the stirrups in the lower and upper beam and in the left column. This can be explained due to a lack of the concrete cover. The average length of those new cracks was around 30 millimetres. These cracks were less than 0,1 millimetres wide.
2	20	Refer to *Figure 3.3*. A new crack arose at the at the beam-column interface at the upper right corner with a length of 100 millimetres. Another crack arose at the right side of the lower beam and had a length of approximately 120 millimetres and made an angle of 60 degrees with the horizontal. A few more cracks were noticed at the beam-column interface at the lower left corner of the first storey beam with a length of 25 millimetres. All these cracks were around 0,1 millimetres wide.
3	25	Refer to *Figure 3.4*. First beam shear crack occurred at the first storey beam and extended nearly through the entire depth of the beam. This crack was 1,5 millimetres wide and made an angle of 45 degrees with the horizontal. Also, the first column flexural cracks appeared at the base at the right side of both columns. Cracks were evenly distributed and developed from the base up to 1000 mm in the column height, and were spaced at approximately 60 millimetres (stirrups were spaced at 45 millimetres). These cracks were around 0,1 millimetres wide.
4	30	Refer to *Figure 3.5*. Collapse of the first storey beam occurred. Then beam shear cracks developed at the second-storey beam. These cracks were 1 millimetres wide and made an angle of 45 degrees with the horizontal. Also, a change in structural stiffness was noticed. The beam shear cracks widened, while the flexural cracks in the beams, interfaces, and columns remained stable. Then flexural yielding of the longitudinal reinforcement bars and the stirrups occurred. Because of this, the shear cracks in the beams widened.
5	31,35	Refer to *figure 3.6*. The specimen failed due to a collapse of the second storey beam after a collapse of the first storey beam. Also, additional flexural cracks were observed at the right side of each column and between the columns at the foundation. At the left side of each column there is also a crushing of the concrete noticed. The opening of these flexural cracks is not increased.

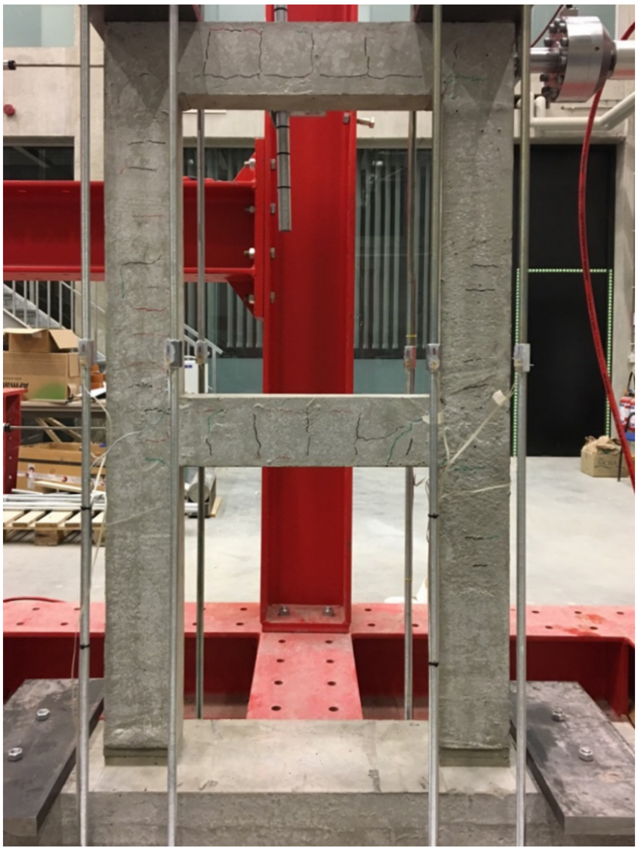

Fig. 3.3: Specimen one at load interval 2 [19]

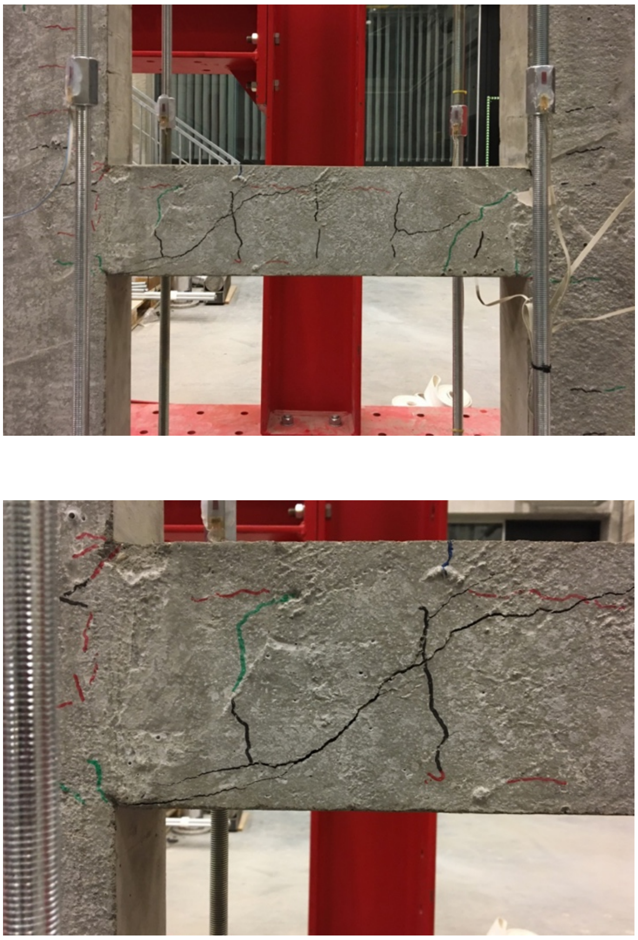

Fig. 3.4: Specimen one at load interval 3 [19]

Fig. 3.5: Specimen one at load interval 4 [19]

Fig. 3.6: Specimen one at load interval 5 [19]

Fig. 3.7: Specimen one after loading and removing measure equipment [19]

In *Figure 3.8* is the crack pattern for the first test specimen depicted. This drawing shows all the cracks including the shrinkage cracks. In *Figure 3.9* is only the crack pattern due to the forward static load shown, so here the shrinkage cracks are not mentioned. The next legend serves as a clarification of the two figures:

- Black = shrinkage cracks;
- orange = cracks mentioned after 10 kN of lateral load;
- green = cracks mentioned after 20 kN of lateral load;
- bleu = opening of the first significant cracks;
- red = shear cracks that causes structure failure of the test specimen.

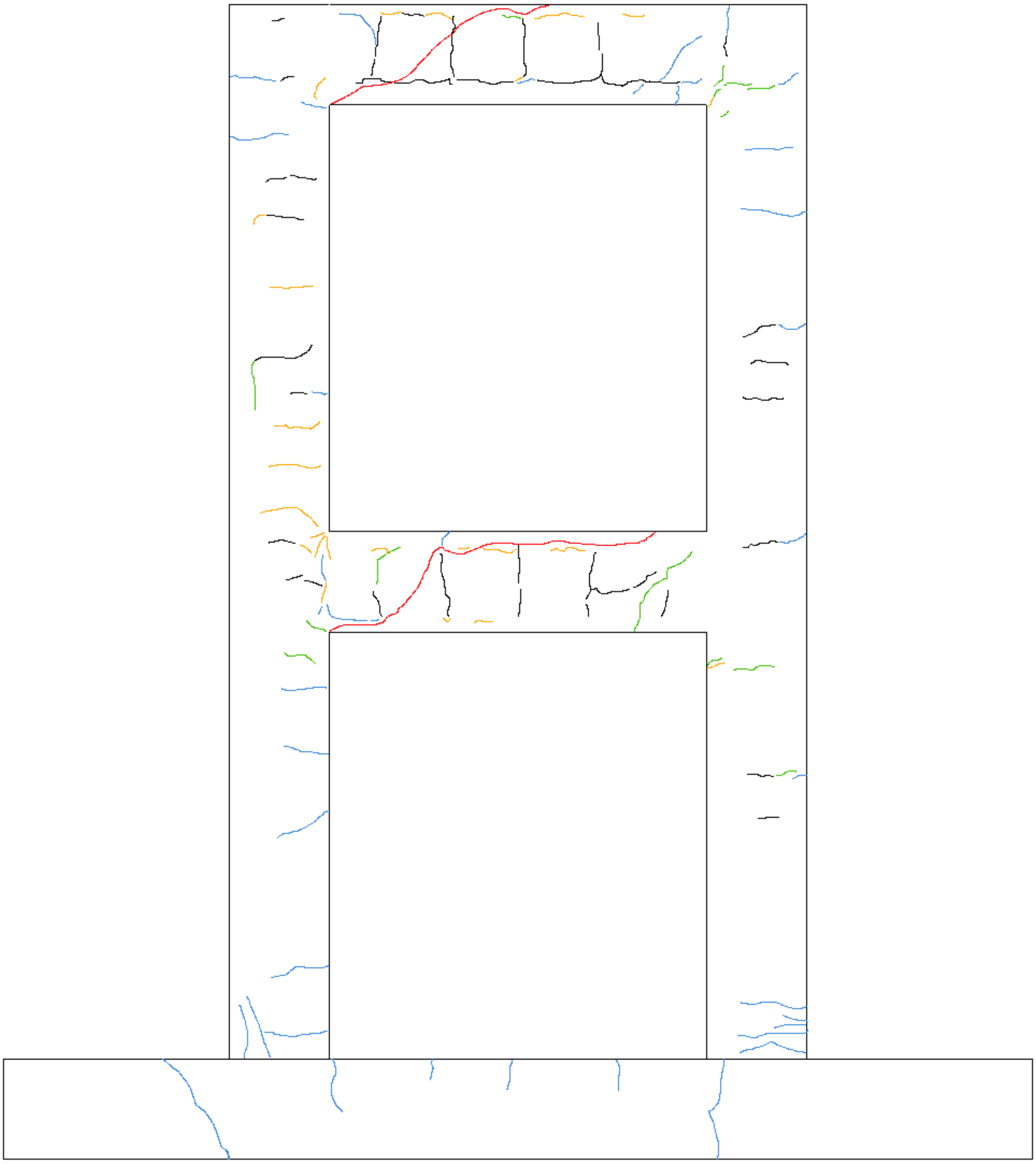

Fig. 3.8: Crack pattern specimen one including shrinkage cracks

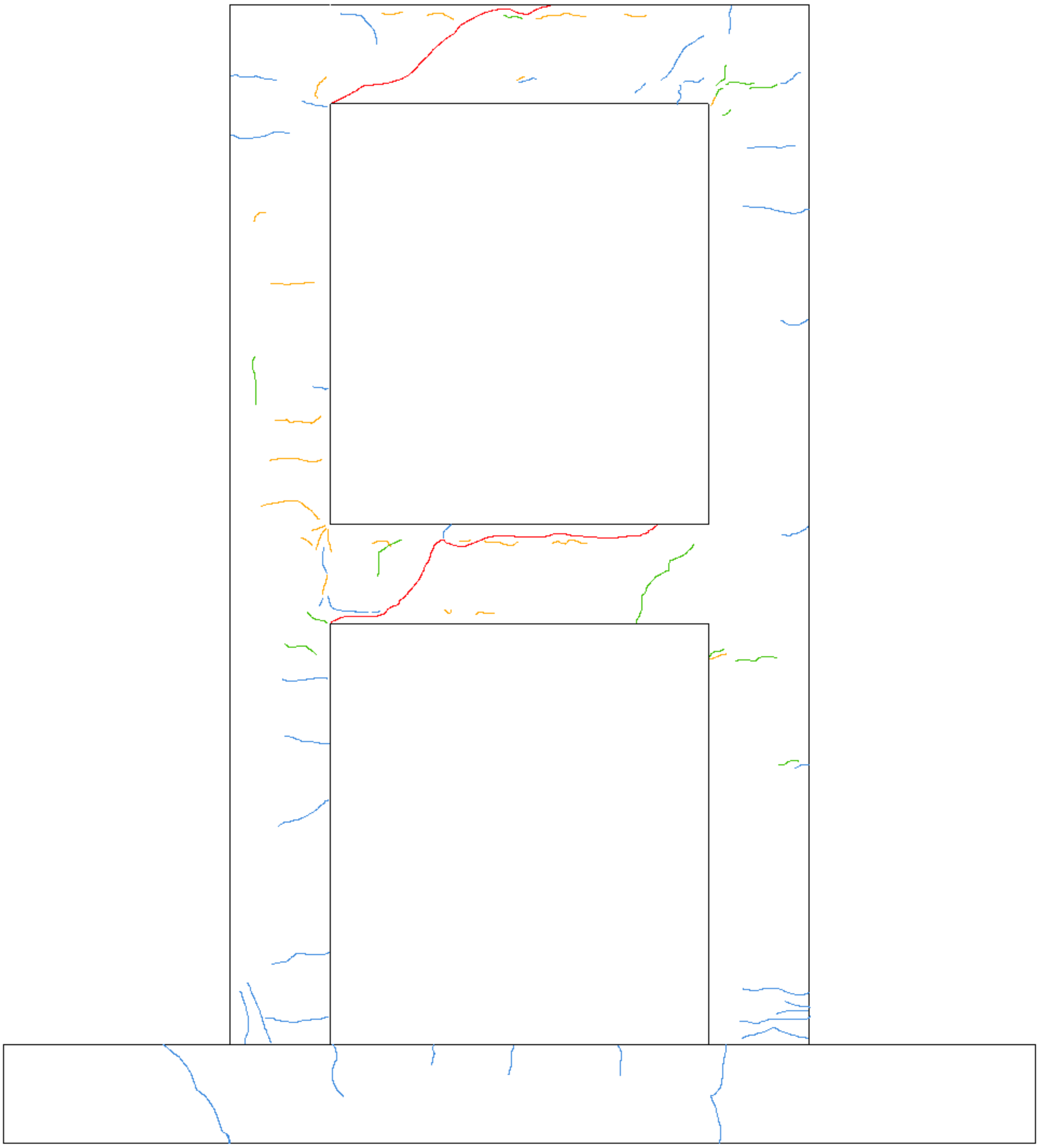

Fig. 3.9: Crack pattern specimen one without shrinkage cracks

The maximum forward static load during de second test reached 27,55 kN with a related lateral displacement of the second storey beam of 26,70 millimetres. After failing of the specimen, the lateral force increased again (like in the first test) until a maximum displacement of 52,40 millimetres was reached. Also, this specimen failed due to shear. Cracks in the lower beam were first observed around 24 kN and failing of the lower beam occurred around 25 kN. Immediately hereafter shear cracks developed in the second storey beam and the whole specimen collapsed at 27,55 kN. The shear crack in the first storey beam was 7,99 millimetres wide and in the second storey beam 14,67 millimetres.

The maximum forward static load in the second test was lower than in the first test because in the second test the stirrups of the second storey beam yielded shortly after 25 kN. Because of this, the stirrups broke and the beam lost its overall strength. This broken stirrup is depicted in *Figure 3.16*.

Table 3.6: Summary of observations during push-over of test specimen two

Specimen Two: Load interval	Load (kN)	Comment
0	0	Application of the compression loads on the columns.
1	10	Existing shrinkage cracks did not continue like in the first test specimen. A small number of new cracks occurred in the right column at the height of the stirrups. This can be explained due to a lack of the concrete cover. The average length of those new cracks was around 35 millimetres. One larger crack arose at the beam-column interface at the lower right corner of the first storey beam with a length of 85 millimetres. These cracks were less than 0,1 millimetres wide.
2	20	Refer to *Figure 3.10*. A new crack arose at the left side of the lower beam and had a length of approximately 125 millimetres and made again an angle of 45 degrees with the horizontal. Another smaller crack continued out of the previous crack at the at the beam-column interface at the upper right corner with a length of 30 millimetres. Also, a crack was noticed at the beam-column interface at the upper left corner of the second storey beam with a length of approximately 100 millimetres. All these cracks widened around 0,1 millimetres.
3	24	First beam shear crack occurred at the first storey beam and extended through the entire depth of the beam like happened in the first test. This crack was 1,0 millimetres wide and made an angle of 45 degrees with the horizontal and developed out of the crack which was mentioned in load interval two. Also, the first column flexural cracks appeared at the base at the right side of both columns. Cracks were evenly distributed and developed from the base up to 700 mm in the column height, and were spaced at approximately 50 millimetres (stirrups were spaced at 45 millimetres). These cracks were around 0,1 millimetres wide.
4	25	Refer to *Figure 3.11*. Collapse of the first storey beam occurred. Then beam shear cracks developed at the second-storey beam. These cracks were 1,5 millimetres wide and made an angle of 45 degrees with the horizontal. Also, a change in structural stiffness was noticed just like in the first test. The beam shear cracks widened, while the flexural cracks in the beams, interfaces, and columns remained stable. Then flexural yielding of the longitudinal reinforcement bars and the stirrups occurred. Because of this, the shear cracks in the beams widened.
5	27,55	Refer to *Figure 3.12*. The specimen failed due to a collapse of the second storey beam after a collapse of the first storey beam. The second storey beam collapsed due to a yielding of the stirrups. Because of this, the stirrups broke and the beam lost its overall strength and the total frame collapsed. Also, additional flexural cracks were observed at the right side of each column and between the columns at the foundation. The opening of these flexural cracks is not increased.

Fig. 3.10: Specimen two at load interval 2 [19]

Fig. 3.11: Specimen two at load interval 4 [19]

Fig. 3.12: Specimen two at load interval 5 [19]

Fig. 3.13: Specimen two after loading and removing measure equipment [19]

In *Figure 3.14* is the crack pattern for the second test specimen depicted. This drawing shows all the cracks including the shrinkage cracks. In *Figure 3.15* is only the crack pattern due to the forward static load shown, so here the shrinkage cracks are not mentioned. The next legend serves as a clarification of the two figures:

- Black = shrinkage cracks;
- orange = cracks mentioned after 10 kN of lateral load;
- green = cracks mentioned after 20 kN of lateral load;
- bleu = opening of the first significant cracks;
- red = shear cracks that causes structure failure of the test specimen.

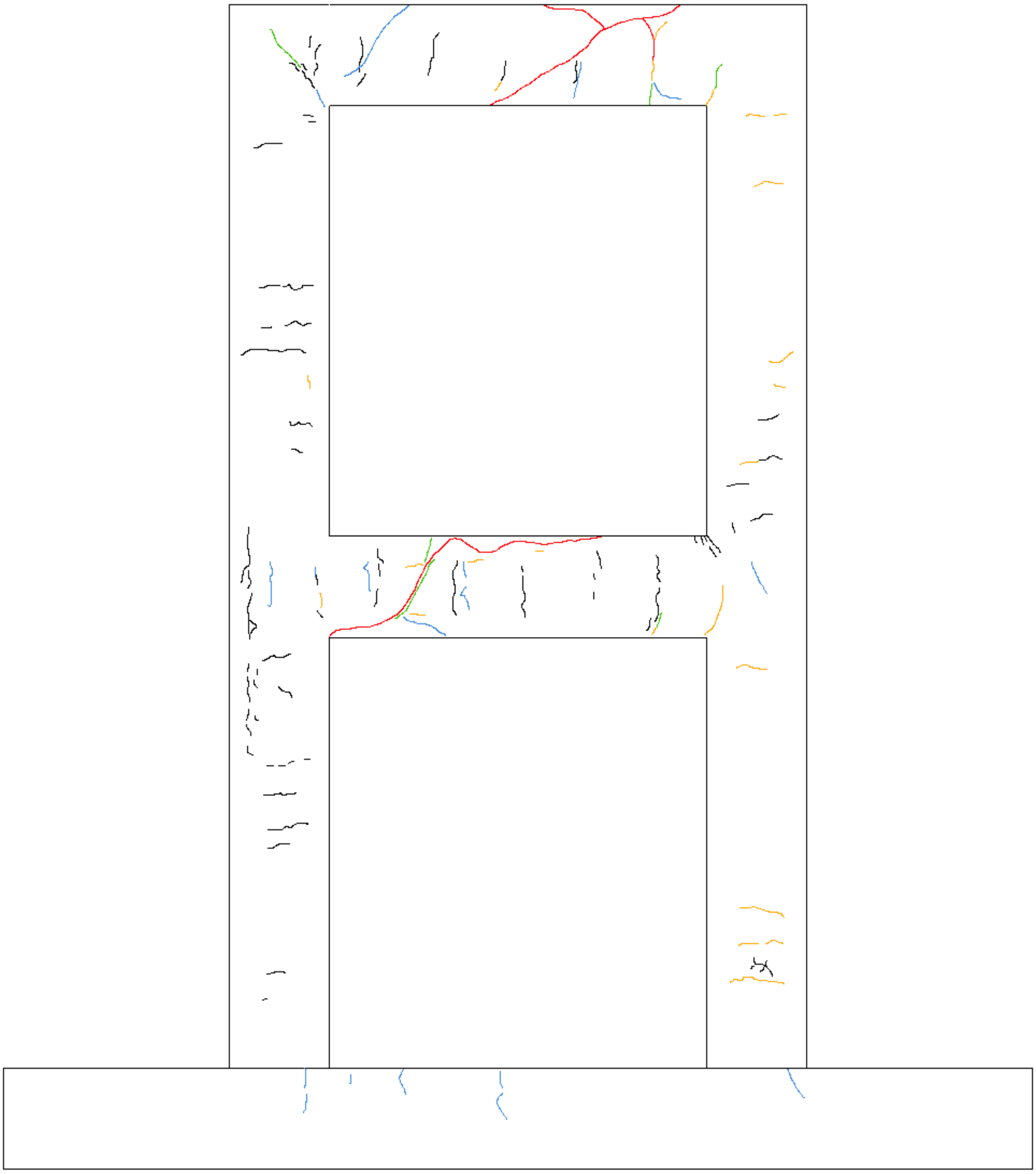

Fig. 3.14: Crack pattern specimen two including shrinkage cracks

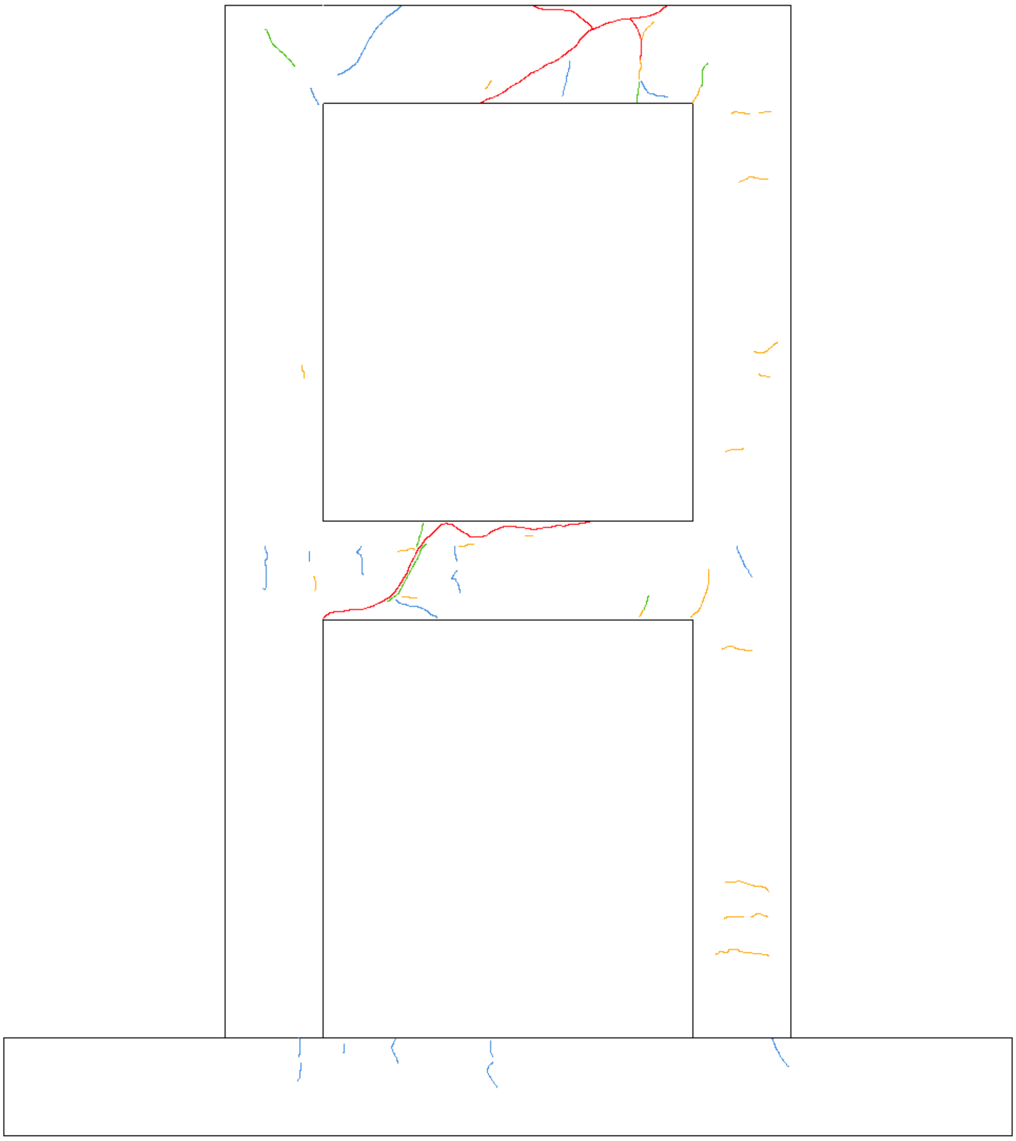

Fig. 3.15: Crack pattern specimen two without shrinkage cracks

Fig. 3.16: Collapse stirrup second storey beam specimen two [19]

3.3.3 Specimens response graphs

This section presents the graphs of the response of the specimens. Only the source data out of the test process and the descriptions of these graphs are mentioned in this section. A comprehensive discussion of these graphs is given in part *3.4 Discussion of results*. In *Graph 3.1* is the absolute second storey displacement perpendicular to the lateral force for specimen one and two plotted. *Graph 3.2* is shown the second storey displacement out of the first test. Similarly, is in *Graph 3.3* the second storey displacement out of the second test depicted. *Graph 3.4* illustrates the two previous graphs to see the similarities and differences in structural behaviour and failing mode between the two specimens.

From *Graph 3.5* to *Graph 3.7* is shown the results of LPT three. This one was located in extension of the first storey beam. The measuring of this LPT related to the lateral force for the first specimen is depicted in *Graph 3.5*. In *Graph 3.6* is the same relation plotted for test specimen two. *Graph 3.7* shows (like in the first case) the two previous graphs to see the similarities and differences in structural behaviour and failing mode between the two specimens related to LPT three.

At each graph is the value given on which the specimen lost its overall strength. Specimen one failed at a lateral load of 31350 N and specimen two failed at a lateral load of 27550 N.

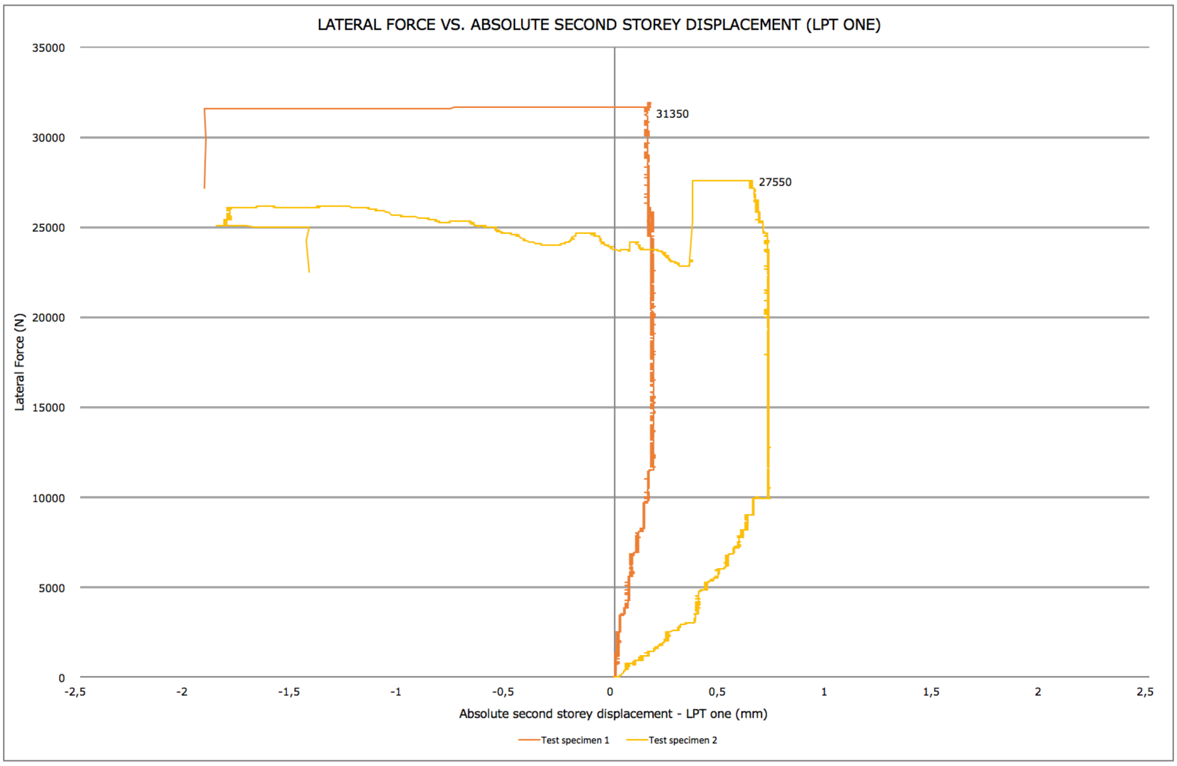

Graph 3.1: Absolute second storey displacement perpendicular to the lateral force – specimen one + two

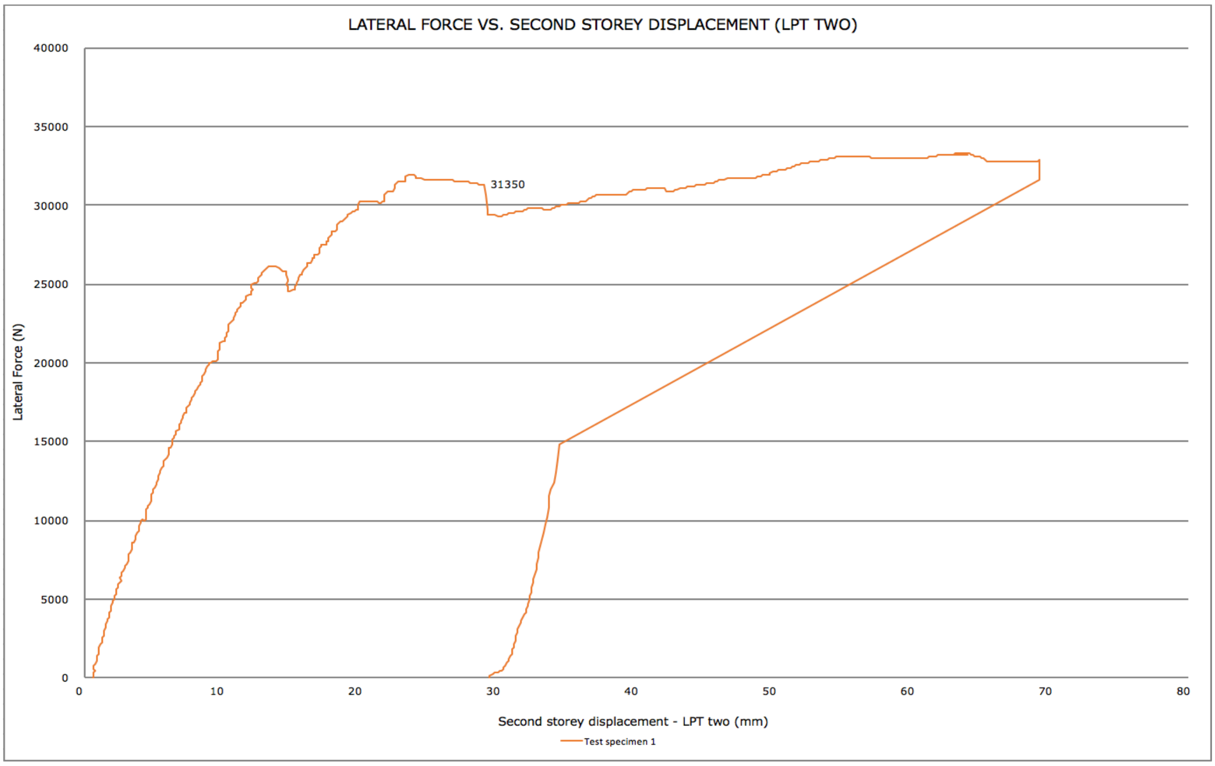

Graph 3.2: Second storey displacement related to the lateral force – specimen one

Graph 3.3: Second storey displacement related to the lateral force – specimen two

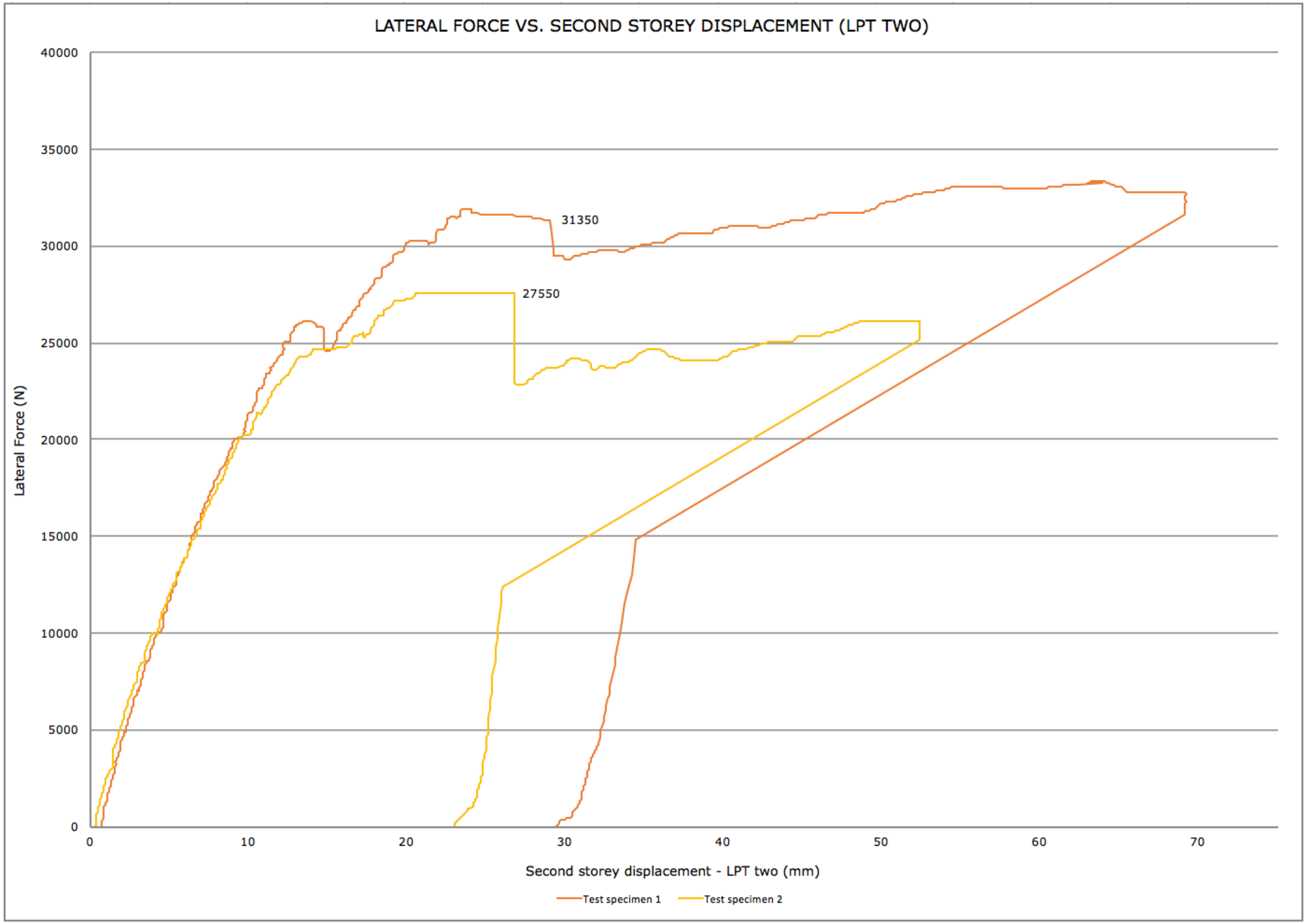

Graph 3.4: Second storey displacement related to the lateral force – specimen one +two

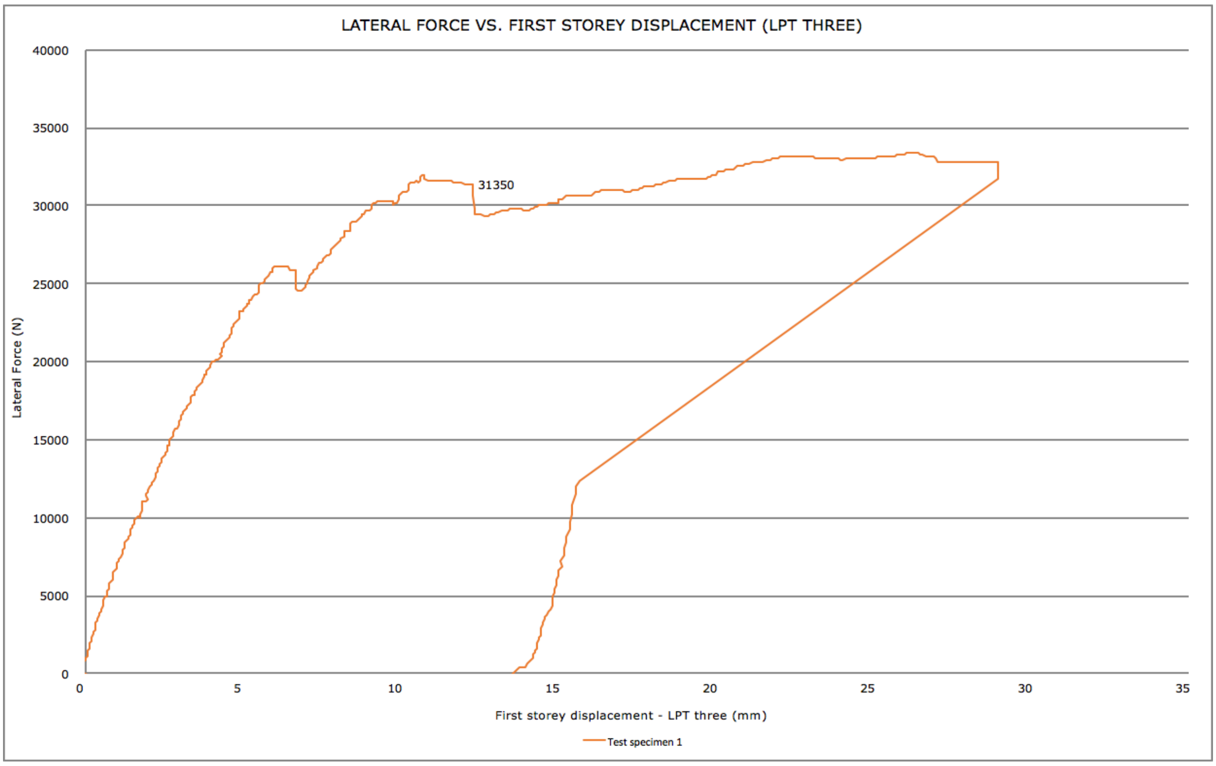

Graph 3.5: First storey displacement related to the lateral force – specimen one

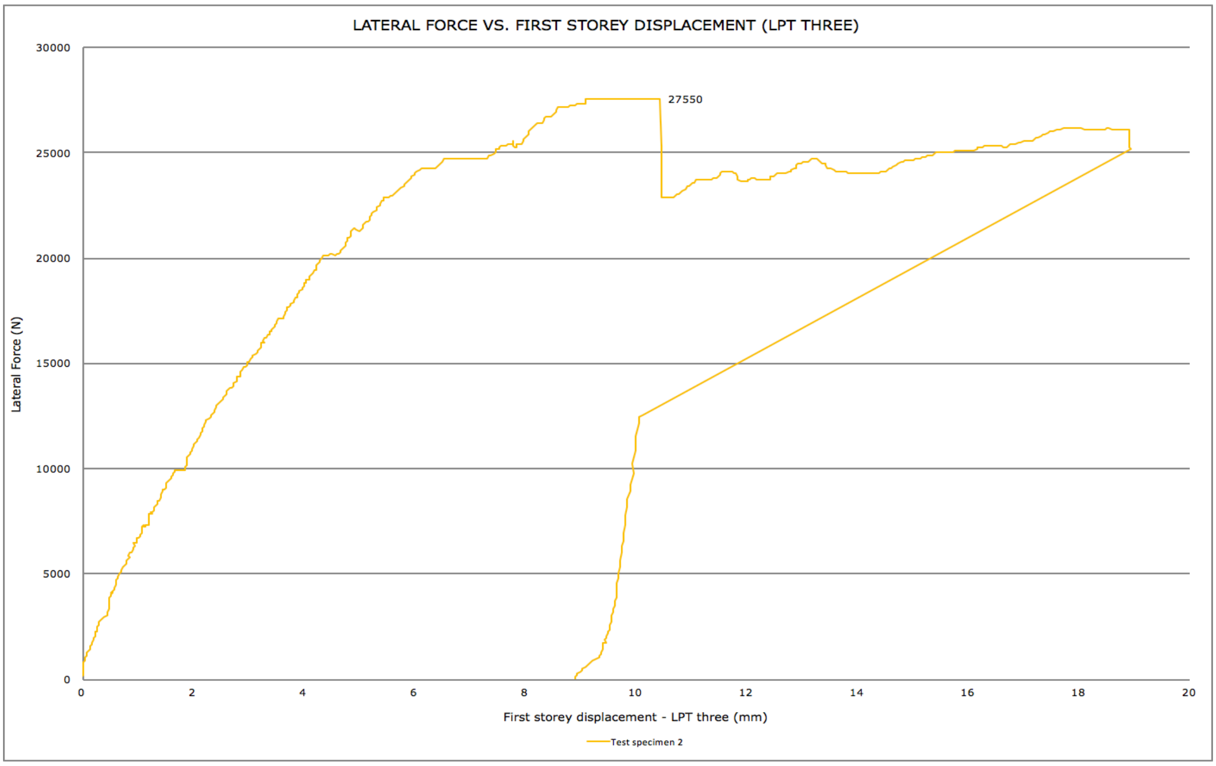

Graph 3.6: First storey displacement related to the lateral force – specimen two

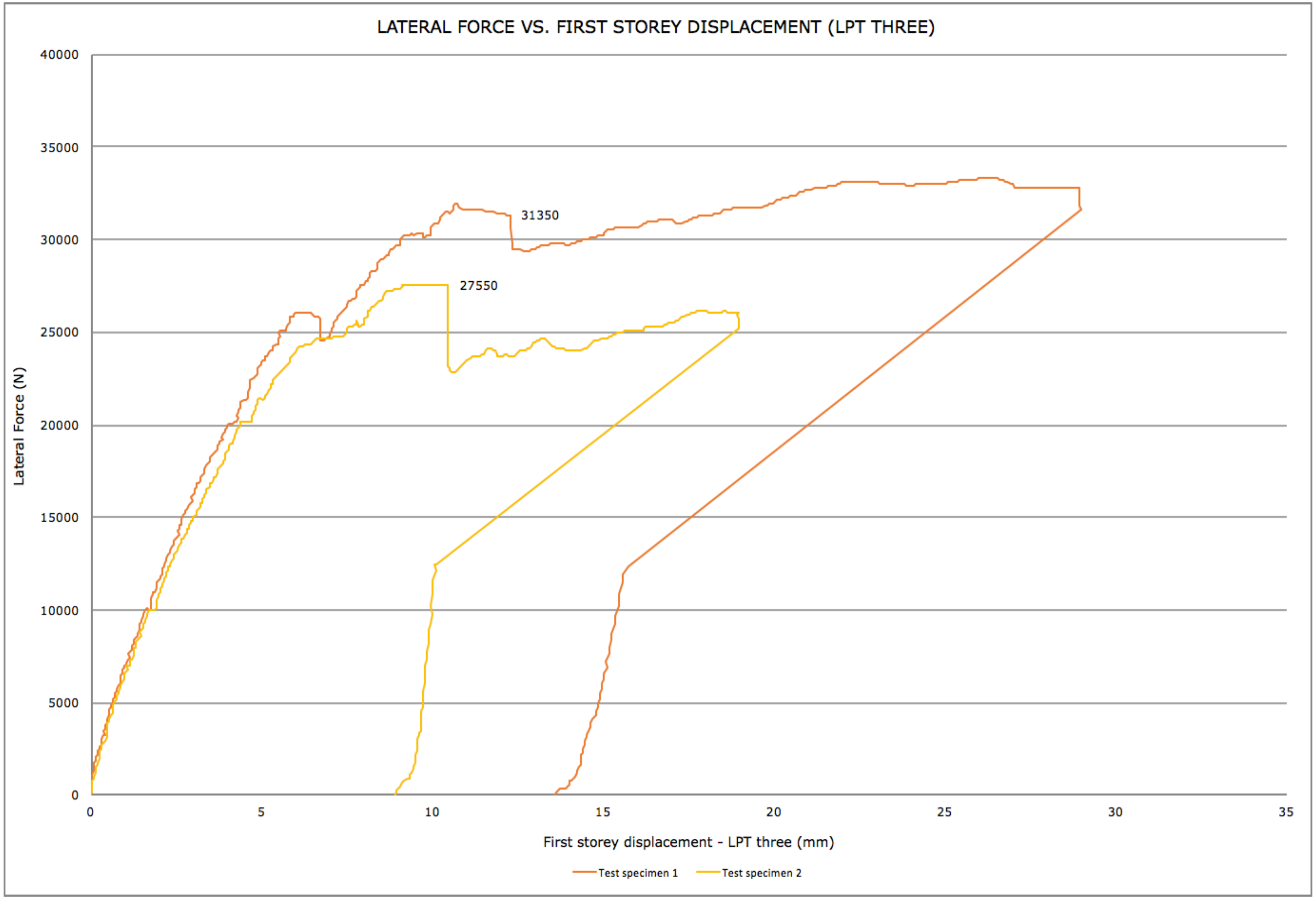

Graph 3.7: First storey displacement related to the lateral force – specimen one +two

3.4 Discussion of results

This section discusses the results out of the experiments from the two specimens with a look to the behaviour of the specimens during the test and the final failing modes. During those tests, there were made analyses on the measuring's of the LPT's. The focus will therefore be on the following topics:

- Progression of the failure mechanism through an analysis of the lateral load versus second-storey displacement graph;
- progression of crack pattern by an increase of the lateral force.

3.4.1 Limitations

Out of these experiments are gathered a big amount of data, so variable points of discussion are possible. Due to a time limit, only the topics mentioned in part *3.4 Discussion of results* are mentioned.

There were also occurring a few problems during the tests. First, the calibration of the inclinometers was not successful. This happened because the cable between the measuring device and the computer was too long. Because of this, the resistance of the cable was bigger than the resistant of the measuring device whereby, the measurement was influenced. Due to this, the inclinometers were not used during the experiment.

The second problem that occurred during the tests was located at the LPT's in extension of the two beams. Due to the deformation of the frame and that the sliding between the LPT and the concrete surface was not possible, the LPT's started to bend in their position. To prevent influence of the measurement results and breakage of the LPT's, the LPT's were released from the concrete surface and put immediately back on. The results gathered due to the replacement of the LPT's are deleted out of the graphs because they do not have any scientific meaning.

3.4.2 Lateral load versus second-storey displacement

The damage mode that was observed in the both tests cases was a primarily shear failure. (Refer to *Figure 3.5* and *Figure 3.11*). Several key moments took place during the tests that affected the structural stiffness of the portal. In general, the moments that had significant changes to the structural stiffness involved either notable shear cracking, or yielding of the stirrups in the beams. Between those key moments, the stiffness of the frame response was linear as depicted in *Graph 3.8*. In this graph is only the second test mentioned because the first test reacted in the same way as the first one. *Table 3.7* serves as a clarification of this graph.

During the forward static load the first initial stiffness was relatively constant until the first significant cracks arose at the beam-column interfaces and in the beams at 20 kN (pt. two). Between 20 kN and 27,55 kN the stiffness decreased. Point three at 27,55 kN occurred shortly after the lower and upper beams collapses due to shear cracks. Due to the ductility phase of the stirrups the displacement increased by a constant force until the portal collapsed (pt. 4). Then, the frame was forced to deform further by an increase of the lateral force. In this phase, the structure found a new stiffness. This came from the flexural strength of the reinforcement bars at the right side in the columns. Also, the friction between the shear planes in the beams provides an increase of the stiffness of the structure. Pont seven forms the end of the forward static loading and in point eight the unloading phase started. The peak lateral load of 27,55 kN was reached at 26,70 millimetres. In test case one the peak lateral load of 31,35 kN was reached at 29,02 millimetres. It is important to point out that in the first test case the frame was forced to deform much further than in the second test. This to investigate or there would occur any significant difference in structural behaviour. This was not the case. This is depicted in *Graph 3.4* and *Graph 3.7* were the graphs have a parallel behaviour.

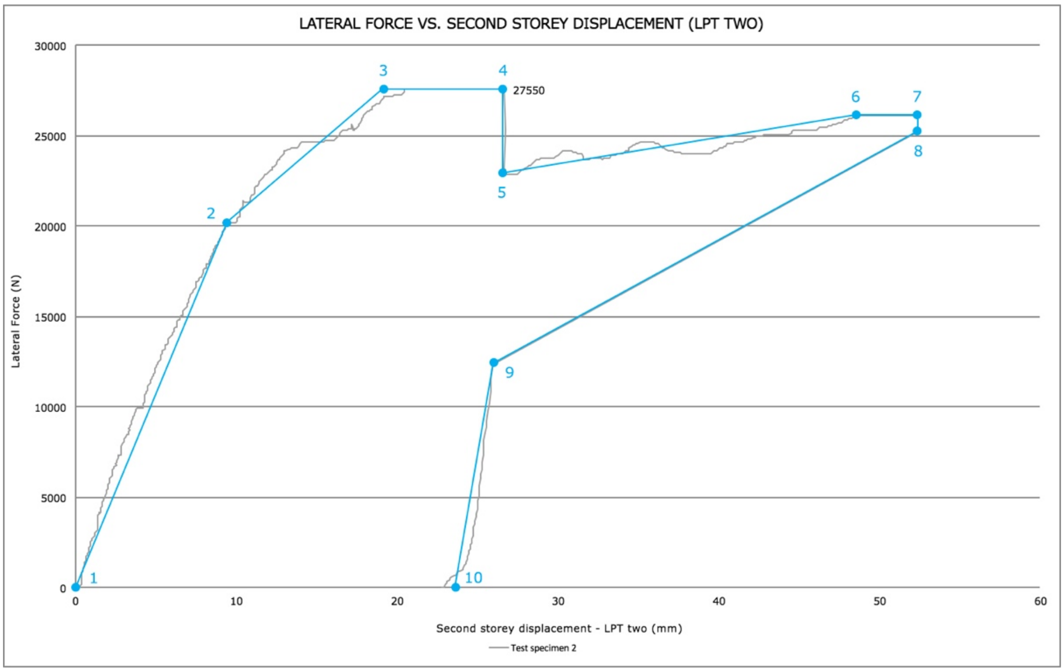

Graph 3.8: Simplified graph of second storey displacement related to the lateral force – specimen two

Table 3.7: Summary of the key moments during the lateral loading

Point	Load (kN)	Load interval	$\Delta\, LPT_2\ (mm)$	Comment
1	0	0	0,23	Initial condition
2	20	2	9,10	Crack arose at the beam-column interface at the upper right corner. Change in structural stiffness shortly after shear cracks in the upper and lower beam. Flexural cracks started to develop in the columns and the foundation.
3	27,55	5	20,72	Ductility phase of the stirrups in the beams.
4	27,55	5	26,70	Collapse of the portal frame.
5	22,85	4	26,80	Two partially isolated vertical cantilevers arose in the structure. Increase of the flexural strength of the reinforcement bars in the columns + increase of the friction capacity between the shear planes in the beams.
6	26,15	5	48,92	Intermediate reading.
7	26,15	5	52,40	End of the static loading.
8	25,15	5	52,40	Start of the unloading phase.
9	12,45	1	26,05	End of the unloading phase.
10	0	0	22,85	Final condition of the test specimen and end of the experimental test.

3.4.3 Crack pattern

The explained crack pattern (Refer to *Figure 3.14* and *Figure 3.15*) is related to the lateral load versus second storey displacement from test specimen two out of section *3.4.2 Lateral load versus second storey displacement*. The crack pattern out of the first test case is almost identical.

The first stage in the developing of the crack pattern was a continuation of the shrinkage cracks. These new cracks became visible by an applied lateral force of 10 kN. At this load stage, also new cracks developed in the front surface of the right column at the height of the stirrups. This can be explained by a lack of the applied concrete cover of ten millimetres. At this load stage the cracks had an average length of 35 millimetres and were less than 0,1 millimetres wide. One crack was larger than the other ones. This was located at the lower right corner of the first storey beam and had a length of 85 millimetres.

In general, when the lateral load and lateral frame deformation increased, the elongation of the beams increased. Due to this elongation, there arise shear cracks. Due to this phenomenon, there arose a first shear crack at 20 kN at the left side of the lower beam and had a length of approximately 125 millimetres. At a lateral load around 24 kN this crack extended through the entire depth of the beam and widened 1,0 millimetres. Also, the first flexural cracks are observed at the base at the right side of both columns. Cracks were evenly distributed and developed from the base up to 700 mm in the column height, and were spaced at approximately 50 millimetres with an opening of 0,1 millimetres.

The next important condition happened at a lateral load of 25 kN, with a collapse of the first storey beam. Immediately after the structural failure of the first storey beam, cracks developed at the second storey beam with an opening of 1,5 millimetres. Then flexural yielding of the longitudinal reinforcement bars and yielding the stirrups occurred. Because of this, the shear cracks in the beams widened. At a peak lateral load of 27,55 kN the second storey beam collapsed. This beam collapsed due to the yielding of the stirrups. Because of this, the stirrups broke and the beam lost its overall strength and the total frame collapsed. Also, additional flexural cracks were observed at the right side of each column and between the columns at the foundation.

A striking determination that can be made is that in both test cases, the first storey beam collapses the first. Immediately after this collapse there arose shear cracks in the second storey beam. This phenomenon can be explained by a calculation of the shear forces and bending moments in the portal frame. This calculation is carried out in SAP2000. In *Figure 3.17* are the static schemes of these calculations depicted. In *Figure 3.17a* are shown the applied forces (45kN compression + 10 kN lateral force), *Figure 3.17b* is a representation of the acting shear forces and *FFigure 3.17c* of the acting bending moments. By this calculation, it becomes clear why the first storey beams first losses his structural strength.

In the SAP2000 model are the specific material parameters out of the experiments used to build the portal frame. On the top of each column is applied a compression force of 45 kN as calculated by *formula 2.3*. A non-increasing lateral load of 10 kN is applied at the upper beam-column interface. The calculation proves that the shear force in the lower beam is higher than the shear force in the upper beam by those applied forces. For this reason, the lower beam first losses his structural strength. After the collapse of the lower beam, there occurs a redistribution of the shear forces. These forces are then largely absorbed by the second storey beam until the acting shear force becomes bigger than the resistance of the second storey beam. After this exceeding of the resistance also this beam will collapse and the frame losses its overall structural strength.

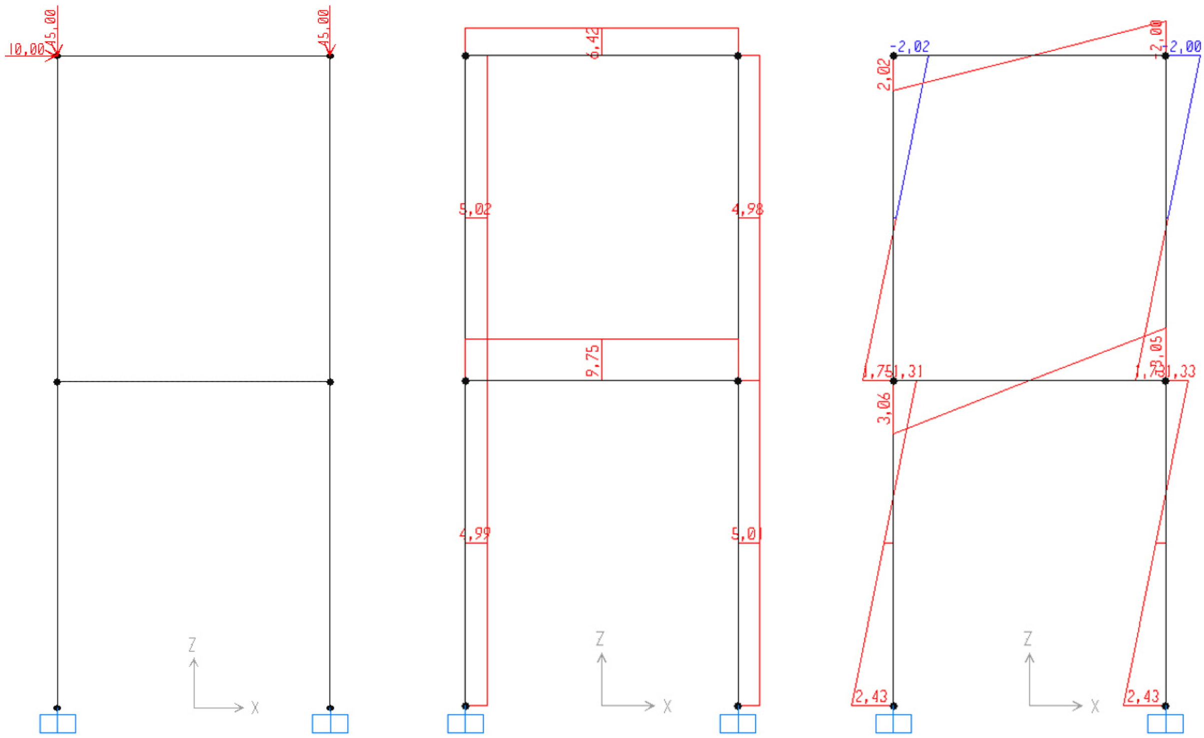

a) b) c)

Fig. 3.17: Static schemes of the test specimen – SAP2000

Fig. 3.18: Cracked specimen one + cracked specimen two [19]

4. FINITE ELEMENT MODELLING

4.1 Introduction

As an augmentation of the experimental analysis, an analytic model of the test specimen is developed using the finite element software TNO DIANA. This software is developed in a spin-off company from the Computational Mechanics department of TNO Building and Construction Research Institute in Delft, The Netherlands. The modelling process is discussed in this chapter. Specifically, the techniques that are used related to the support conditions and, concrete- and reinforcement elements. Results of this finite element analysis and a discussion of these results are mentioned in chapter *5. Finite Element Results*. A comparison between the experimental- and numerical results is given in chapter *6. Comparison Experimental- vs. Finite Element Results*.

4.2 TNO DIANA modelling

By using TNO DIANA as modelling software, there is the advantage that there is no external pre-processor needed to build the finite element mesh. In contrast to other software such as VecTor2 where the mesh is built in the pre-processor FormWorks, it is possible in this software to build the mesh in the software itself. The portal frame was completely modelled using quadratical elements that were a representation of the concrete and the reinforcement bars. Refer to the TNO DIANA manual for a complete summary of the possible functions of the program. The version that is built in this master's thesis is a model where perfect bond between the concrete and reinforcement is assumed. In part 4.3 follows a summary of the characteristics of the model. This part is focusing on the used procedures and on the several facets of the finite element mesh. The build mesh is depicted in *Figure 4.1*.

In structural analysis, a commonly used type of analysis, using numerical techniques, involves the assumption of small strains and linear elastic behaviour. However, this is only valid for small applied loadings. Therefore, linear analyses are usable in cases where simple direct solution are expected or in superposition cases. So, a linear equation can just be solved in a single iteration and has a unique solution. However, there are situations where nonlinear effects must be incorporated for a realistic assessment of the structural response. These non-linearity's are categorized into three cases.

The first case is a physical nonlinear analysis wherein the plasticity or the cracking of a structural model will be studied. The second case is a geometric nonlinearity, wherein significant changes in geometry are observed due to large deformations. The third case is a material nonlinearity, which arises when stress-strain behaviour ceases to be linear or, more precisely, when material properties change due to the applied loads. So, a nonlinear analysis is also usable for situations where there need to be done an analysis of the failure mechanism of a structure or an evaluation of the failure mode of an existing structure. So, to solve nonlinear analyses, there are required multiple iterations.

The use of a nonlinear analysis has also several consequences. For example, the superposition method can no longer be applied, only one load situation can be handled at a time, the response of the structure can be non-proportional to the applied loading because there are several solutions possible, et cetera. The difference between a linear and a nonlinear behaviour is schematic depicted in *Figure 4.2*. Out of this summary there can be concluded that in this master's thesis is chosen to obtain a nonlinear analysis. This, because the specimen is loaded until structural failure occurs. [20]

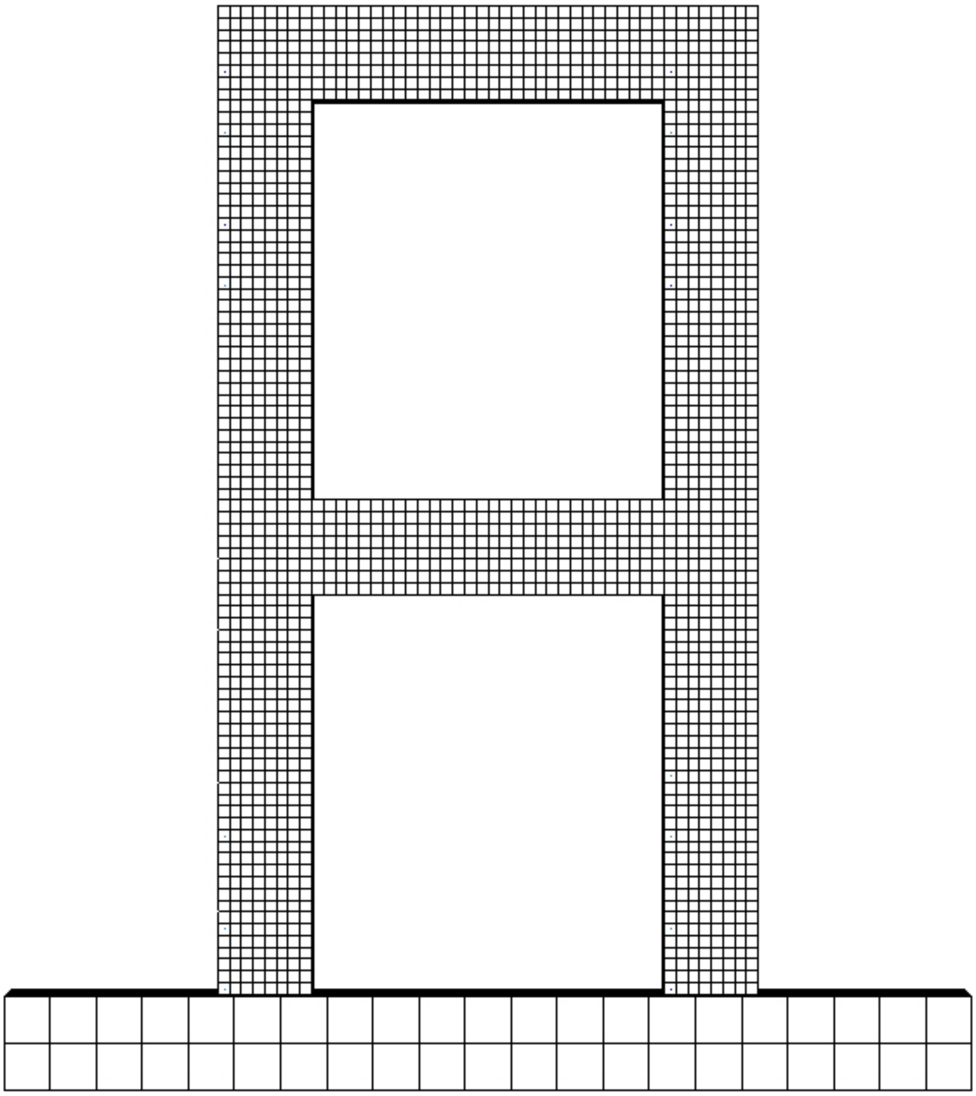

Fig. 4.1 Concrete Finite Element Mesh

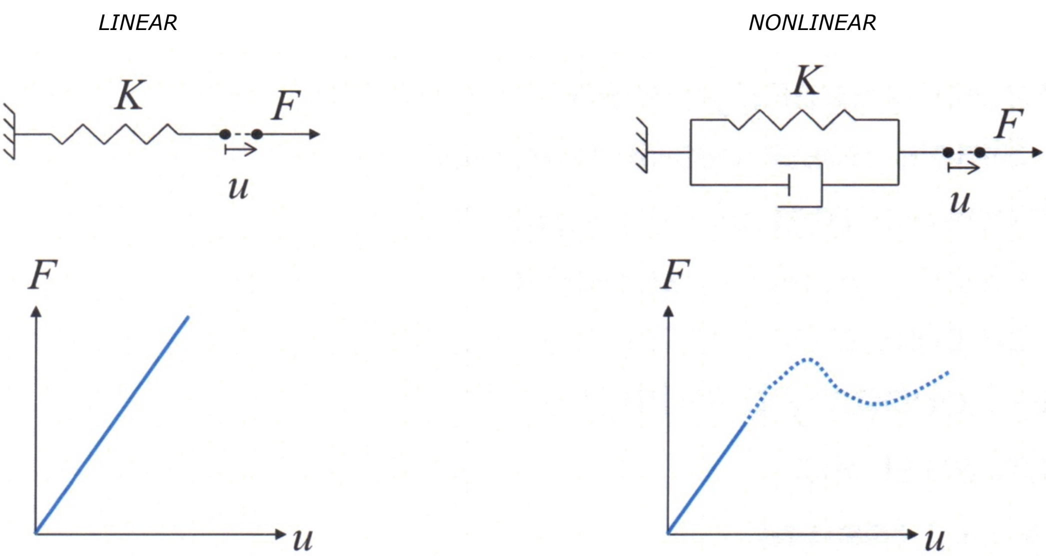

Fig. 4.2 Difference between a linear and a nonlinear behaviour [20]

4.2.1 Support conditions

In the experimental setup, the frame was connected to the test bench with four threaded bars diameter sixteen millimetres to obtain a fixed support. There were two sets of two threaded bars located at the outside of the columns. This tensioning force was introduced into the finite element model by applying five clamped supports at the left side of the foundation. Next, the foundation was supported by an infinite rigid floor whereby no deformation of the floor would occur. These are suggested by 105 pinned supports.

The experiment showed that the foundation not slide during the application of the lateral increasing force, which justifies that the pinned supports in the finite element model are correct. The foundation stayed intact with a low amount of damage patterns. The support condition of the foundation is depicted in *Figure 4.3*.

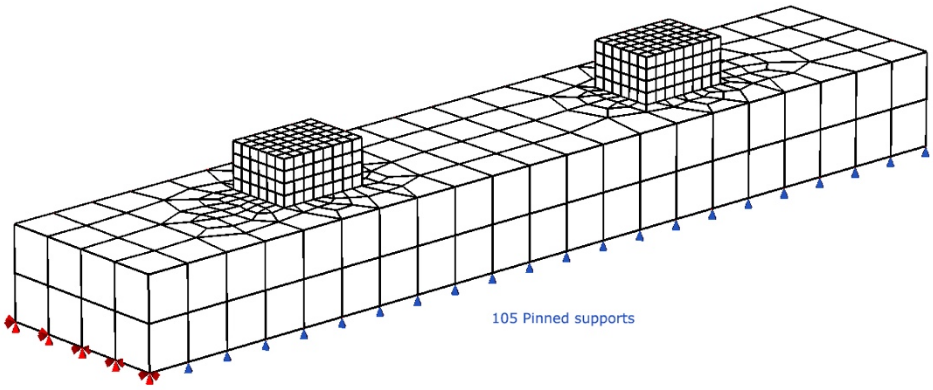

Fig. 4.3 Support condition of the foundation

4.2.2 Concrete elements

Plane stress square elements were used to model the reinforced concrete and to model the concrete cover. In total 11154 concrete elements were used. The elements were 16,67 millimetres on 16,67 millimetres for the columns and the beams and 66,67 millimetres on 66,67 millimetres for the foundation. There is made a difference in mesh size between the foundation and the rest of the frame because the behaviour of the foundation is not the major research topic in this master's thesis. Also, the foundation is oversized whereby the influence of the applied forces on this structural element is very small. By using a larger mesh size for the 'less important foundation' the model must solve less equations and iterations whereby the overall results of each analysis are faster available.

The material model that is used for the mathematical FE modelling of the concrete is the EN 1992-1-2 compressive stress-strain model, depicted in *Graph 4.1*. The section EN 1992-1-2 of the Eurocode is related to the design of structures with a considering of the fire resistance. As creep effects are not considered explicitly, the material models in this part of the Eurocode can be applied for heating rates between 2 and 50 K/min. The compressive stress-strain relationship given in *Figure 4.1* is defined by the compressive strength fc, θ and the strain εc1, θ. The values for these parameters are given in *Table 3.1* of part 3.2.2 Concrete of Eurocode 1992-1-2. The parameters specified in this table can be used for normal weight concrete with aggregates out of pebbles or lime. [20]

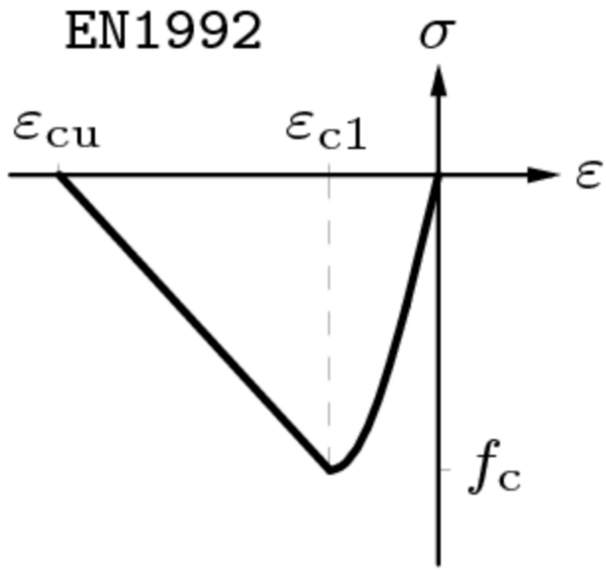

Graph 4.1: EN 1992-1-2 compressive stress-strain model [20]

4.2.3 Reinforcement elements

The used reinforcement is modelled as truss elements. These truss elements are elements with a node one each side and a homogeneous cross-section. Each node has three freedom degrees (x, y, z). The reinforcement is modelled as ductile longitudinal and transversal (stirrups) reinforcement bars in the foundation, columns and beams. The length of each reinforced element in the foundation is 66,67 millimetres and 16,67 millimetres for the rest of the frame. In total 9472 reinforcement elements were used. *Figure 4.4* and *Figure 4.5* illustrates respectively the applied reinforcement layout and the applied reinforcement layout together with the finite element mesh of the concrete.

The reinforcement bars in this model are designed in such a way that complete yielding is possible. There is also assumed a perfect bond between the reinforcement bars and the concrete because out of the experimental tests there can be concluded that there was no slippage between these two constructive elements.

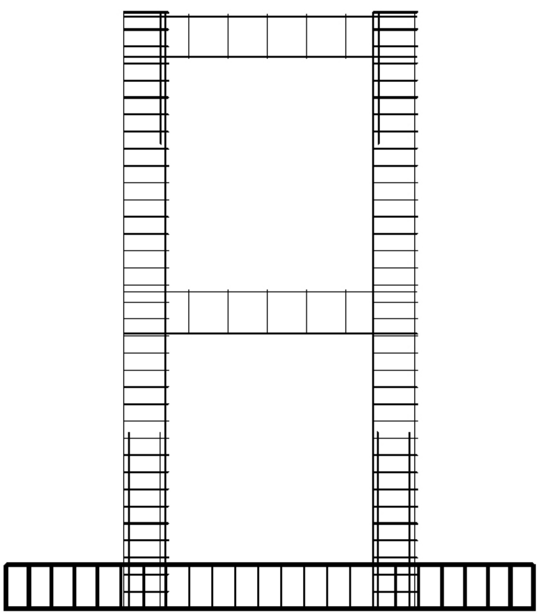
Fig. 4.4 Reinforcement layout

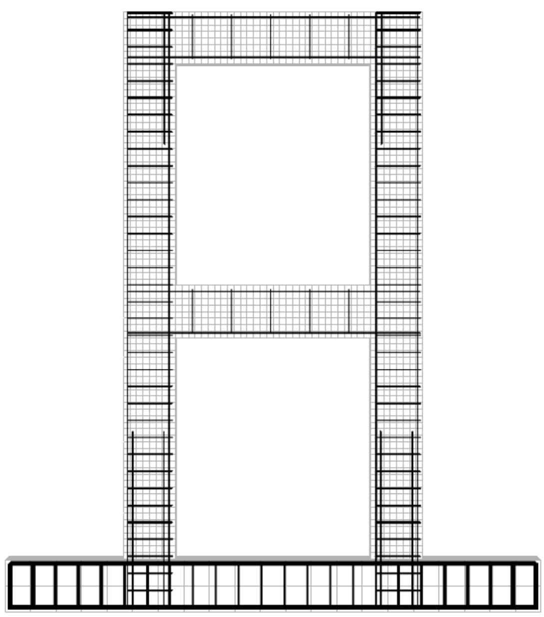
Fig. 4.5 Reinforcement layout + finite element mesh

The material model that is used for the mathematical FE modelling of the reinforcement is the Von Mises plasticity model with pure kinematic hardening, depicted in *Graph 4.2*. This material model is defined by a bilinear inelastic curve and is used in cases where an elastic material is loaded past the yield strength of the material. When this is achieved, a plastic deformation of the material will occur. The Von Mises plasticity model uses this bilinear inelastic curve to calculate the stresses in the materials (cfr. reinforcement). The elastic part of the stress versus strain curve has a slope equal to the elasticity modulus, and the plastic part of this curve has a slope equal to the strain hardening modulus.

It is important to point out that there are two types of hardening material models available. The isotropic hardening model which yields uniform through the entire surface of the material and the kinematic hardening model which is used is this master's thesis. This kinematic hardening model involves a shifting of the yield surface. The most important zones are the yield strength and the strain hardening modulus and are marked in *Graph 4.1*. The yield strength of a material is the point in the stress-strain curve where the material starts to deform into the plastic strain of the material. After this yielding point, the new yield stress depends on the way of hardening and the history of loading. The strain hardening modulus of the curve is the slope of the stress-strain curve after the yielding point.

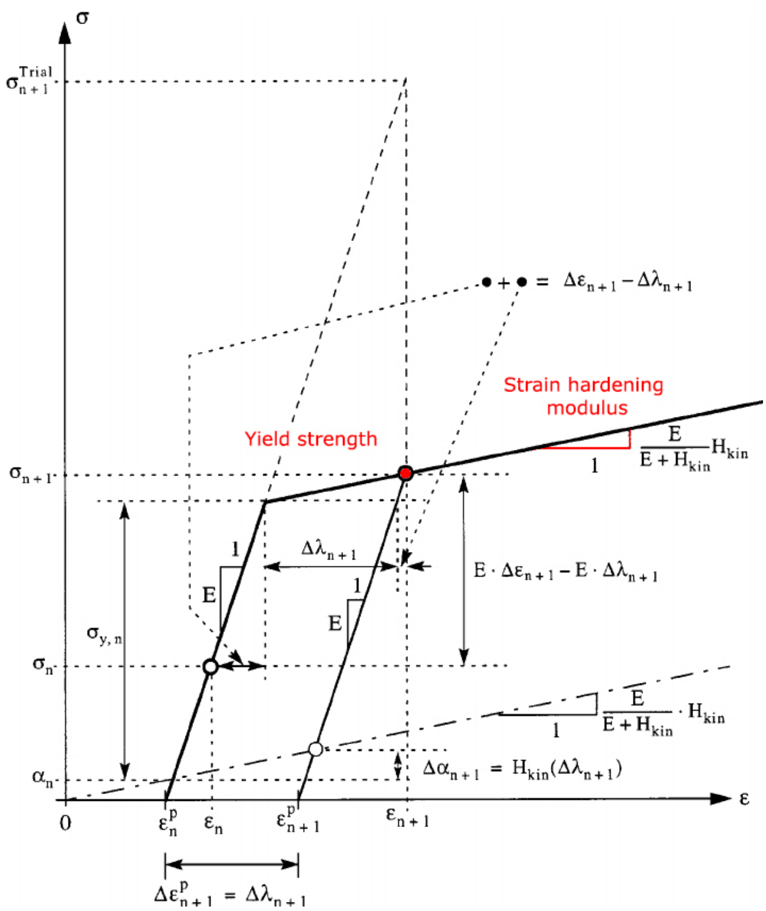

Graph 4.2: Von Mises plasticity model with pure kinematic hardening [20]

4.2.4 Loading conditions and procedures

In the experimental part of this master's thesis, a stabilizing force of 45 kN as calculated by *formula 2.3* was applied at the top of each column along steel distribution plates. In the FE model is a load of 0,71 kN applied at 63 nodes at the top of each column. This stabilizing load was held constant through the entire analysis procedure. The lateral increasing load at the right side of the right column at the height of the second storey beam is also applied at 63 nodes. The complete loading combination used in the FE model is illustrated in *Figure 4.6*.

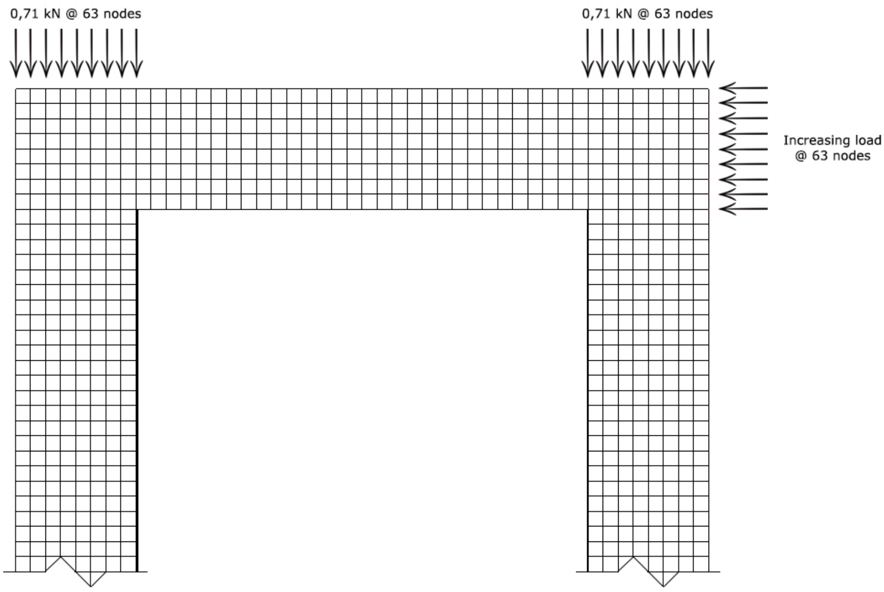

Fig. 4.6 Lateral – and horizontal loading

4.2.5 Analysis procedure

The solution of an analysis of a nonlinear finite element model, is a system of nonlinear equations, for which an incremental-iterative solution procedure need to be applied. The incremental-iterative method that is used in this FE model is the regular Newton-Raphson method whose curve is depicted in *Graph 4.3*.

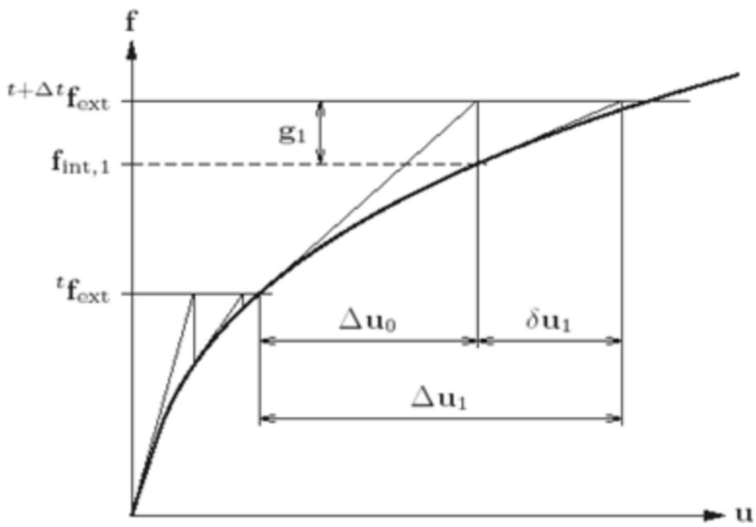

Graph 4.3: Regular Newton-Raphson method [20]

In this incremental-iterative method is the tangent stiffness matrix derived at every iteration. The general mathematical formula behind the model has the form:

$$[K_T(U_t)]\,.\{\Delta U\} = \{F_{EXT}(U_t)\} - \{F_{INT}(U_t)\} \tag{4.1}$$

In this formula is $\{\Delta U\}$ the displacement increment, and $[K_T(U_t)]$ the tangent stiffness matrix in function of (U_t) at step t. The result out of this equilibrium is:

$$\{F_{EXT}(U_{t+\Delta t})\} - \{F_{INT}(U_{t+\Delta t})\} = 0 \tag{4.2}$$

$U_{t+\Delta t}$ out of *formula 4.2* is the total displacement at step $t + \Delta t$ and can be defined as:

$$U_{t+\Delta t} = U_{t+\Delta t} + \Delta U \tag{4.3}$$

Before *equation 4.1* can be used, there need to be done first a determination of the load incrementation, which is the linearization of the nonlinear problem. Depending on the shape of the equilibrium path, there are three types of load incrementations possible: force control, displacement control and arc-length control. In this FE model are used the force control (*graph 4.4a*) and arc-length control with a snap-through approach (*Graph 4.4b* + *Graph 4.4c*).

In the force control are the loads incrementally applied. A load control analysis is applied to models with continuous force increasing or without softening behavior and limits. Consequently, if there is a softening behavior or there are limits in the model then, the pure load incremental procedure does not lead to a solution. This in the case that the applied load is bigger than load capacity of the model.

In the arc-length method are the incremental displacements constrained. In this method, the applied load factors are varying from load steps defined by the user. Because step sizes are not applied to the applied load but to the combination of force and displacement. This arc-length method is combined with the snap-through procedure. This is a procedure to predict the behaviour of the model, wherein the iteration process is searching for solutions that are always laying in front of the previous calculated value and never behind the previous calculated value [20].

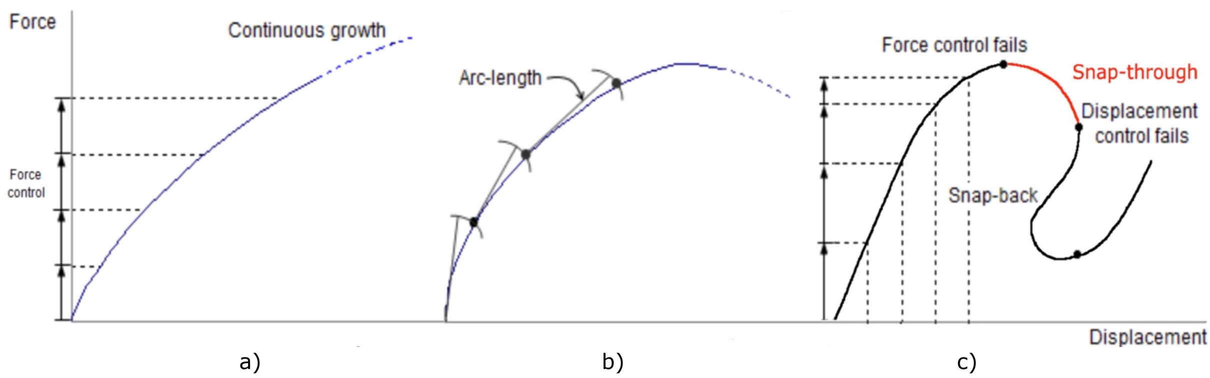

Graph 4.4: Used load incrementation procedures – TNO DIANA [20]

5. FINITE ELEMENT RESULTS

5.1 Introduction

The results of the finite element analysis for both prototype and the scaled model are mentioned in the different subdivisions of part *5.2 Results*. In this part, the emphasis of the results is placed on the crack-widths in the z-direction, the total compression stresses in the concrete, the displacement of the frame and its element in the x-direction and, the total stresses in the reinforcement in the x- and z-direction. A discussion of these results is given in part *5.3 Discussion of results*. Out of this discussion of the results is the failure mode formulated.

5.2 Results

5.2.1 Prototype

A. Crack-widths (z-direction)

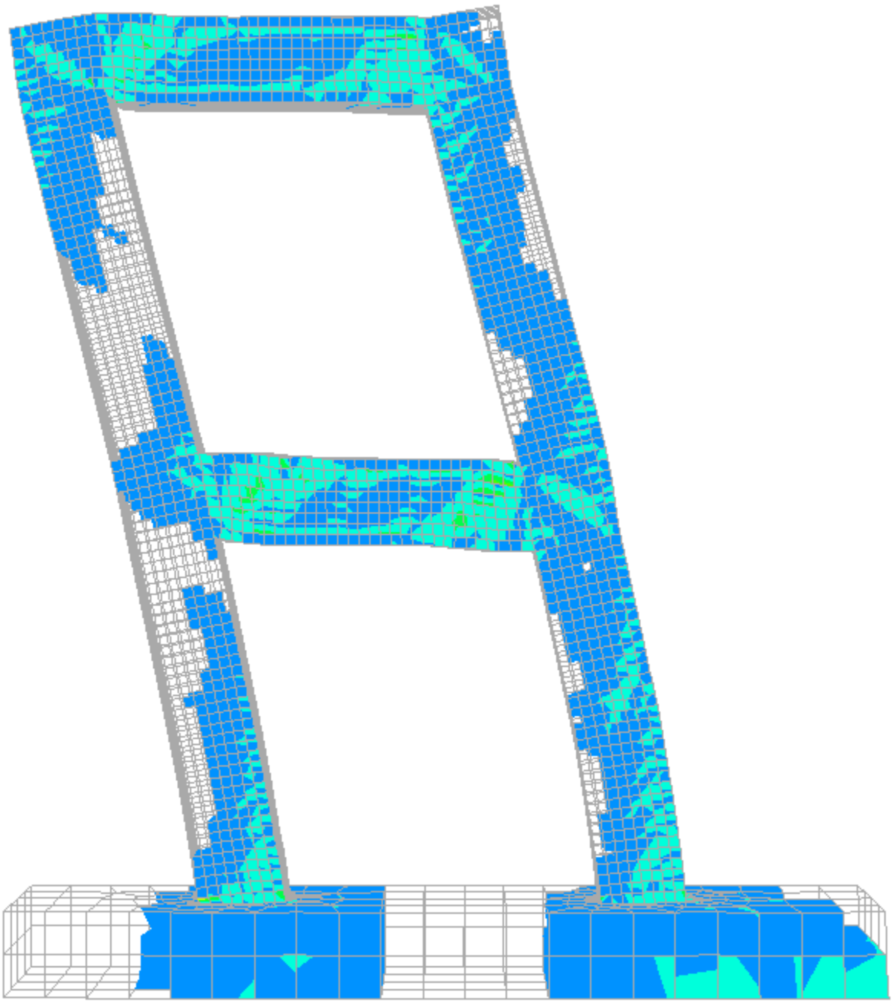

Fig. 5.1: Crack pattern in the z-direction – Prototype

B. **Displacements (x-direction)**

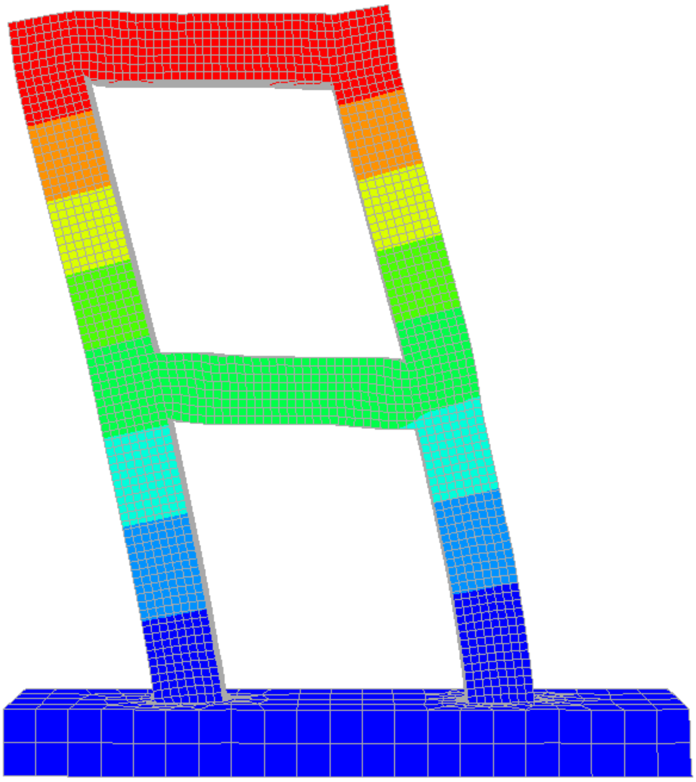

Fig. 5.2: Total displacement in the x-direction – Prototype

C. **Total compression stresses concrete S3**

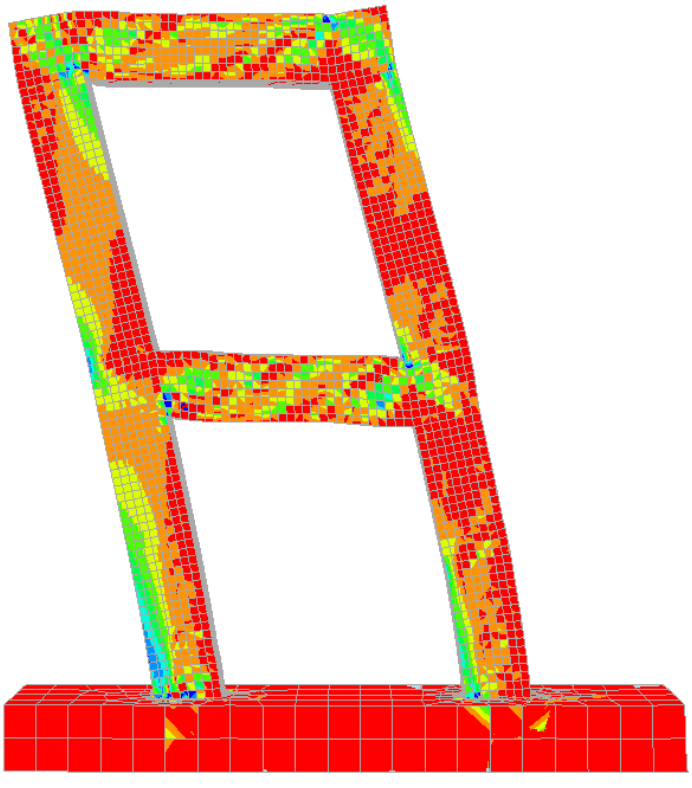

Fig. 5.3: Total compression stresses in the concrete in the 3th direction – Prototype

D. **Total stresses reinforcement (x-direction)**

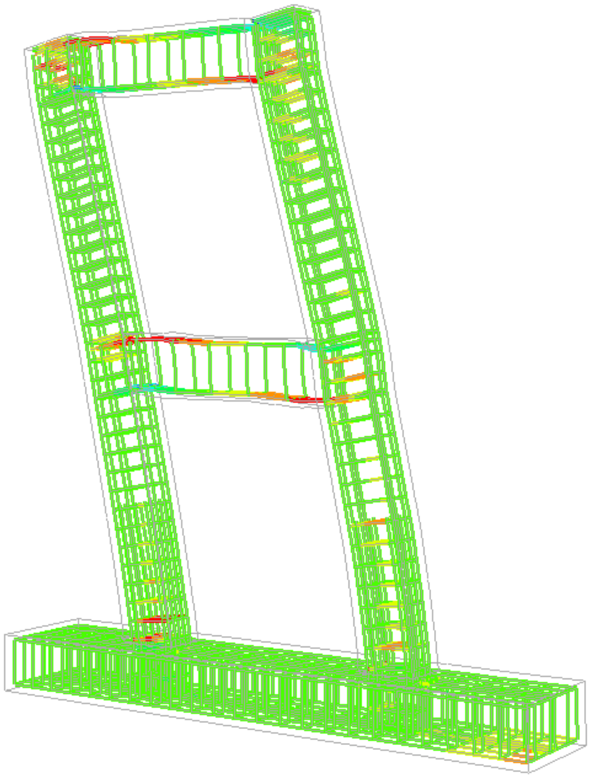

Fig. 5.4: Total stresses in the reinforcement in the x-direction – Prototype

E. **Total stresses reinforcement (z-direction)**

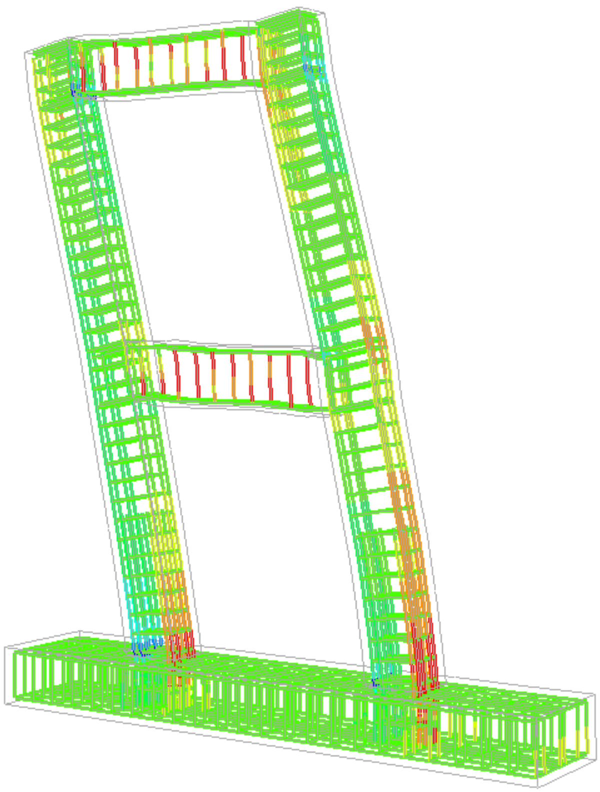

Fig. 5.5: Total stresses in the reinforcement in the z-direction – Prototype

F. Load-displacement second storey

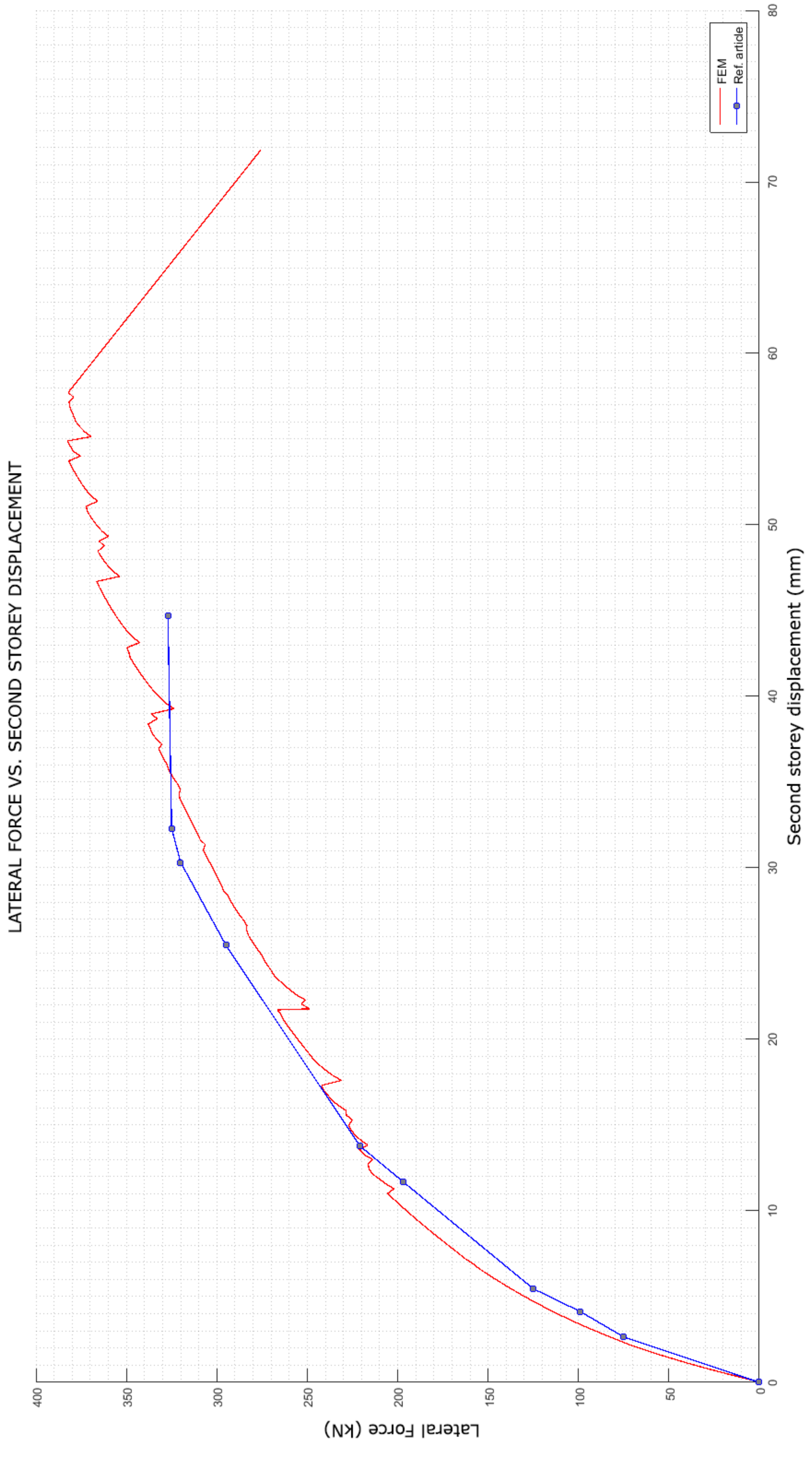

Graph 5.1: Second storey displacement related to the lateral force – Prototype

G. Failure mode

The frame design was based on a weak beams and strong columns. The failure mode of the prototype can be derived out of the crack pattern that is depicted in *Figure 5.1*. Finally, the frame failed due to a combination of bending + shear. Bending occurred in the beams and in the right side of each column. These flexural cracks had a maximum opening of 0,56 millimetres (light blue zones in *Figure 5.1*). The flexural cracks in the beams are showed by the long horizontal cracks. These cracks show a failure (friction loss) between the concrete and the longitudinal reinforcement bars.

The shear cracks occurred exclusively in the beams. These shear cracks are showed by the diagonal cracks visible in the beam with a maximum opening of 0,56 millimetres. These arose due to an activation of the compressed strut in the concrete. These typical cracks are also visible at the joint between the columns and the beams. Due to this shear force, the stirrups started to yield. First, the stirrups at the lower beam yielded and after that the stirrups of the upper beam.

H. Discussion of results

Figure 5.2 shows the deformation of the frame. It is obvious that the second storey beam has the highest lateral deformation because the lateral force is applied at this level. This maximum deformation is 59,83 millimetres, and the lowest deformation is zero millimetres at the level of the clamped foundation.

In *Figure 5.3* is the total compression stress in the concrete depicted. In this figure are the compressed struts in the beams clearly visible (diagonals). The maximum compression occurs at the left side of the left column with a value of 35 N/mm^2. Refer to *Figure 3.7* for a similar concrete crushing.

Figure 5.4 shows the maximum stresses in the reinforcement in the x-direction. The maximum of 473,49 N/mm^2 occurs at the upper left side and at the lower right side of the beams. This value is higher than the yielding point of the longitudinal bars (447 N/mm^2 – refer to *Table 1.4*) and for this reason the reinforcement started to yield in these areas.

In *Figure 5.5* are also the stresses in the reinforcement depicted but for the reinforcement in the z-direction. In this figure, it is clearly visible that the highest stresses are located in the stirrups of the beams. Due to this, the stirrups started to yield and the beams failed due to shear. Also, in the right side of the columns are observed high stresses. These are linked to the bending of the columns. The maximum value for the shear stresses out of this figure is 501,97 N/mm^2 and is almost equal to the yielding point of the stirrups (506 N/mm^2 – refer to *Table 1.4*).

In *Graph 5.1* is the second storey displacement related to the lateral force plotted. The red line out of this graph shows the obtained calibration of the own numerical model. This graph shows a pretty good approach of the results obtained in the experiments at the University of Toronto. At the early stage of the elastic zone, the red curve is almost equal to the blue one. A difference between the two curves arise in the ultimate zone. This is because of a continuation of the numerical model till the failure point was reached. In the experiments at the University of Toronto they did not go till the failing point because they wanted to have the potential to repair the frame, and to test those repaired zones.

5.2.2 Scaled model

A. Crack-widths (z-direction)

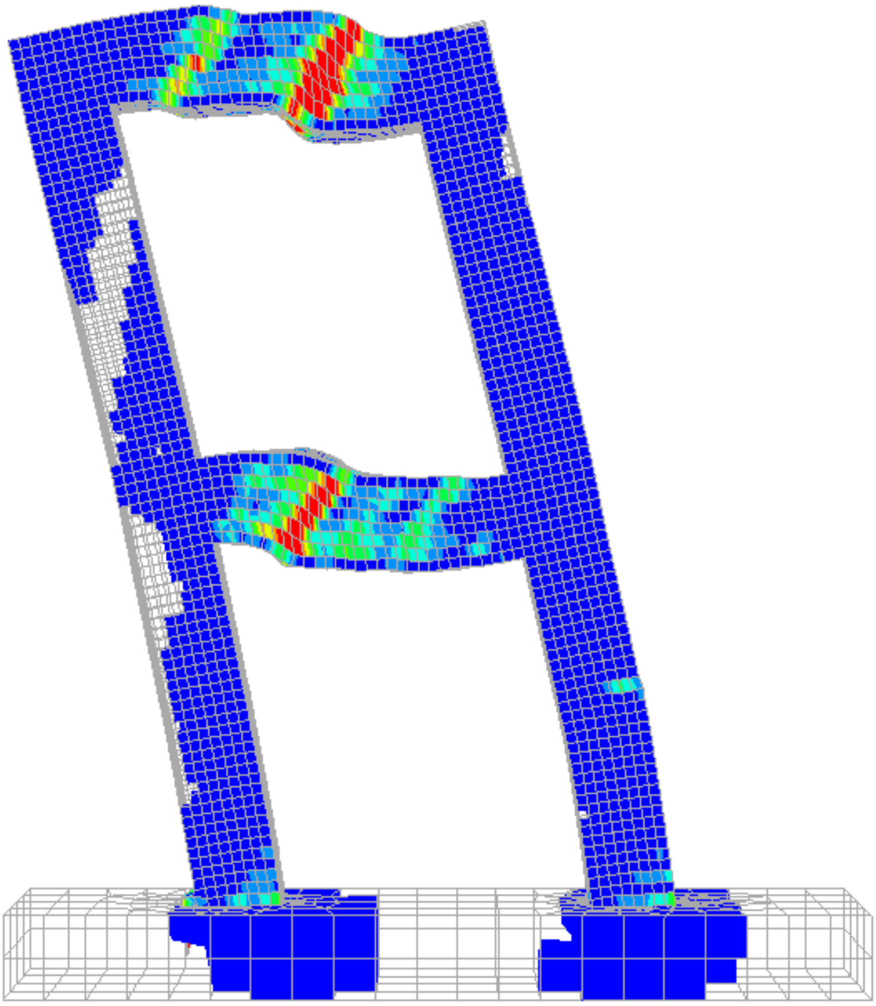

Fig. 5.6: Crack pattern in the z-direction – Scaled model

B. Displacements (x-direction)

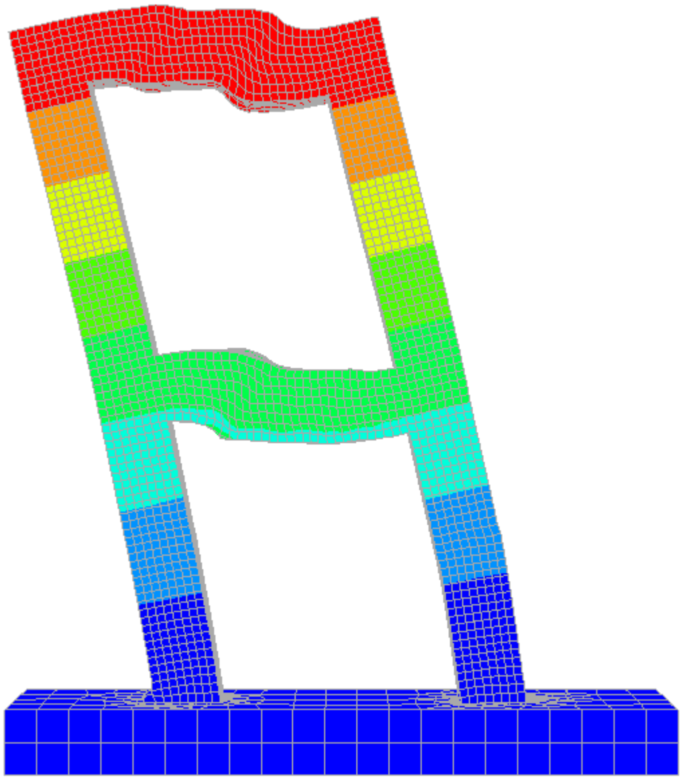

Fig. 5.7: Total displacement in the x-direction – Scaled model

C. Total compression stresses concrete S3

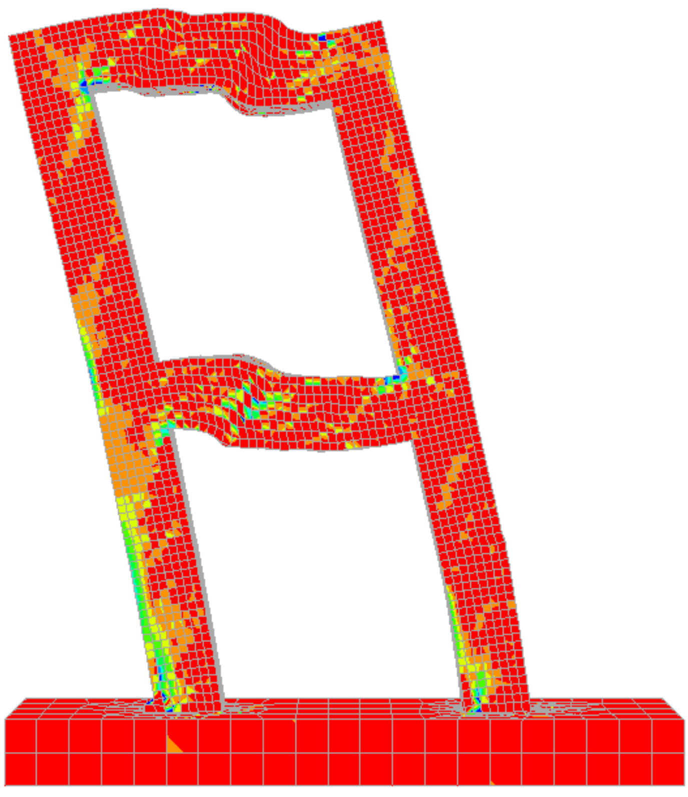

Fig. 5.8: Total compression stresses in the concrete in the 3th direction – Scaled model

D. Total stresses reinforcement (x-direction)

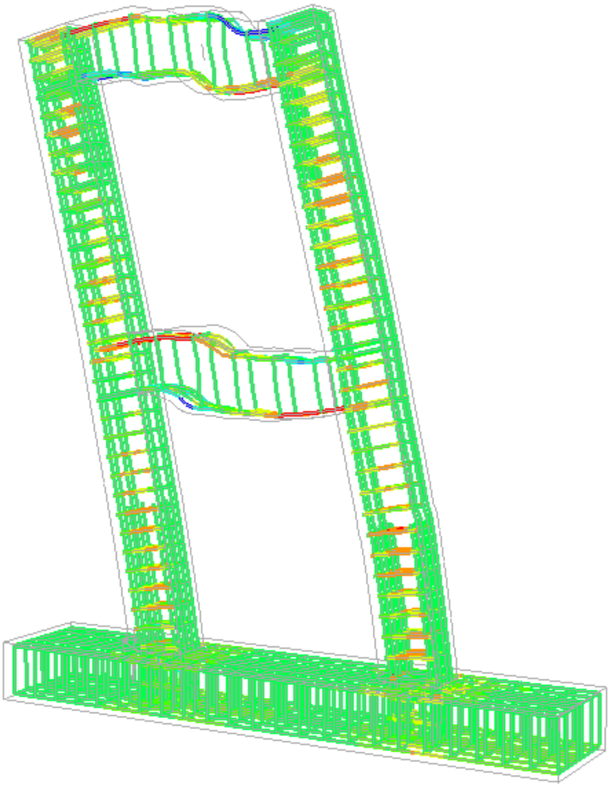

Fig. 5.9: Total stresses in the reinforcement in the x-direction – Scaled model

E. Total stresses reinforcement (z-direction)

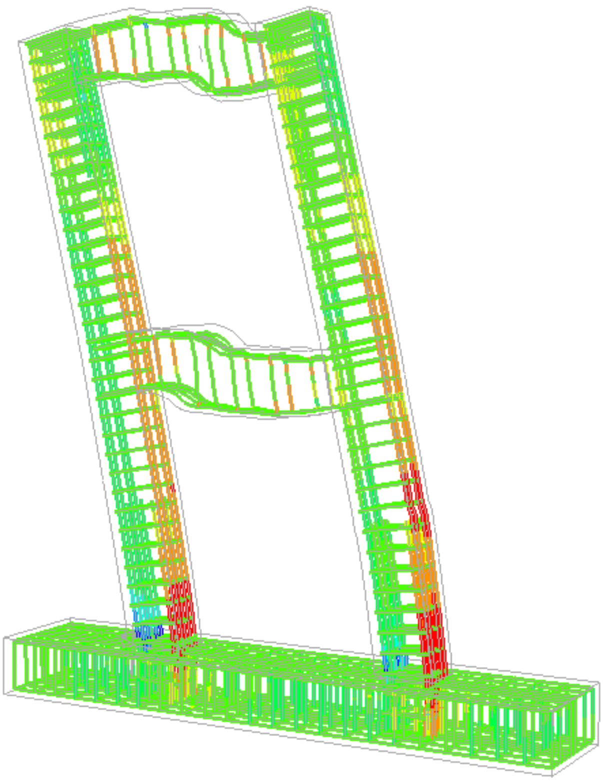

Fig. 5.10: Total stresses in the reinforcement in the z-direction – Scaled model

F. **Load-displacement second storey**

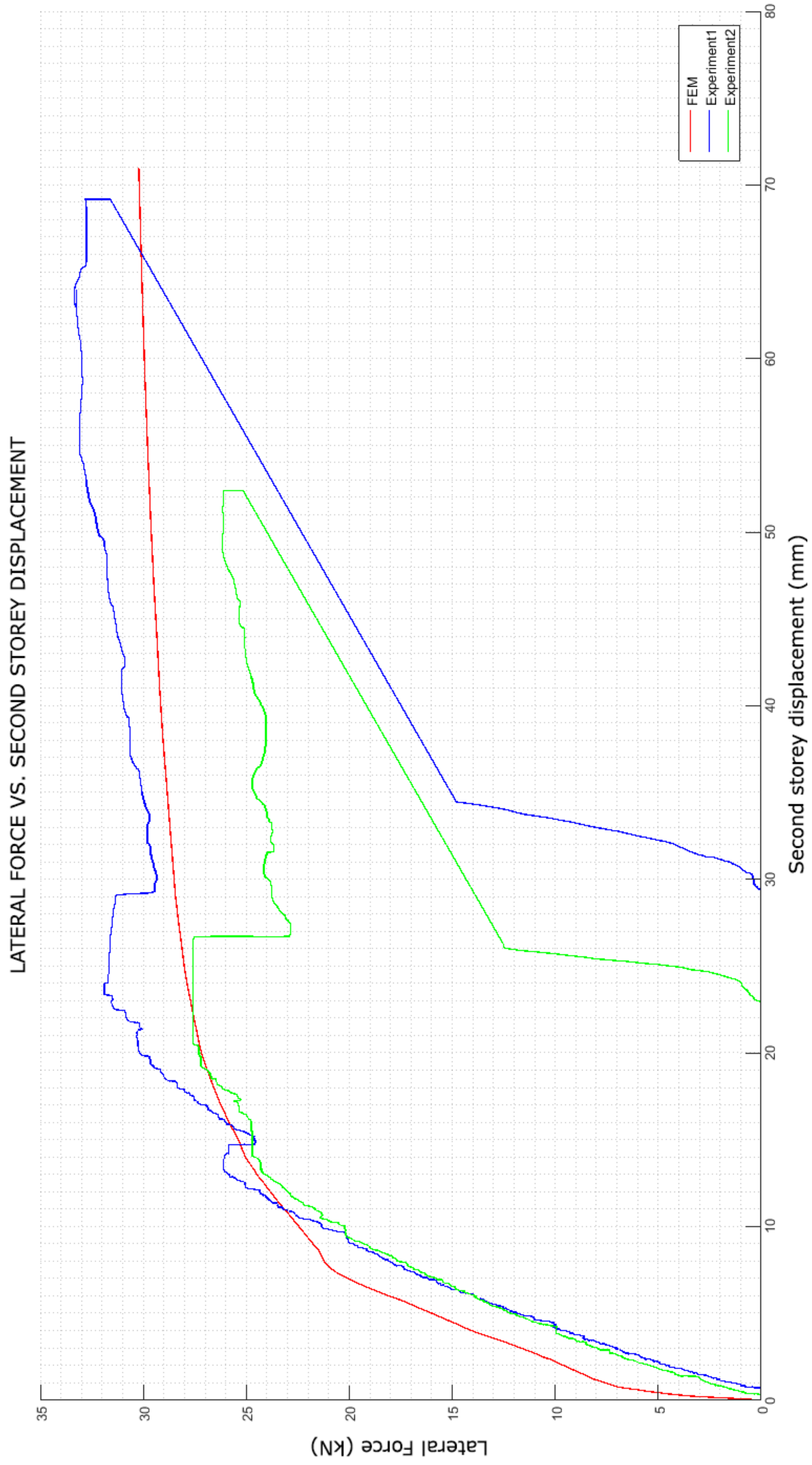

Graph 5.2: Second storey displacement related to the lateral force – Scaled model

G. Failure mode

The failure mode of the scaled model can be derived out of the crack pattern that is depicted in *Figure 5.6*. At the final stage, the frame failed due to shear. The shear cracks occurred exclusively in the beams. These shear cracks are showed by the diagonal cracks visible in the beam with a maximum opening of 3,00 millimetres (red zones). These arose due to an activation of the compressed strut in the concrete. Due to this shear force, the stirrups also started to yield. First, the stirrups at the lower beam yielded and after that the stirrups of the upper beam. Failing due to bending was not the case here.

So, there arose a difference in behaviour and failure mode between the prototype (bending + shear) and the scaled model (pure shear). This is remarkable conclusion and will be further examined in chapter *7. Comparison reference article vs. own research results*.

H. Discussion of results

Figure 5.7 shows the deformation of the frame. It is obvious that the second storey beam has the highest lateral deformation because the lateral force is applied at this level. This maximum deformation is 74,55 millimetres, and the lowest deformation is zero millimetres at the level of the clamped foundation. Related to the prototype, this deformation is a little bit higher because in this case the failing point is reached.

In *Figure 5.8* is the total compression stress in the concrete depicted. In this figure are the compressed struts in the beams not so clearly visible (diagonals) as in *Figure 5.3* because there did not occur a bending failure in the scaled model. The maximum compression stress is 53 N/mm^2.

Figure 5.9 shows the maximum stresses in the reinforcement in the x-direction. The maximum of 418,05 N/mm^2 (red zone) occurs at the upper left side and at the lower right side of the beams. The negative value of the compression occurs at the upper right side of the second storey beam and has a value of -407,06 05 N/mm^2 (blue zone). These values are higher than the yielding point of the longitudinal bars (refer to *Graph 2.7*) and for this reason the reinforcement started to yield in these areas.

In *Figure 5.10* are also the stresses in the reinforcement depicted but for the reinforcement in the z-direction. In this figure, it is clearly visible that the highest stresses are located in the stirrups at the left side of the beams. Due to this, the stirrups started to yield and the beams failed due to shear (Refer to *figure 3.5)*. Also, in the right side of the columns are observed high stresses. These are linked to the bending of the columns. These stresses reaching higher in the column height compared with the prototype. This because the beams do not take any bending (pure shear failure). The maximum value for the shear stresses out of this figure is 548,67 N/mm^2 and is higher than the yielding point of the stirrups (refer to *Graph 2.6*).

In *Graph 5.2* is the second storey displacement related to the lateral force plotted. The red line out of this graph shows the obtained calibration of the numerical model for the scaled model. The blue line is a plot of the experimental results of specimen one and the green line shows the experimental results of specimen two. The FEM approach reacts in the early stages (0 kN – 10 kN) a little bit stiffer than the experimental values. Between 10 kN and 20 kN the stiffness is equal to the experimental results. After the elastic zone the curve fits in between the two experimental curves and after the failure point the curve approaches the average of those two experimental curves.

6. COMPARISON EXPERIMENTAL- VS. FINITE ELEMENT RESULTS

6.1 Introduction

A comparison between the results of the experimental- versus the numerical method are carried out in the different subdivisions of part *6.2 Results*. In this part, the emphasis of the comparison of the results is placed on the crack-widths in the z-direction, the displacement of the frame and its element in the x-direction, the total compression stresses in the concrete and the total stresses in the reinforcement in the x- and z-direction. A general conclusion of these comparisons is given in chapter *8. Conclusion*.

6.2 Results

6.2.1 Crack-widths (z-direction)

Generally, the finite element model gave a good prediction of the failure mode and the location of the first major cracks (Refer to *Figure 3.7, 3.13, 3.18, 5.6* and *Graph 5.2*). Experimentally, the progression of first cracking was as follows: first storey beam shear, right side of columns flexure, collapse of first storey beam, second storey beam shear, flexure at the base of both columns and collapse of the second storey beam. The finite element model predicted the same behaviour except the flexural cracks at the right side of the columns. These were underestimated. But the model predicted the same failure mode, namely pure shear failure in the beams. The maximum average of the crack opening in the second storey beam was 14,70 millimetres and in the first storey beam 7,80 millimetres. The finite element model predicted a shear crack of 12 millimetres for the second storey beam and 7 millimetres for the first storey beam. So, the predictions about the opening of the cracks was also correct.

6.2.2 Displacements (x-direction)

Refer to *Graph 3.4*, *3.7* and *Figure 5.7*. The finite element model predicted that the second storey beam would experience the highest lateral displacement. The foundation would not deform (because it was a clamped foundation) and the displacement of the first storey beam is laying between the displacement values of the second storey beam and the foundation. This prediction corresponds to the results gathered out of the experimental tests, so the prediction of the displacement of the frame by the finite element model was correct.

6.2.3 Total compression stresses concrete S3

The finite element response of the compression stresses in the concrete was compatible to the experimental results. Refer to *Figure 5.8* for the prediction by the analytical model and to *Figure 3.7* for an example of the concrete crushing during the experiment. The finite element model predicted the highest compression stresses at the left side of the left column (blue marker elements out of *Figure 5.8*) with a value of 53 N/mm^2. The maximum average compression strength of the concrete during the two experimental tests was 53,33 N/mm^2. So, the analytical model predicted correct the place, were the crushing of the concrete would occur.

6.2.4 Total stresses reinforcement (x-direction)

When the stresses in the longitudinal reinforcement bars were checked, the following observations were made. Prior to the shear failure, the response of the finite element model seemed reasonable with the experiment. Like the experiment, the highest stresses occurred in the bars at the upper left side and lower right side of each beam (refer to *Figure 5.9* for the prediction and to *Figure 3.6* and *3.12* for the experimental results). Out of the material test, the yielding point of the longitudinal reinforcement was determined at 400 N/mm^2. The value of the stresses at the previous mentioned places was predicted by the analytical model and was 418,05 N/mm^2. This means that the reinforcement at those places was beyond the yielding point. This prediction could be linked to the experimental observations.

6.2.5 Total stresses reinforcement (z-direction)

When the analytically predicted transversal reinforcement stresses were compared to the actual behaviour of the frame, the following observations were made (refer to *Figure 3.5, 3.6, 3.11, 3.12* and *3.16* for the experimental behaviour and to *Figure 5.10* for the analytical prediction). The model predicted high stresses at the right side of each column and in the stirrups of the beams (orange marked elements). The predicted value of these stresses was 274,19 N/mm^2. Out of the material tests is the yielding point for both transversal- and longitudinal reinforcement determined. The yielding point for the bars with diameter six was, 400 N/mm^2 (column reinforcement) and for the bars with diameter three, 246 N/mm^2 (stirrups). This means that the stirrups in the beams are beyond their yielding point and the reinforcement bars in the columns were not beyond their yielding point. Therefore, the beams failed due to shear because in these zones was the yielding point of the reinforcement reached first.

6.2.6 Load-displacement second storey

Refer to *Graph 5.2*. In this graph is the second storey displacement related to the lateral force for the experiments plotted together with the prediction of the finite element model. The red line out of this graph shows the obtained calibration of the numerical model for the scaled model. The blue line is a plot of the experimental results of specimen one and the green line shows the experimental results of specimen two. The FEM approach predicts in the early stages (0 kN – 10 kN) a little stiffer behaviour than the experimental values. Between 10 kN and 20 kN the prediction of the stiffness is equal to the experimental results. After the elastic zone the curve fits in between the two experimental curves and after the failure point the curve approaches the average of those two experimental curves. The predicted value for the peak load is an average between 31,35 kN (specimen one) and 27,55 kN (specimen two). The unloading phase is not predicted by the finite element model.

Finally, it can be concluded that the general prediction of the numerical model on all previous facets, a very good approach is of the values gathered out of the experimental tests. This means that the finite element model is calibrated correctly, and that it widely can be used to predict the behaviour of a reinforcement concrete frame based on a scaled model.

7. COMPARISON REFERENCE ARTICLE - VS. OWN RESEARCH RESULTS

Table 7.1: Summary of the calculations of the behaviour between prototype and scaled model – SAP2000

Prototype 1/1				Scaled model 1/3			
Lateral Force (kN)	Shear Force V_{Ed} (kN/m)	Bending Moment M_{Ed} (kNm)	V_{Ed}/ M_{Ed} (-)	Lateral Force (kN)	Shear Force V_{Ed} (kN/m)	Bending Moment M_{Ed} (kNm)	V_{Ed} / M_{Ed} (-)
10	8,89	8,45	1,05	1	0,975	0,306	3,19
100	88,89	84,58	1,05	10	9,75	3,06	3,19
200	177,80	169,17	1,05	20	19,50	6,12	3,19
300	266,70	253,76	$\boxed{1,05}$	30	29,26	9,18	$\boxed{3,19}$

--->

$\approx\ x\,3$

Out of *Table 7.1* there can be concluded that there is a difference in behaviour (V_{Ed}/M_{Ed}) between the prototype and the scaled model. The occurring difference is almost equal to the scale factor three. This means that due to a geometrical downscaling of all the dimensions and the reinforcement diameters, the failure mode changes. In this case, from bending + shear failure (prototype) to a pure shear failure (scaled model). Refer to *Figure 5.*1 for the failure mode of the prototype and to *Figure 5.*7 for the failure mode of the scaled model.

Out of this analysis can be concluded that there is no linear downscaling possible between the prototype and the scaled model. So, to apply the downscaling correctly, the change in behaviour must be considered. *Equation 7.1* shows the mathematical equation of this phenomenon:

$$\frac{M_{Rd}^{1/1}\Big/M_{Ed}^{1/1}}{V_{Rd}^{1/1}\Big/V_{Ed}^{1/1}} = \frac{M_{Rd}^{1/3}\Big/M_{Ed}^{1/3}}{V_{Rd}^{1/3}\Big/V_{Ed}^{1/3}} \tag{7.1}$$

Only the green marked parameters out of the previous equation can be modified to obtain the same behaviour and failing mode between the prototype and the scaled model. Next, the calculations of all the resistant parameters out of *equation 7.1* are mentioned. A calculation of the shear force resistance for the prototype and the scaled model is given in *equation 7.2.* The calculations of the bending resistance for both models are given in *equation 7.3*. The design values for both models are already given in *Table 7.1* and are calculated in SAP2000.

$$minimum\ of: \tag{7.2}$$

$$V_{Rd,s}{}^{1/1} = \frac{A_{sw}}{S} \,.\, z \,.\, f_{yd} \,.\cot\theta$$

$$V_{Rd,max}{}^{1/1} = \frac{\alpha_{cw} \,.\, b_w \,.\, z \,.\, v_1 \,.\, f_{cd}}{\cot\theta + \tan\theta}$$

$$Refer\ to\ figure\ 1.14\ and\ 1.15 +\ table\ 1.2\ and\ 1.3\ for\ the\ used\ values$$

$$V_{Rd,s}{}^{1/1} = \frac{\left(\frac{(\pi.\,9{,}5\ mm^{\,2})}{4}\right).\,2}{300\ mm} \,.\, 0{,}9 \,.\, 350\ mm \,.\, 506\ \ N/mm^2\ \,.\cot 45° = 75{,}32\ kN$$

$$V_{Rd,max}{}^{1/1} = \frac{1 \,.\, 300\ mm \,.\, 0{,}9 \,.\, 350\ mm \,.\, 0{,}6 \,.\, 42{,}9\ \ N/mm^2}{\cot 45° +\ \tan 45°} = 1216{,}22\ kN$$

$$V_{Rd}{}^{1/1} =\ V_{Rd,s}{}^{1/1} = 75{,}32\ kN$$

$$Refer\ to\ figure\ 2.2\ \ and\ 2.3 +\ table\ 2.1\ and\ 2.4\ for\ the\ used\ values$$

$$minimum\ of:$$

$$V_{Rd,s}{}^{1/3} = \frac{A_{sw}}{S} \,.\, z \,.\, f_{yd} \,.\cot\theta$$

$$V_{Rd,max}{}^{1/3} = \frac{\alpha_{cw} \,.\, b_w \,.\, z \,.\, v_1 \,.\, f_{cd}}{\cot\theta + \tan\theta}$$

$$V_{Rd,s}{}^{1/1} = \frac{\left(\frac{(\pi.\,3\ mm^{\,2})}{4}\right).\,2}{100\ mm} \,.\, 0{,}9 \,.\, 116\ mm \,.\, 246\ \ N/mm^2\ \,.\cot 45° = 3{,}63\ kN$$

$$V_{Rd,max}{}^{1/1} = \frac{1 \,.\, 100\ mm \,.\, 0{,}9 \,.\, 116\ mm \,.\, 0{,}6 \,.\, 53{,}33\ \ N/mm^2}{\cot 45° +\ \tan 45°} = 167{,}03\ kN$$

$$V_{Rd}{}^{1/3} =\ V_{Rd,s}{}^{1/3} = 3{,}63\ kN$$

$$M_{Rd}{}^{1/1} = A_{sl} \, . f_{yd} \, . z \tag{7.3}$$

$$Refer\ to\ figure\ 1.14\ and\ 1.15 + \ table\ 1.2\ and\ 1.3\ for\ the\ used\ values$$

$$M_{Rd}{}^{1/1} = \left(\frac{(\pi . 20\ mm\ ^2)}{4}\right) . 4\ bars\ . 447\ N/mm^2\ \ . 0,9\ . 350\ mm = 176,94\ kNm$$

$$Refer\ to\ figure\ 2.2\ \ and\ 2.3 + \ table\ 2.1\ and\ 2.4\ for\ the\ used\ values$$

$$M_{Rd}{}^{1/3} = \left(\frac{(\pi . 6\ mm\ ^2)}{4}\right) . 4\ bars\ . 400\ \ N/mm^2 . 0,9\ . 116\ mm = 4,72\ kNm$$

Then, the found values are returned in *equation 7.1* to determine the needed $V_{Rd}^{1/3}$ to obtain the same failure mode as the prototype:

$$\frac{M_{Rd}^{1/1} \big/ M_{Ed}^{1/1}}{V_{Rd}^{1/1} \big/ V_{Ed}^{1/1}} = \frac{M_{Rd}^{1/3} \big/ M_{Ed}^{1/3}}{V_{Rd}^{1/3} \big/ V_{Ed}^{1/3}} \tag{7.1}$$

$$\frac{176,94\ kNm \big/ 253,76\ kNm}{75,32\ kN \big/ 266,70\ kN} = \frac{4,72\ kNm \big/ 9,18\ kNm}{V_{Rd}^{1/3} \big/ 29,26\ kN}$$

$$V_{Rd}^{1/3} \quad = \quad 6,09\ kN$$

Next, the new reinforcement diameter for the stirrups is obtained out of the new value of $V_{Rd}^{1/3}$:

$$V_{Rd,s}{}^{1/3} = \frac{A_{sw}}{S} \, . \, z \, . \, f_{yd} \, . \cot\theta \tag{7.4}$$

$$A_{sw} = \frac{V_{Rd,s}{}^{1/3} \, . \, S}{z \, . \, f_{yd} \, . \cot\theta}$$

$$A_{sw} = \frac{6{,}09 \, . \, 10^3 \, N \, . \, 100 \, mm}{0{,}9 \, . \, 116 \, mm \, . \, 246 \, N/mm^2 \, . \cot 45°} = 23{,}73 \, mm^2$$

$$A_{sw} = \frac{\pi \, . \, d^2}{4}$$

$$d_{sw} = \sqrt{\frac{4 \, . \, A_{sw}}{\pi}}$$

$$d_{sw} = \sqrt{\frac{4 \, . \, 23{,}73 \, mm^2}{\pi}} = 5{,}496 \, mm$$

There is also a small difference in bending resistance whereby the diameter of the longitudinal bars also changes. This difference can be calculated as:

$$M_{Rd}^{1/1} \Big/ M_{Ed}^{1/1} = M_{Rd}^{1/3} \Big/ M_{Ed}^{1/3} \tag{7.5}$$

$$176{,}94 \, kNm \Big/ 253{,}76 \, kNm = M_{Rd}^{1/3} \Big/ 9{,}18 \, kNm$$

$$M_{Rd}^{1/3} = 6{,}40 \, kNm$$

$$M_{Rd}{}^{1/3} = A_{sl} \, . \, f_{yd} \, . \, z$$

$$A_{sl} = \frac{M_{Rd}{}^{1/3}}{f_{yd} \, . \, z}$$

$$A_{sl} = \frac{6{,}40 \, . \, 10^6 \, Nmm}{400 \, N/mm^2 \, . \, 0{,}9 \, . \, 116 \, mm} = 153{,}28 \, mm^2$$

$$A_{sl} = 2\ rows\ .\frac{\pi\ .\ d^2}{4}$$

$$d_{sl} = \frac{\sqrt{\frac{4\ .\ A_{sl}}{\pi}}}{2\ rows}$$

$$d_{sl} = \frac{\sqrt{\frac{4\ .\ 153{,}28\ mm^2}{\pi}}}{2\ rows} = 6{,}985\ mm$$

To summarize these calculations, there can be concluded that it is possible to neutralize the change in behaviour by increasing the diameters of the longitudinal - and transversal reinforcement. The longitudinal reinforcement should be changed from diameter six millimetres into a diameter of 6,985 millimetres by a scale factor of three. The transversal reinforcement should be changed from diameter three millimetres into a diameter of 5,496 millimetres. So, the diameters that will be applied for the building of these models are dimensions that are widely available on the market. For this reason, a longitudinal reinforcement with diameter seven millimetres should be used and for the transversal reinforcement should be used a diameter of six millimetres when a scale factor of three is applied. *Table 7.2* serves as a summarization.

Table 7.2: Summary of the modified diameter related to the original diameter

Original diameter (mm)	Modified diameter (mm)	Area cross-section (mm^2)	Location in specimen
3	6	28	Transversal
6	7	38	Longitudinal

The best way to prove that these calculations have a scientific value, is building a new model with the modified diameters. But due to a lack of time this was not possible anymore. For this reason, these modified diameters are applied in the calibrated numerical model to prove that the calculations are correct. In the first modified model are both modified diameters out of *Table 7.2* applied. In the second modified model is the original diameter for the stirrups used, but is the amount of the applied transversal reinforcement doubled to investigate our this also could be a solution. Besides, the modified diameter for the longitudinal reinforcement is also applied is this model.

In *Figure 7.1* is the crack pattern of the prototype depicted, in *Figure 7.2* the crack pattern of the scaled model and in *Figure 7.3* the crack pattern of the first modified scaled model. This comparison shows very clear that the failing mode of the prototype (bending + shear) (*Figure 7.1*) is totally different than the one of the scaled model (pure shear) (*Figure 7.2*). In addition, the failing mode of the modified scale model (*Figure 7.3*) is approximately the same than the one of the prototype. So, by applying the modified diameters out of *Table 7.2*, the same failure mode (bending + shear) as the prototype is obtained. This proves that the previous calculations are correct. *Graph 7.1* shows the lateral force vs. second storey displacement of the modified scaled model related to the lateral force vs. second storey displacement out of the experimental results and the scaled model.

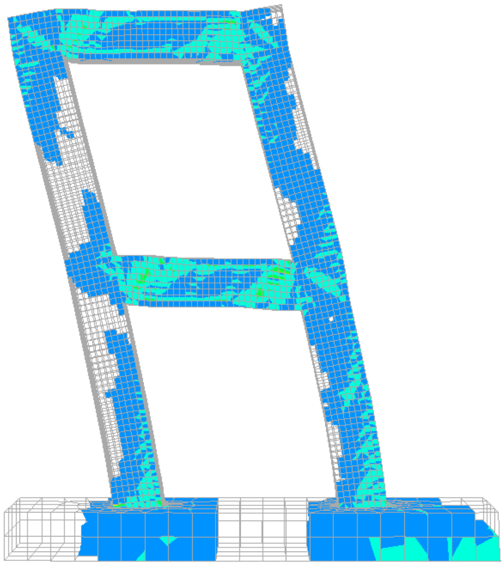

Fig. 7.1: Crack pattern in the z-direction – Prototype

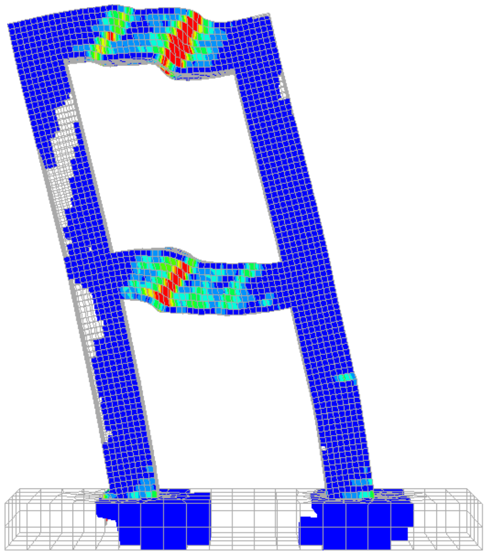

Fig. 7.2: Crack pattern in the z-direction – Scaled model

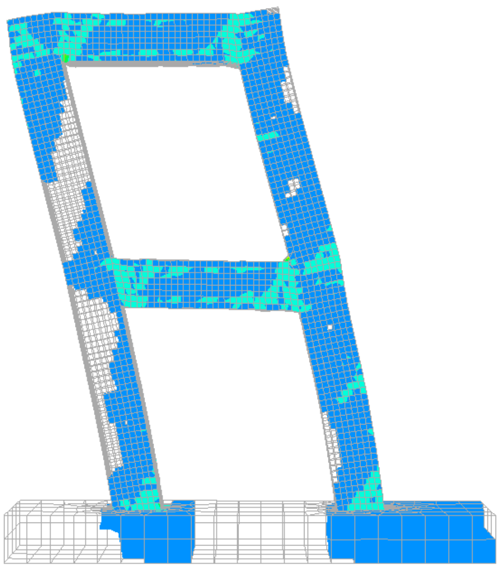

Fig. 7.3: Crack pattern in the z-direction – Modified scaled model one

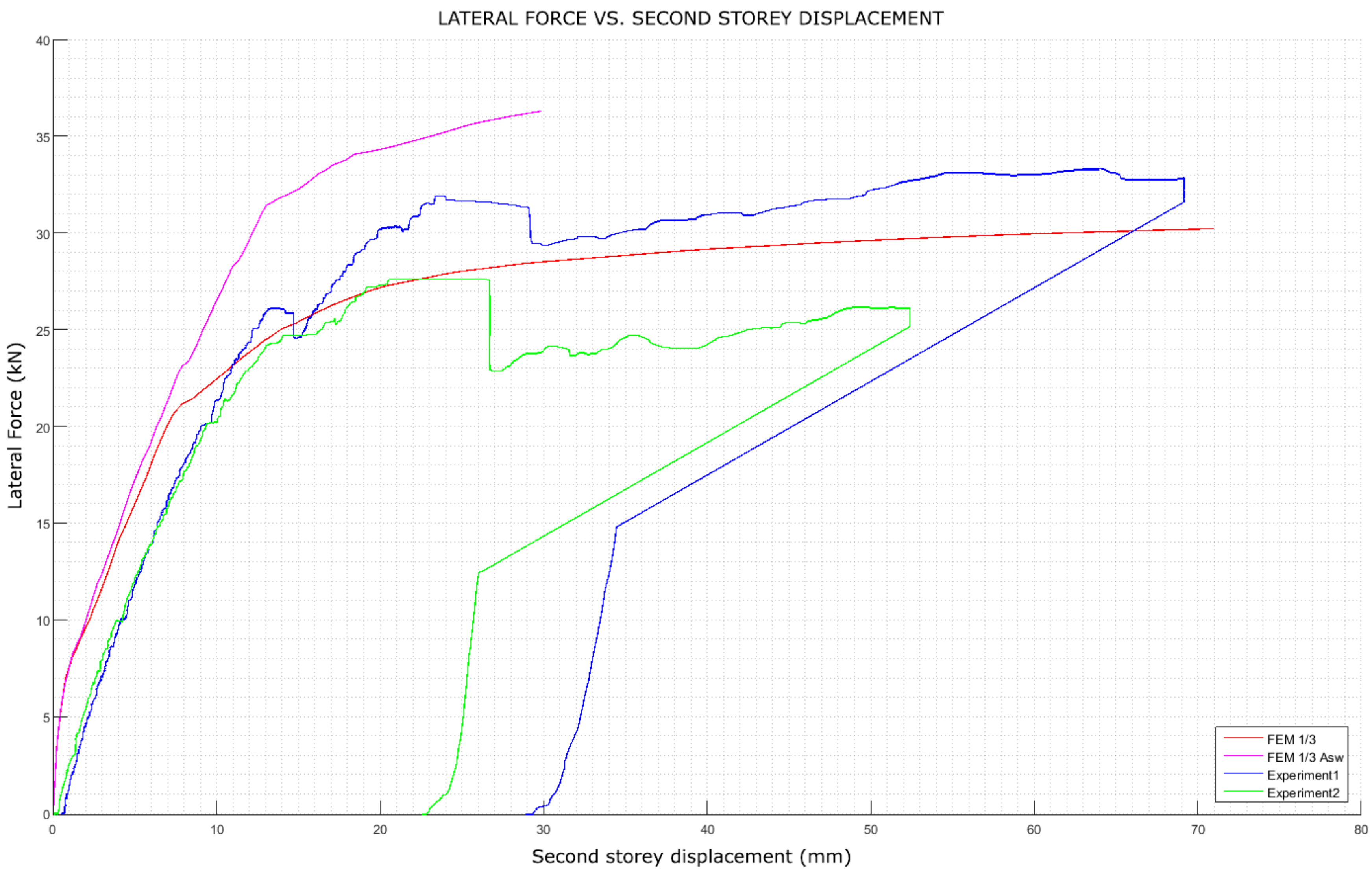

Graph 7.1: Second storey displacement related to the lateral force – Scaled model + Modified scaled model one

In *Figure 7.4* is the crack pattern of the second modified scaled model depicted. When this figure is compared to *Figure 7.1* or *Figure 7.3* it is very clear that this crack pattern is totally different. In this model, there occurs a failure in the compressed zone of the concrete at the left side of the left column. There also occurs a crack at the upper left joint between column and beam. Thus, in this modified model there is a shifting from the place of first failure from the first storey beam to the second storey beam and a shifting from the crack from the right side to the left side of the beam. So, a doubling of the transversal reinforcement is not a good solution, because a total different failure mode is obtained compared to the failure mode of the prototype and the failure mode of 'modified scaled model one'. *Graph 7.2* shows the lateral force vs. second storey displacement of the two modified scaled models related to the lateral force vs. second storey displacement out of the experimental results and the scaled model. Here, it is visible that the curve of the second modified scaled model (black) is laying in between the curve of the first modified scaled model (magenta) and the curve out of the experiment of specimen one (bleu). As general conclusion can be said that 'modified scaled model one' is a good solution to obtain the same failure mode as the prototype. The curve related to this model reacts much stiffer than the first calibrated finite element model (red).

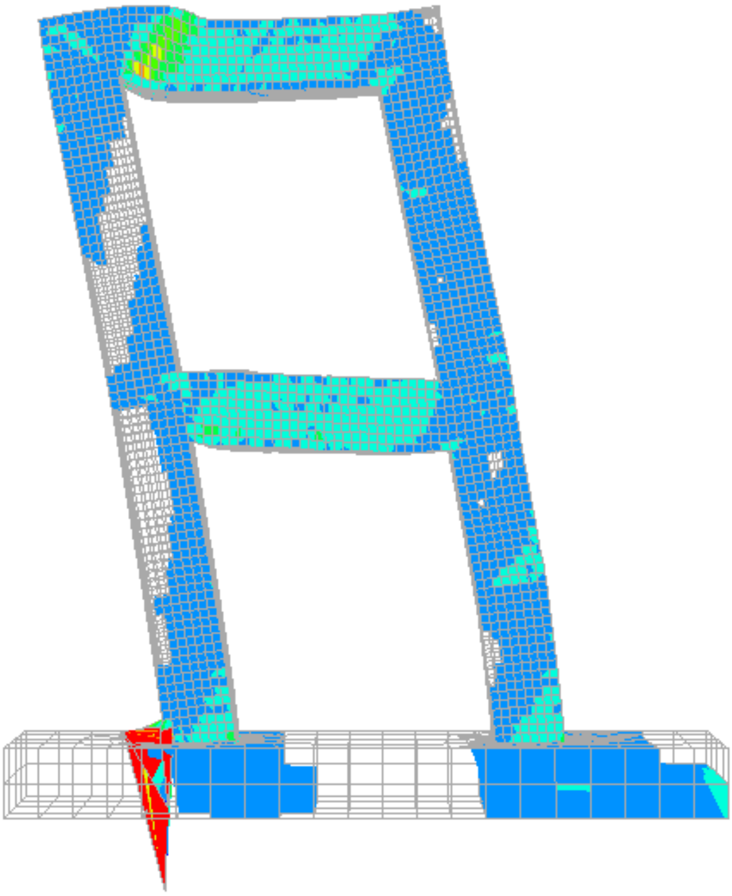

Fig. 7.4: Crack pattern in the z-direction – Modified scaled model two

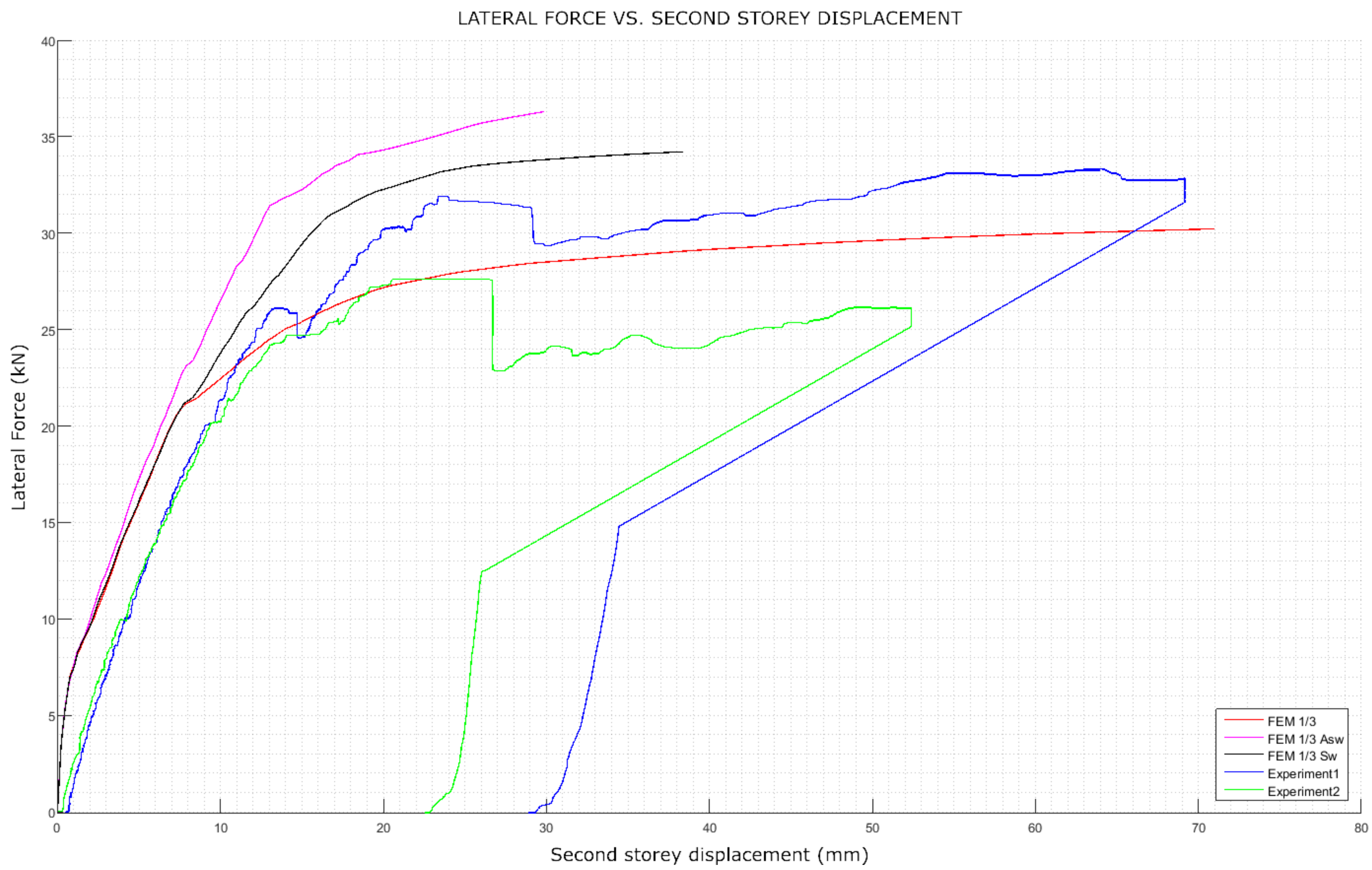

Graph 7.2: Second storey displacement related to the lateral force – Scaled model + Modified scaled model one + two

8. CONCLUSION

To conclude, a difference in behaviour (V_{Ed}/M_{Ed}) and failure mode arose between the prototype and the scaled model. The occurring difference is approximately equal to the scale factor of three. This means that due to a geometrical downscaling of all the dimensions and the reinforcement diameters, the failure mode changed. In this study, the failure mode changed from bending + shear failure (prototype) to a pure shear failure (scaled model). From the analysis, it can be concluded that there is no linear downscaling possible between the prototype and the scaled model. So, to apply the downscaling correctly, the change in behaviour must be taken into consideration.

This change in behaviour between the prototype and the scaled model is removed by a modification of the reinforcement diameters. The diameter of the longitudinal reinforcement is changed from diameter six millimetres into a diameter seven millimetres. The diameter of the transversal reinforcement is changed from diameter three millimetres into a diameter six millimetres. The finite element model proves that this modification is accurate and that due to this modification there is no longer a difference in behaviour and failure mode between the prototype and the scaled model.

In sum, downscaling of a reinforced concrete frame is possible, when the failure mode does not change. If the failure mode changes, the reliability of the prediction of the behaviour of the structure significantly decreases. When the failure mode between the prototype and the scaled model remains identical, the prediction of the behaviour of the structure is correct. This prediction can be obtained by an experimental test or by using the calibrated finite element model that is elaborated is this master's thesis.

9. FUTURE WORK

For future experimental work, it could be interesting to carry out the same tests on the same frames, but with the modified reinforcement diameters. This would make it possibe to check physical of the failure mode changes from pure shear to bending + shear like predicted by the modified numerical model. Next, it would be interesting to conduct a cyclic test on specimens with equal geometrical parameters but with the modified reinforcement diameters as the ones tested in this master's thesis. This can be done to investigate the behaviour of the portal frame in an area that is sensitive for earthquakes. Subsequently, there could also be done a calibration of a numerical model whereby the behaviour from other structures in an earthquake sensitive area could be predicted.

Another approach is to change the shear reinforcement (cfr. stirrups of the beams) of the frames into fibres. As a result, the shear capacity of the beams would increase, whereby more force could be absorbed in the beams and the frame would resist a lateral increasing load much longer.

For future numerical work, it would be valuable to determine exactly the bond coefficient between the steel reinforcement and the concrete. This is interesting as in the numerical model of this master's thesis, a bond coefficient is used that assumes a perfect bond between the steel reinforcement and the concrete. This is a pure theoretical assumption because in a real-life situation there will always be a friction loss between the reinforcement and the concrete.

After a modification of the numerical model with an adjusted bond coefficient it is also possible to carry out a parametrical study. The advantage of such methods is that it is possible to change the material properties, the dimensions of the model, etcetera. This could easily be done by using a software that considers parametrical material properties and model dimensions.

REFERENCES

[1] M. A. B. Embong, Finite element analysis of 3D reinforced concrete frame using Ansys, Pahang: Faculty of Civil Engineering & Earth Resources, 2015.

[2] K. V. Duong, Seismic behaviour of a shear-critical reinforced concrete frame: an experimental and numerical investigation, Toronto, 2006.

[3] C. Murty, "Concrete Coalition," 2005. [Online]. Available: http://www.concretecoalition.org/wp-content/uploads/2013/08/RC_frame.jpg. [Accessed 2017].

[4] F. J. Vecchio and M. P. Collins, The Modified Compression-Field Theory for Reinforced Concrete Elements Subjected to shear, Toronto: ACI Journal, 1986.

[5] M. Celebi and J. Penzien, Experimental investigation into the seismic behavior of critical regions of reinforced concrete components as influenced by moment and shear, Berkley: UCB/EERC Report 73-04, Earthquake Engineering Center, University of California, 1973.

[6] A. Ghobarah, T. Aziz and A. Biddah, Seismic rehabilitation of reinforced concrete beam-column connections, Oakland: Earthquake Spectra, Allen Press, 1996, pp. 12, 4: 761-780.

[7] F. J. Vecchio and S. Balopoulou, On the nonlinear behaviour of reinforced concrete frames, Toronto: Canadian Journal of Civil Engineering, 1990, pp. 17, 5: 698-704.

[8] F. J. Vecchio and M. B. Emara, Shear deformations in reinforced concrete frames, Toronto: ACI Structural Journal, 1992, pp. 89, 1: 46-56.

[9] J. Goodier and W. Thomson, Applicability of similarity principles to structural model, Washington: NACA Tech, 1944, p. Note 933.

[10] J. Goodier, Dimensional analysis, hanbook of experimental stress analysis, New York: Wiley & Sons Inc., 1950, pp. 1035 - 1045.

[11] H. Krawinkler, Scale Effects in Static and Dynamic Model Testing of Structures, Tokyo-Kyoto: World Conference on Earthquake Engineering, 1988, pp. 865 - 876.

[12] H.-K. Man, Analysis of SD Scale and Size Effects in Numerical Concrete, Zürich: ETH Zürich, 2010, p. 13.

[13] E. Szücs, Similitude and modeling, Amsterdam: Elsevier Scientific Publishing Company, 1980.

[14] D. Barr, A survey of procedures for dimensional analysis, Glasgow: International Journal of Mechanical Engineering Education, Vol 11, 1983, pp. 147 - 159.

[15] D. Schuring, Scale models in engineering: fundamentals and applications, Pennsylvania: Pergamon Press, 1977.

[16] H. Langhaar and M. Stippes, Three-dimensional Stress Functions, Philadelphia: Elsevier Ltd., 1954, pp. 371-382.

[17] S. Kline, Similitude and approximation theory, New-York: McGraw-Hill, 1965.

[18] S. Timoshenko and S. Woinowsky-Krieger, Theory of plates and shells, New-York: McGraw-Hill, 1959.

[19] M. Renette, [Own image archive], Diepenbeek, Limburg, 2017.

[20] J. Manie, DIANA - Finite Element Analysis User's Manual FX+ for DIANA, Delft: TNO DIANA BV, 2015.

Auteursrechtelijke overeenkomst

Ik/wij verlenen het wereldwijde auteursrecht voor de ingediende eindverhandeling:
Experimental and numerical analysis on a reinforced concrete structure using structural similitude laws

Richting: **master in de industriële wetenschappen: bouwkunde**
Jaar: **2017**

in alle mogelijke mediaformaten, - bestaande en in de toekomst te ontwikkelen - , aan de Universiteit Hasselt.

Niet tegenstaand deze toekenning van het auteursrecht aan de Universiteit Hasselt behoud ik als auteur het recht om de eindverhandeling, - in zijn geheel of gedeeltelijk -, vrij te reproduceren, (her)publiceren of distribueren zonder de toelating te moeten verkrijgen van de Universiteit Hasselt.

Ik bevestig dat de eindverhandeling mijn origineel werk is, en dat ik het recht heb om de rechten te verlenen die in deze overeenkomst worden beschreven. Ik verklaar tevens dat de eindverhandeling, naar mijn weten, het auteursrecht van anderen niet overtreedt.

Ik verklaar tevens dat ik voor het materiaal in de eindverhandeling dat beschermd wordt door het auteursrecht, de nodige toelatingen heb verkregen zodat ik deze ook aan de Universiteit Hasselt kan overdragen en dat dit duidelijk in de tekst en inhoud van de eindverhandeling werd genotificeerd.

Universiteit Hasselt zal mij als auteur(s) van de eindverhandeling identificeren en zal geen wijzigingen aanbrengen aan de eindverhandeling, uitgezonderd deze toegelaten door deze overeenkomst.

Voor akkoord,

Renette, Maikel

Datum: **4/06/2017**